Universitat d'Alacant
Universidad de Alicante

Synthesis of hybrid silica-organic materials for the development of electrochemical biosensing applications

Halima Djelad

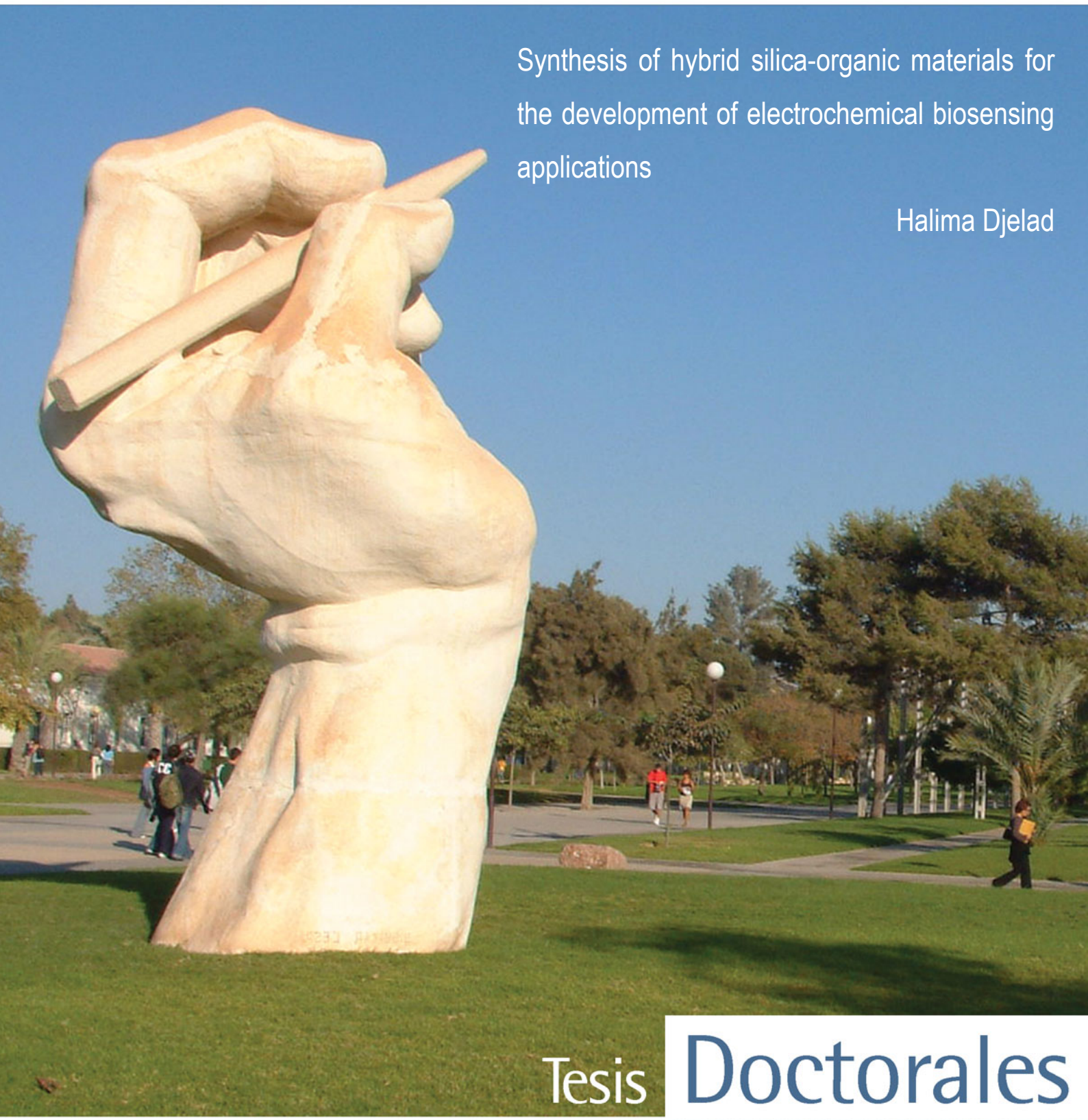

Tesis Doctorales

www.eltallerdigital.com

UNIVERSIDAD de ALICANTE

Synthesis of hybrid silica-organic materials for the development of electrochemical biosensing applications

Halima Djelad

Doctoral Thesis

Universitat d'Alacant
Universidad de Alicante

Instituto Universitario de Materiales

Facultad de Ciencias

Universidad de Mascara

Mustapha Stambouli

Synthesis of hybrid silica-organic materials for the development of electrochemical biosensing applications

Halima Djelad

Tesis presentada para aspirar al grado de

Doctora por la Universidad de Alicante

y la Universidad de Mascara (Mustapha Stambouli) – Cotutelle.

DOCTORADO EN CIENCIA DE MATERIALES

Dirigida por:

Francisco Montilla Jiménez

Prof. Titular de Química Física

Abdelghani Benyoucef

Prof. Ingeniería de procesos

Remerciements

Je commence tous d'abord à remercier mes directeurs de thèse : Francisco Montilla Jiménez, Emilia Nuñez Morallón et Abdelghani Benyoucef, de m'avoir accepté dans leur groupe de recherche et m'offrir l'opportunité d'acquérir de nouvelles connaissances.

Merci à toi PACO pour ta patience et ton aide dans les moments difficiles.

Mes plus sincères remerciements à M. César Quijada Tomas, Professeur de l'université polytechnique de Valence et à M. Raul Berenguer Betrian, de l'université d'Alicante et M. Mohammed Issam Ferahi, Professeur de l'université d'Oran pour avoir mobilisé leur temps et leur compétence pour examiner et juger ce travail.

A notre technicien Javier Medina, à Toya, les choses sont très simples et faciles avec vos aides.

A mes amis de groupe (GEPE): Sara, Mª José, María, Felipe, Alejandro, Fabián, José Quintero, Javi Quilez, Asma, Atsushi, Ana Belen, Andrés, Edwin, Camilo, Raúl, Maribel, Sarai, Sandra, Carolina, Ana Cristina, David Salinas, Alonso, Omar Ornelas, Ramiro, Carlos Sanchís, Zakaria, Juan Manuel Sieben, Adilene, Maali, Samiha, Mounia, Asmaa, Isabel Piñeiro e Isa Fuentes.

A Alonso, merci pour ton aide durant ma première année.

A toutes les personnes qui ont servis pour ma formation, et mon enseignement.

Je dédie ce travail qui est le fruit de toutes mes années d'études :

A ma grand-mère (***TOUMI HALIMA***), qui s'est éteinte en novembre 2009; Je ne t'oublierai jamais.

A mon très cher père ***DJELAD ABDALLAH***, je me rappel toujours de tous les moments où tu m'as poussé à travailler et à réussir. Cher père j'avoue que si je suis devenue quelque chose actuellement c'est grâce à tes efforts, à tes conseilles et à ta surveillance. Tu m'as toujours aidé, encouragé et dirigé sur le bon chemin en donnant la volonté et la confiance en soi, que dieu te garde pour moi, cher père. Merci et j'espère que vous trouvez dans ce travail l'expression de ma gratitude et mon respect.

A ma très chère mère ***BOUHADIBA YAMINA***, j'aimerai toujours te remercier pour tous ce que tu as fais jusqu'à notre jours là pour assurer l'éducation et la formation, chère mère j'avoue vraiment que tu été pour moi la lumière qui guide mes routes et qui m'emmène aux chemins de la réussite, tu as été toujours à mes côtés avec tes précieuses prières qui m'ont énormément poussé vers le mieux, c'est grâce à toi que je dois toute ma réussite. J'espère que mon travail sera le témoignage de ma gratitude et mon respect le plus profond.

A mon très cher mari ***HADJ DJILANI EL HOUARI (SID AHMED)***, aucun mot ne saurait t'exprimer mon profond attachement et ma reconnaissance pour tout l'encouragement, le respect, la gentillesse et l'amour que tu m'as offert, je te dédis ce travail. Tu es un modèle d'honnêteté et de loyauté. J'espère te combler et te rendre toujours heureux. Que dieu réunisse nos chemins pour un long commun serein et que ce travail soit le témoignage de ma reconnaissance et de mon amour sincère et fidèle.

A ma très chère princesse ***HADJ DJILANI AHLEM***, c'est à toi mon adorable ange, mon amour, ma joie, mon petit trésor que maman dédie ce travail pour te dire que tu resteras pour toujours le rayon du soleil qui égaye ma vie. Je t'aime mon bébé et je te souhaite tous le bonheur du monde.

A mes très chers frères : **SOFIANE**, **DJAWED**, **WALID**, **YACINE** et **ABDERAHMANE,** à toi **WALID** spécialement cher frère pour ta compagnie depuis mes études les plus première, tu m'a toujours aidé par ta soutenance, tes encouragements et ton aide. J'avoue vraiment que si je suis arrivée à être là c'est grâce à toi.

A mes très chères sœurs : **RADIA**, **DJIHENE**, **CHAHINEZ**, **NASSIRA** et **HALIMA**.

A mes adorables neveux et nièces : **ABDALLAH 1**, **OUSSAMA**, **YOUNES**, **YAMINA**, **SULTANA**, **ABDALLAH 2** , **DJOUMANA** et **RADIA**.

A ma très chère belle mère ***SARI CHERIFA***. Je profite de la présente occasion pour vous remercier pour tout l'amour et la sympathie que vous m'accordez. Que Dieu le tout puissant vous comble de santé. A la mémoire de mon beau père **HADJ DJILANI MOHAMMED** ainsi toute ma belle famille.

A ma très chère copine **KEDIR NAWEL CHAHINEZ** dont la présence, l'attention ont été si importantes dans la réalisation de ce modeste travail. Qui est ma meilleure amie, avec qui j'ai eu un immense plaisir de partager dix années de moments intenses.

…. Et à tous ceux qui me sont chers.

Que dieu le tout puissant nous accorde un avenir meilleur.

Lire, c'est boire et manger. L'esprit qui ne lit pas maigrit comme le corps qui ne mange pas.

VICTOR HUGO

Index

1.Introduction: Sensors and biosensors

In recent years, the importance of monitoring and controlling many different parameters in fields such as clinical diagnoses, food industry, environment, forensics or drug development has been increasing. Thus, there is a need to have reliable analytical devices capable to carry out fast and accurate analyses. Conventional methods provide high sensitivity and selectivity, but they are expensive, time consuming and require highly trained personal. One way to overcome many disadvantages of these methods is to develop sensors.

Chemical sensors are devices that convert the concentration of target compounds into an analytical signal. The term analytical implies the concept of measurability. Then a chemical sensor converts the information about the presence of target compounds into a measurable quantity. Currently, electronics is the technology that enables not only the measurement, but also the efficient use of the acquired information. Examples of this are storage, processing, communication, and active utilization of the information to control machines. Sensor technology has been pivotal in the latest spread of microelectronics, and the continuous extension of sensor properties is gaining unprecedented fields of applications. The number of articles increased considerably in the last twenty years, as shown in Figure 1.1, demonstrating a high level of interesting in this area.

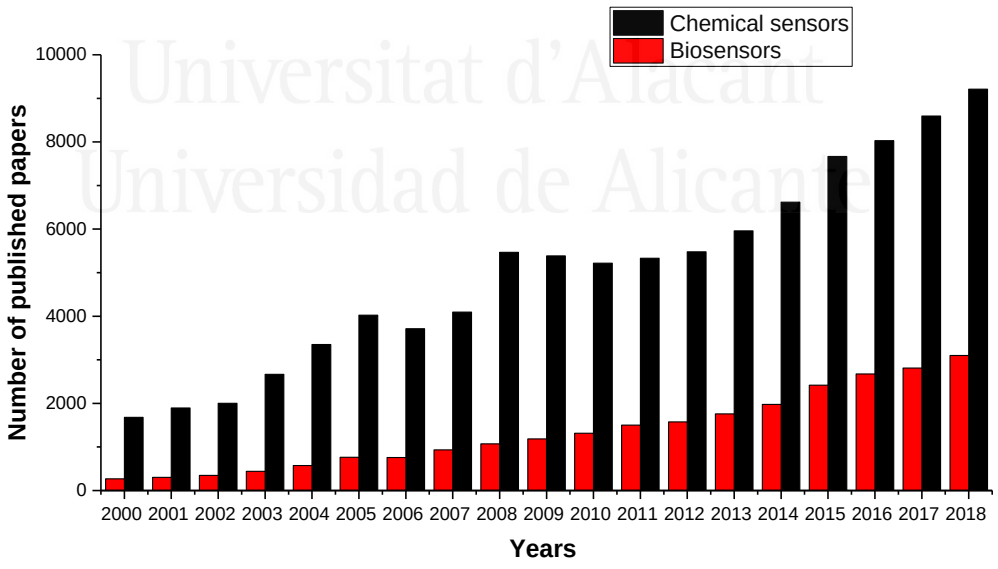

Figure 1.1. Number of published papers searching “Chemical sensors and biosensors” in topic in Scopus.

1.1. Sensors

1.1.1. Definition of sensor

A sensor can be defined, in a very general manner, as a device that responds to a signal, or stimulus. A stimulus can be understood as any quantity, property or condition.
In their vast majority, modern sensors are not standalone devices. They are part of larger systems that may incorporate other detectors, signal conditioners and processors, memory devices, data recorders and transducers. In consequence, sensors need to provide a signal which is readable by all other elements of the system they are incorporated in. This is why in the majority of artificial systems, information on the stimulus, first carried by the sensor's response, is processed and transmitted as an electrical signal: a voltage, a current or a charge. This electrical signal can be further described typically in terms of amplitude, frequency, and/or phase[1,2].

1.1.2. Sensors, transducers and actuators

A sensor can be interpreted as a device that converts any form of energy to electrical energy. Consequently, sensors are a subclass of transducers, which are simply defined as energy converters, from one kind into another. Devices referred to as actuators also constitute a subclass of transducers and are the counter part of sensors: they convert electrical energy into another kind of energy.

- *Direct and complex sensors*

When one or more transducers are necessary to convert the initial stimulus into an electrical signal, the system formed is a complex sensor. In opposition, a direct sensor uses physical effects for straight forward conversion of the stimulus into an electrical signal generation or modification.

- *Passive and active sensors*

According to sensor theory [1,2], all sensors can be classified into two large categories: passive sensors and active sensors. An active sensor requires an external source of energy, referred to as an excitation signal, whereas active sensors directly generate an electrical signal in response to a stimulus, without the need for an external excitation.

A further classification of sensors can be achieved by considering all of their properties[3]: stimulus, targeted applications, specifications, physical effect(s) for transduction, type of energy conversion, materials, etc. . .

1.1.3. Chemical sensors

A chemical sensor is a self-contained analytical device that can provide information about the chemical composition of its environment, that is, a liquid or a gas phase[4]. The information is provided in the form of a measurable physical signal that is correlated with the concentration of a certain chemical species (termed as analyte). Two main steps are involved in the functioning of a chemical sensor, namely, recognition and transduction. In the recognition step, analyte molecules interact selectively with receptor molecules or sites included in the structure of the recognition element of the sensor. Consequently, a characteristic physical parameter varies and this variation is reported by means of an integrated transducer that generates the output signal. A chemical sensor based on a recognition element made of a biological compound is a biosensor.

However, as synthetic biomimetic materials are going to substitute to some extent, recognition biomaterials, a distinction between a biosensor and a standard chemical sensor may be difficult. Typical biomimetic materials used in sensor development are molecularly imprinted polymers and aptamers.

1.1.4. Electrochemical Sensors

Till the nineties, the term electro-analytical chemistry was used to indicate the development of novel devices and techniques, and of novel methodologies for the correct use of electrochemical techniques in analytical chemistry. It also included all techniques (spectroscopic, morphologic, structural, etc.) suitable for characterizing the electrically conducting materials constituting the electrode or the species used as a component of the electrode. The term also included these non-electrochemical techniques whenever used to identify the effects induced by the polarization of the electrode, such as transformation of species, of the electrode surface itself, etc. The Bard's series[5] defined what we would like to define as electro-analytical chemistry in a wider meaning.

An electrochemical sensor is a device that transforms electrochemical information into a useful analytical signal. An electrochemical sensor is normally comprised of a working electrode,

reference electrode and a counter electrode connected to a potentiostat/galvanostat. The working electrode acts as receptor and is a component of the transducer as well. In a typical three electrode electrochemical sensor, a transducer is composed of working electrode, reference electrode, counter electrode and the other components of sensing device involved in the analysis. Electrochemical sensing is a promising analytical field and it has found its applicability in the fields of energy, health, environment, food and pharmaceutical industry[6]. Electrochemical sensing can be divided into chemical and biosensing. Chemical sensor provides the analytical information about a particular quantity of certain chemical species in the surrounding environment. A biosensor is an integrated device that provides quantitative and semi-quantitative analytical information by using a biological recognition element which is in direct spatial contact with a transduction element[7]. Electrochemical sensors carry certain advantages which include their cost effectiveness, applicability to a vast range of chemicals, ease of use and functionalization, robust nature, high sensitivity and selectivity.

Most part of the activity of the electro-analysis starts from a more restricted view of Electroanalytical Chemistry, which is in most cases identified with Electrochemical Sensing.

Electrochemical Sensing is linked to:

- Fabrication and physico-chemical characterization of novel materials or molecules acting as the sensitive elements of the sensors;
- Use of some benchmark species to test the effectiveness of the developed system and of the relevant analytical procedure;
- Finalization of the newly synthesized or already established sensing devices to detect specific substances in specific matrices, developing suitable procedures to achieve best values for “performance indicators”.

As to the first identified issue, the extraordinary upsurge of material science has induced electroanalysts to exploit a number of novels, conductive materials either as the sensitive elements of sensors or as a part of composites bearing molecules or functionalities suitable to more or less specifically interact with certain analytes. A minor portion of new materials, actually not necessarily conductive, have been exploited in potentiometry, to prepare effective selective electrodes.

Novel materials have been least frequently used as such; they most often need to be supported on a conductive conventional substrate, such as Pt, Au or glassy carbon, leading to the so-called (chemically)modified electrodes. The role of the modification is essentially that of pursuing electrocatalytic effects and of possibly preventing adsorption of species present in solution that poison the electrode surface. In particular, electrocatalysis may anticipate the potential at which

some analytes are electroactive, favoring higher resolution or even allowing detection of species otherwise “hidden” by the solvent discharge[8]. Discussing the approaches followed in order to induce electrocatalysis and prevent electrode fouling, we can work out a concise examination of the most often preferred amperometric system. In [9] 3D-ensembles of gold nanowires were fabricated by electroless Au deposition in polycarbonate membranes by partial membrane etching. These electrode systems, characterized by a particularly high signal-to-noise (Faradic-to-capacitive currents) ratio are applied to the anodic stripping voltammetric determination of inorganic arsenic, which constitutes an analyte of particular interest. For many reasons, among which the fact that excellent repeatability of the responses is not mandatory, and that the cost is very low, outstanding interest has been recently acknowledged to disposable systems consisting of Screen-Printed Electrodes (SPEs). A simple carbon black dispersion on a SPE is effectively used for determination of a number of phenolic compounds [10]. The effectiveness of composites is coupled to the advantages of SPEs in a sensing system in which Au-NPs are anchored to carbon black microparticles[11].

1.2. Brief history of Biosensors

The history of biosensors started with the development of enzyme electrodes by the Professor Leland C Clark Jnr. In 1962, Clark published his paper on the oxygen electrode [12]. The concept was illustrated by an experiment in which glucose oxidase was entrapped at a Clark oxygen electrode using dialysis membrane. A few years later, in 1975 Clark's biosensor became commercial with the successful launch of the Yellow Springs Instrument Company (Ohio) glucose analyzer based on the amperometric detection of hydrogen peroxide.

In 1969 the potentiometric urea electrode was introduced by George Guilbault and Joseph Moltavo using immobilized urease and a pH-sensitive sensor[13]. Then, in 1973 Ph. Racinee and W. Mindt developed the first lactate electrode [14]. In 1976, Clemens and co-workers incorporated an electrochemical glucose biosensor in an artificial pancreas, and a few years later this biosensor was marketed by Miles Laboratories [15,16]. Finally, Karl Cammann introduced the term “biosensor” in 1977 [17], but it was not until 1997 when IUPAC introduced for the first time the definition for biosensors in analogy to the definition of chemosensors [18]. According to the classical IUPAC definition, a biosensor is an analytical device which is capable of providing specific quantitative or semi quantitative analytical information using a biological recognition element (biochemical receptor) which is in direct

spatial contact with a transducer element[7].

Nowadays, the work on biosensors and papers published continues to make progress using different biological elements in combination with various types of transducers. In commercial term, biosensors are quickly acquiring popularity in the global market due to their wide variety of applications in the fields of medical diagnostics, pharmaceuticals, biodefense, food industry and industrial processes. The greatest application for biosensors continues to be blood glucose devices. However, the market is changing towards other applications such as infectious disease screening, cholesterol testing, blood gas analyses, pregnancy testing and applications in industrial biology, food toxicity detection and military field [19].The term biosensors means that the device is a combination of three parts: (i) a biorecognition element or bioreceptor, (ii) a sensor element also called transducer and (iii) a signal processing system. The basic concepts of a biosensor operation can be illustrated in Figure 1.2. A bioreceptor generally consists of an immobilized biocomponent that is able to detect the specific target analyte. On the other hand, the transducer is a converter. The reaction between the analyte and the bioreceptor causes a chemical change, and this change is converted into an electrical signal by the transducer. Finally, the electrical signal is amplified and sent to microelectronics and data processor.

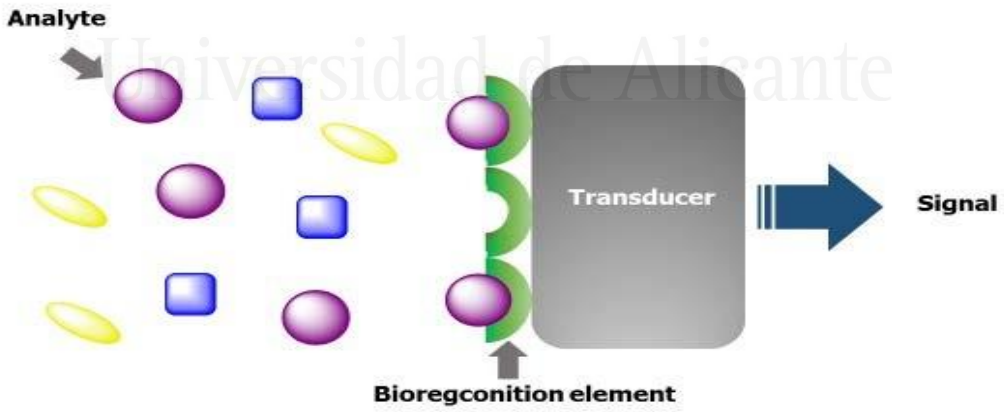

Figure 1.2. Schematic representation of a biosensor.

Biosensors can be classified into four different basic groups on the basis of signal transduction: electrochemical, optical, mass sensitive and thermal sensors. Additionally, can be classified depending on the bioreceptor as: immunochemical, enzymatic, non-enzymatic receptor, whole-cell, nucleic acid biosensors and biomimetic sensors.

1.2.1. Types of bioreceptors in biosensors

As indicated biosensors can be classified depending on the type of bioreceptor used. Generally, they can be divided into six major groups: enzyme-based sensors, protein-based sensors, nucleic acid-based sensors (called genosensors), cell-based sensors, immune (or antibody) sensors and biomimetic sensors, see Figure 1.3.

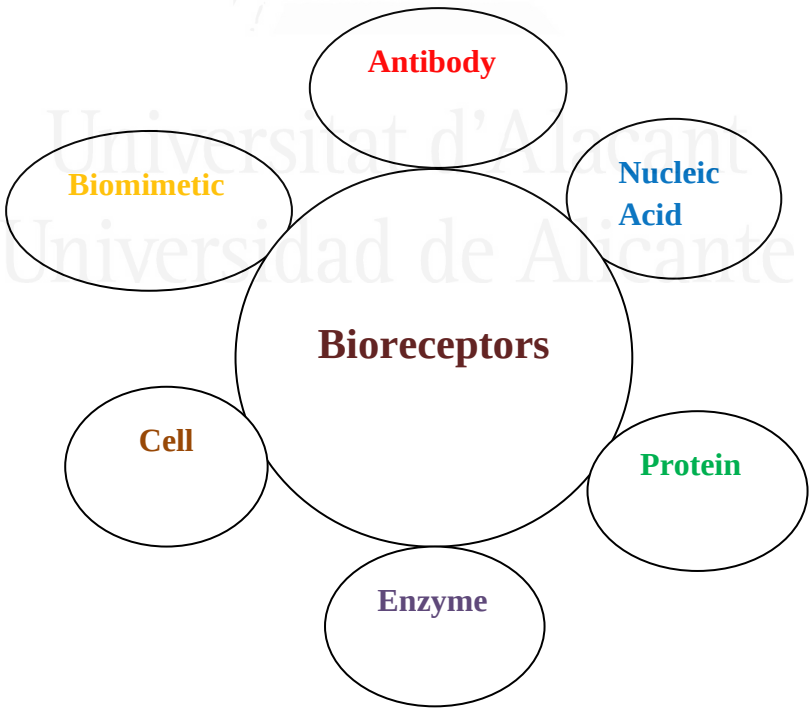

Figure 1.3. Classification of bioreceptors used in biosensors.

1.2.1.1. Antibody-based biosensors

Immunosensors are based on the principles of solid-phase immunoassays, where the immune reagent, either the antibody (Ab) or the antigen (Ag), is immobilized on a solid support, so that the interaction takes place on the solid–liquid interface. Apart from the sensitivity and selectivity, additional benefits derive from the possibility of conveniently tailoring their affinity and selectivity with new binding properties [20]. Rahman, et al achieved label-free detection of BPA (bisphenol A) with an impedimetric immunosensor[21].

In this example, the immunosensor was fabricated by the covalent bond formation between a polyclonal antibody and a carboxylic acid group functionalized onto a nanoparticle comprised conducting polymer. By using a commercial reagent4,4-bis(4-hydroxyphenyl) valeric acid (BHPVA), they have prepared the antigen through the conjugation of BHPVA with bovine serum albumin (BSA) and then produced a specific polyclonal antibody. The immobilization of antibody and the interaction between antibody and antigen were studied using quartz crystal microbalance (QCM) and electrochemical impedance spectroscopic (EIS) techniques. The immunosensor showed specific recognition of BPA with less interference than 4.5% from other common phenolic compounds. The linear dynamic range of BPA detection was between 1 and 100 ng/mL. The detection limit of bisphenol A was determined to be 0.30± 0.07 ng/mL.

1.2.1.2. Biomimetic biosensors

Molecularly imprinted polymer (MIP)-based sensors mimic the biological activity of antibodies, receptor molecules, etc [22]. MIPs combine highly selective molecular recognition, comparable to biological systems, with typical properties of polymers such as high thermal, chemical and stress tolerance, and an extremely long shelf life without any need for special storage conditions. MIP optical sensors have been developed for detection of pesticides[23] and for polycyclic aromatic hydrocarbons [24]. Systems still under development are thin MIP membranes on an electrode or optode. The selective transport through the polymeric barriers has to be considered.

1.2.1.3. Protein receptor-based biosensors

Non-catalytic proteins of non-immune origin constitute the recognition element in the so-called protein receptor-based biosensors. These proteins, which span cell membranes, allow the binding signal to be transduced through the membrane by producing the activation of an enzyme (metabotropic receptors) or by opening an ion channel of the membrane (Ionotropic receptors). New biorecognition molecules provided by genetic engineering constitute a step further in the development of these biosensors Hock et al [25]. In contrast to simple chemical information, by using living intact microorganisms rather than isolated biological components, it is possible to obtain functional information (i.e. information about the effect of a stimulus on a living system) to determine if a substance is toxic to cells.

1.2.1.4. Whole cell-based biosensors

In addition, microorganisms themselves can be used specifically for sensing the bioavailability of a particular pollutant, are usually more tolerant to assay conditions than enzymes or protein and can be prepared in almost unlimited quantities. The diffusion of substrate and products through the cell wall also results in a slow response relative to enzyme-based sensors. Whole cell biosensors can monitor the metabolism of cells by the measurement of pH, O_2 consumption, CO_2 production, redox potential, and electric potential on nervous system cells or bioluminescence in bacteria. In some bioluminescence bacteria, for example, the increase in light is induced by the presence of a certain contaminant. Genetically engineered microorganism-based biosensors have also been developed for the monitoring of specific contamination. In these ones, genes that code for luciferase are placed under the control of a promoter that recognizes the analyte of interest[26]. In the presence of organic pollutants, the genetic control mechanism turns on the synthesis of luciferase, which produces a measurable light emission. Recently, methods that use mammalian cells have been investigated, since they can better resemble the toxicity observed in people. Nerve cells growing on array structures, for example, have been implemented in the development of chips and sensors[27].Tissue-based biosensors such as potato slices for the determination of mono and polyphenols, and cultured human hepatoblastome Hep G_2 cells for the on-site evaluation of environmental waters[28] are of current interest.

1.2.1.5. DNA-based biosensors

Two main strategies have been developed in the area of DNA biosensors. One is the hybridization of nucleic acid sequences from infectious microorganisms detection in which a single stranded DNA molecule immobilized in a sensor is able to seek out or hybridize to its complementary strand in a sample. However, for the monitoring of endocrine disruptors a second type of DNA biosensors is applied. In this approach, biosensors monitor the interaction of small pollutants with affinities for DNA with the immobilized DNA layer. These biosensors may therefore be used as a general indicator of pollution, integrated in a panel of tests, since they can give rapid and easy to evaluate information on the presence of such compounds.

1.2.1.6. Enzyme-based biosensors

The catalytic biosensors rely on the enzyme-catalyzed conversion of anon-detectable substrate into an optically or electrochemically detectable product or vice versa. In general, enzymatic biosensors are based on the selective inhibition of specific enzymes by different classes of compounds. Several enzyme-catalyzed reactions involve the production or consumption of a detectable product or low molecular weight species, such as O_2, CO_2, and ions. A common way of measuring these species is through the use of suitable transducers, usually electrochemical, coupled to the immobilized enzyme. The most important enzymes from an analytical point of view are the oxidoreductases and hydrolases. The use of acetylcholinesterases (AChEs) in biosensor technology has gained enormous attention, in particular with respect to insecticide detection [29].

1.2.2. Types of transducers in biosensors

Among all types, electrochemical biosensors are especially attractive because of the remarkable high sensitivity, low cost, fast-response and experimental simplicity. Moreover, they are the most frequently used in commercialized biosensors, for instance for blood glucose testing. The small size of electrodes and the possibility to miniaturization permit the construction of hand devices or/and in field devices. Transducers generally can be classified into four major groups: optical, piezoelectric, calorimetric and electrochemical, see figure 1.4.

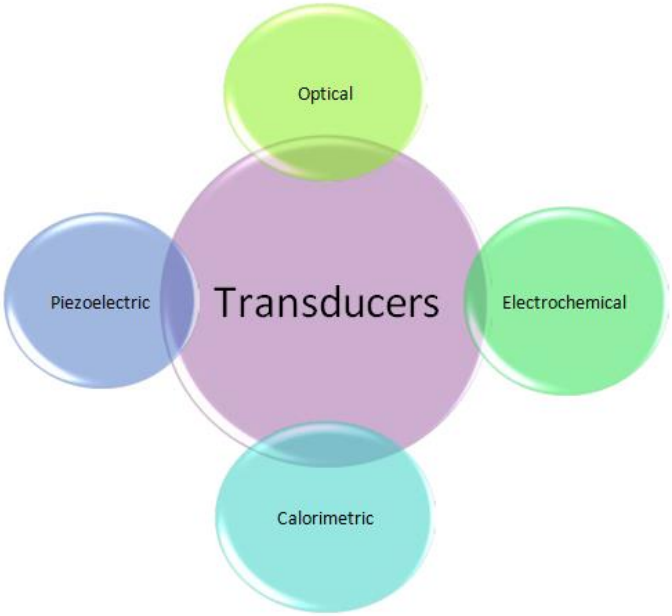

Figure 1.4. Classification of transducers used in biosensors.

1.2.2.1. Optical biosensors

Optical biosensors are the most common, after amperometric and potentiometric biosensors. The various types of optical transducers exploit properties such as simple light absorption, fluorescence/phosphorescence, bio/chemiluminescence, reflectance, Raman scattering and refractive index. Apart from speed, sensitivity and robustness, other attractive features of optical sensors include their suitability to component miniaturization, remote sensing and their multi-analyte sensing capabilities. In addition, the increasing market of telecommunications has supported development in new optical materials research. Examples of optical techniques usually utilized in biosensors are fiber optic, optical waveguide structures and surface Plasmon resonance (SPR).

1.2.2.2. Mass-sensitive biosensors

Within mass-sensitive biosensors, acoustic wave biosensors operate on the basis of an oscillating crystal that resonates at a fundamental frequency. The crystal element is coated with a layer containing the biorecognition element designed to interact selectively with the target analyte. A measurable change in the resonance frequency occurs after the binding of the analyte on the sensing surface according to the mass change of the crystal. Most of these biosensors

utilize piezoelectric materials as signal transducers[30]. An emerging group of mass-sensitive biosensors are the so-called cantilever biosensors, which are based on the bending of microfabricated silicon cantilevers[30,31]. The mass change, originating from the adsorption of target molecules on the microcantilever surface (where receptor molecules are immobilized), causes a differential surface stress change, and therefore a bending or deflection of the cantilever [31]. The deflection of a few nanometers can be detected by electric or optical methods. Micro cantilever biosensors offer various advantages due to their microscopic dimensions (in the range of 10^{-3} mm^2): only small quantities of receptor and analyte are necessary and limits of detection achieved are often lower than those obtained by classical methods[32]. The feasibility of mass production, real-time monitoring and operation in air, vacuum or liquid environments, are other advantages of these biosensors[33].

1.2.2.3. Thermometric biosensors

Thermometric biosensors, finally, exploit the absorption or evolution of heat in biological reactions. This is reflected as a change in the temperature within their action medium and is transduced by a change in the resistance of a thermistor, which acts as a temperature transducer. As reviewed by Ramanathan and Danielsson [34], thermistor-based calorimetric biosensors have mainly been applied to clinical and industrial process monitoring. Up to now, only several pesticides have been measured by thermometric biosensors.

1.2.2.4. Electrochemical biosensors

Based on the developing label-free electrochemical biosensors, there are various methods that can be used in electrochemistry. Many electroanalytical techniques have inherent advantages with variable purposes, and therefore may be utilized in a multitude of different fields of study, encompassing enzyme catalysis [35], free radical generation [36], solar energy conversion [37] and myriad of others. The main advantages of using voltammetric methods over optical spectroscopy or chromatography include their high sensitivity, precision, accuracy and cost effectiveness.

Concurrent with the greater knowledge of electrochemistry and a better understanding of electrode synthesis and modification, sensors will improve considerably in terms of both

sensitivity and detection limits. Micro- and nano-sensors will likely constitute the next disruptive paradigm in the field of sensing and biosensing.

Types of electrochemical sensors

Electrochemical sensors can be divided into three types based on their nature and working principle, i.e. potentiometric, conductimetric and amperometric/voltammetric sensors. Here we briefly discuss all types but will focus more on amperometric sensors.

Potentiometric sensors

As the name suggests, potentiometric sensors measure the potential difference between a sample solution and a reference solution with the help of a reference electrode and an indicator electrode. The two solutions are separated by a membrane *m* which contains an ionophore that is selective to target ion. The Nernst equation provides the relationship between potential difference and target ion activity.

$$E = E_0 + \frac{RT}{zF} \ln \frac{a^s}{a^m} \qquad \textbf{Eq. 1}$$

Where E_0 is the standard potential of sensor electrode, F is Faraday's constant, T is absolute temperature, R is universal gas constant, s is sample, *z* is valency of ion and *a* is the target ion activity[38]. Potentiometric sensors have been widely used since 1930's due to their simplicity and ease of use. There are three main types of potentiometric devices used which include ion-selective electrodes (ISE), coated wire electrodes (CWES) and field effect transistors (FETS)[39].

The ion-selective electrode measures the activity of particular ionic species in the surrounding solution. The principle of ISE devices is based on permselective, ion conducting membrane which separates the electrode from outside solution. The composition of membrane is very important for producing the ISE for particular ionic species. In working principle of ISE, the reference electrode potential is kept constant while the potential of working electrode is determined by the surrounding environment. The change in working electrode potential or potential difference is considered as the concentration of the target ion[40]. pH electrode is the best and most widely used example of potentiometric sensor, the success of this electrode lays

in its robust nature, easy handling, reproducibility, wide range of application and cost effectiveness [39]. Bakker and Pretsch discussed in detail the breakthrough developments in nanoscale potentiometry, limit of detection and sensor stability[41].

Conductimetric sensors

Conductimetric sensors are based on the principle of providing sensor and information as a result of changes in the electrical conductivity of material (used in the construction of the sensing device) which is in contact with the analyte. Conductimetric sensors are basically non-selective, but as a result of more precise miniaturization and surface modification, selectivity can be improved. Conductimetric sensors do not require reference electrode for functioning and hence reduce the cost as well as make these sensors simpler for use. Reports for different kind of thin films modifications are available in literature mainly for the detection of gases. Examples of these thin film modified conductimetric sensors include, Copper doped oxides are used for the detection of H_2S [42]. CH_4 detection done by using Ga_2O_3 semiconductor films[43], modification by conductive polymers such as polypyrrole for volatile amine detection[44], CdS films modification for the detection of oxygen [45] and modification by $MnWO_4$ films to be used as humidity sensors [46].

Amperometric sensors

In amperometric sensing, the current is measured as a result of an electron transfer reaction in a working electrode while its potential is controlled with a potentiostat. The potential can be kept constant (potentiostatic detection) or it can be scanned between two values (potentiodynamic detection). The principle is based on the electron transfer between the analyte and working electrode. The basic instrumentation for amperometric sensing includes a potentiostat and three electrodes (working, reference and counter) dipped in a suitable electrolyte to form an electrochemical cell. The auxiliary or counter electrode is made up of an inert conducting material such as graphite, platinum, stainless steel, etc. In amperometric sensing the electron transfer reaction takes place at the surface of working electrode. The reference electrode provides a reference potential to working and counter electrode[39]. A typical amperometric sensing system and its principle is shown in Figure 1.5.

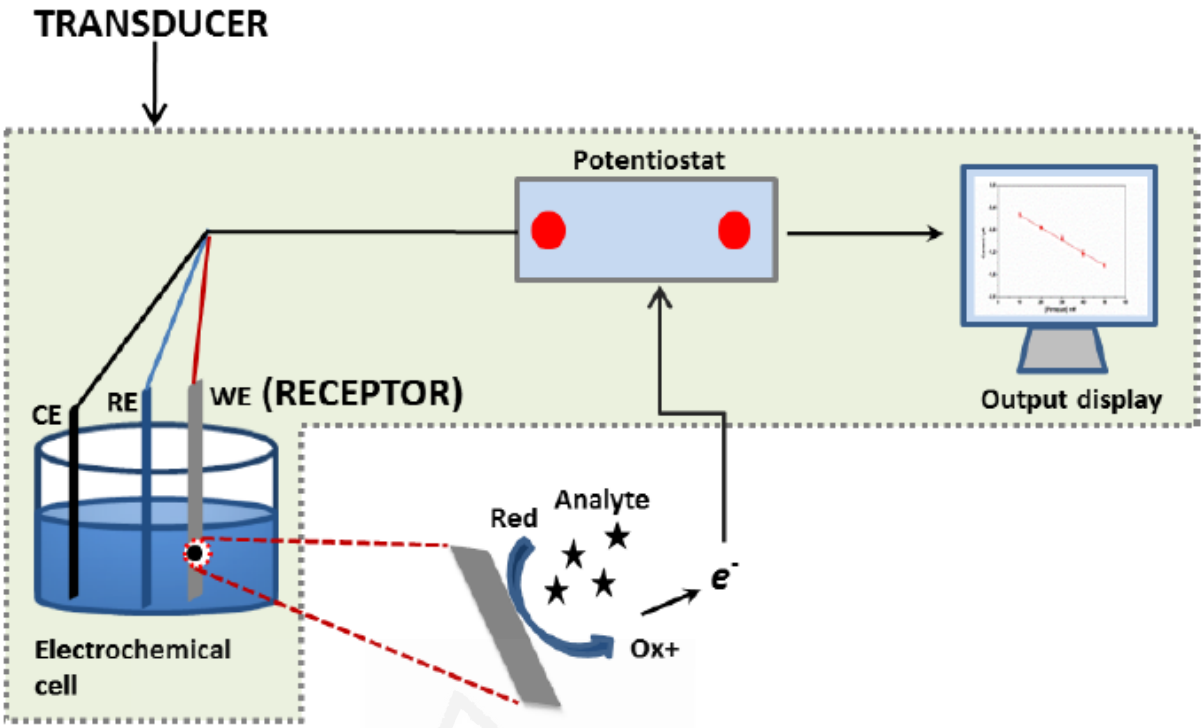

Figure 1.5. Schematic representation of a typical amperometric sensing system.

1.2.3. Electrode modification for biosensors: Immobilization strategies

Many immobilization strategies have been reported. Main protocols can be envisioned: adsorption, covalence, entrapment, cross-linking or affinity. In many cases, the immobilization methods are based on combination of several immobilization methods. For these five basic methods, a comparison is presented as following.

According to binding nature, adsorption involves weak bonds; covalent coupling is chemical binding between functional groups of biomolecules and those on the support; entrapment is incorporation of biomolecules within a gel or a polymer; cross-linking is bond between biomolecules, cross linker and insert molecule; affinity is bonds between a functional group on the support and affinity tag on a protein sequence.

The advantages of each method are: adsorption is simple, easy and there is limited loss of biomolecules activity; covalent coupling is no diffusion barrier method, more stable and short response time are obtained; entrapment presents no chemical reaction between the monomer and the biomolecules that could affect the activity and several types of biomolecules can be

immobilized within the same polymer; cross-linking is simple; affinity presents a controlled and oriented immobilization.

For the drawbacks, for each method are: in adsorption there are desorption and non-specific adsorption; covalent coupling leads to not regenerable matrix, coupling involving toxic product leads to high biomolecules activity loss; entrapment leads to diffusion barrier biomolecules leakage and high concentrations of monomer and biomolecules; cross-linking leads to high biomolecules activity loss; affinity needs the presence of specific groups on biomolecules.

The immobilization protocols appear as a key factor to develop efficient biosensors with appropriate performances such as good operational and storage stability, high sensitivity, high selectivity, short response time and high reproducibility.

Immobilized biomolecules have to maintain their structure, their function, to retain their biological activity after immobilization, to remain tightly bound to the surface and not to be desorbed during the use of the biosensor. Moreover, an ideal biosensor has to be stable for long-term application. The type of immobilization method affects activity and stability of biosensors. Factors such as accuracy of measurements, the sensor-to-sensor reproducibility and operational lifetimes are drastically influenced by biomolecules stability. Since the analytical performances of a biosensor are strongly affected by the immobilization process, intensive efforts have been done to develop successful immobilization strategies in order to assure greater sensitivity and stability of biosensors. The choice of the most appropriate and judicious technique also depends on the biomolecules nature, the transducer and the associated detection mode. The best method of biomolecules immobilization varies if the biosensor application requires maximum sensitivity or rather focuses on stability. Reproducibility, cost and difficulty of the immobilization process also need to be considered.

1.3. Chemical synthesis of silica

Introduction

Porous silica materials made by low-temperature sol-gel process are promising host matrixes for encapsulation of biomolecules. To date, researchers have focused on sol-gel routes using alkoxides such as tetramethylorthosilicate (TMOS) and tetraethylorthosilicate (TEOS) for encapsulation of biomolecules. These routes lead to formation of alcohol as a by-product that can have a detrimental effect on the activity of entrapped biomolecules. Synthesis of silica nanoparticles have drawn great interest of research owing to their potential application in industries (electronic devices, insulators, catalysis, etc.) and pharmaceuticals (enzyme encapsulation, drug delivery and cell markers) [47,48]. Sol–gel process has become an attractive research area, in which extensive studies have been made on the synthesis of silica nanoparticles [49–51].

The encapsulation of enzymes and other proteins into inorganic host materials using sol-gel processing has attracted considerable attention over the past few years [52,53]. This research has demonstrated that the biomolecules immobilized in the sol-gel derived matrix retain their functional characteristics to a large extent. These new composite materials are of interest for their applications as optically based biosensors. The porosity of sol-gel glasses allows small analyte molecules to diffuse into the matrix while the large protein macromolecules remain physically trapped in the pores. The transparency of the matrix enables one to use optical spectroscopy methods to characterize the reactions that occur in the pores of the glass. Sol-gel materials are ideal candidates as hosts for biomolecules dopants because they are synthesized at low temperatures under fairly mild reaction conditions [54]. The variation of synthesis conditions has enabled researchers to tailor the sol-gel chemistry so that the encapsulation of a variety of proteins, enzymes and other biological molecules has been reported. Among the various biomolecular dopants studied to date are alkaline phosphatase, glucose oxidase, cytochrome c, trypsin, urease, Cu-Zn superoxide dismutase as well as yeast cells [8, 9]. Electrochemistry has been introduced as a powerful tool in order to prepare new organometallic reagents for functionalizing of mesoporous silica. Preparation of the reagents was based on electrochemical oxidation of dihydroxybenzene derivatives in the presence of 3-(trimethoxysilyl)-1-propanethiol as a nucleophile [55].

1.3.1. The chemistry of the sol-gel process

In this thesis a study of the modification of electrodes by means of thin films of silica is carried out by means of the sol-gel method. Sol–gel chemistry offers a flexible approach to obtaining a diverse range of materials. It allows differing chemistries to be achieved as well as offering the ability to produce a wide range of nano-/ micro-structures [56]. Silica exists under a wide variety of forms, with crystalline and amorphous structure. It is a material that has been examined exhaustively [47], both its physical and chemical properties are well known [54], which gives it an extraordinary number of applications, such as its use in chromatography, thermal insulation, catalysis and as support for catalysts, it is used in the reinforcement of polymers and as a support to immobilize enzymes, among others.

Silica can be found naturally or prepared by synthetic procedures. There are three ways of silica synthesis using silicon compounds as a precursor [57]. By pyrolytic, by the thermal decomposition of silicon halides in the gas phase, usually between 1000 and 1100 ºC in a hydrogen and air flame. The resulting product is a silica aerogel. An alternative to this method is the fusion of sand in plasma from soluble silicates, mainly Na_2SiO_3. The third synthesis method consists of the hydrolysis of alkoxysilanes in a hydroalcoholic medium, which leads to the formation of silica after two reactions, one of hydrolysis and the other of condensation. This method is that we will use throughout this thesis for the preparation of silica, so it will be described in detail below.

Sol-gel method

The sol-gel method consists on the production of glass or ceramic materials, through the hydrolysis and condensation of suitable metal alkoxides [54]. For the preparation of silica materials, one of the most used alkoxides as a precursor is tetraethoxysilane (TEOS). This precursor can be hydrolyzed and condensed under relatively mild conditions, as indicated below.

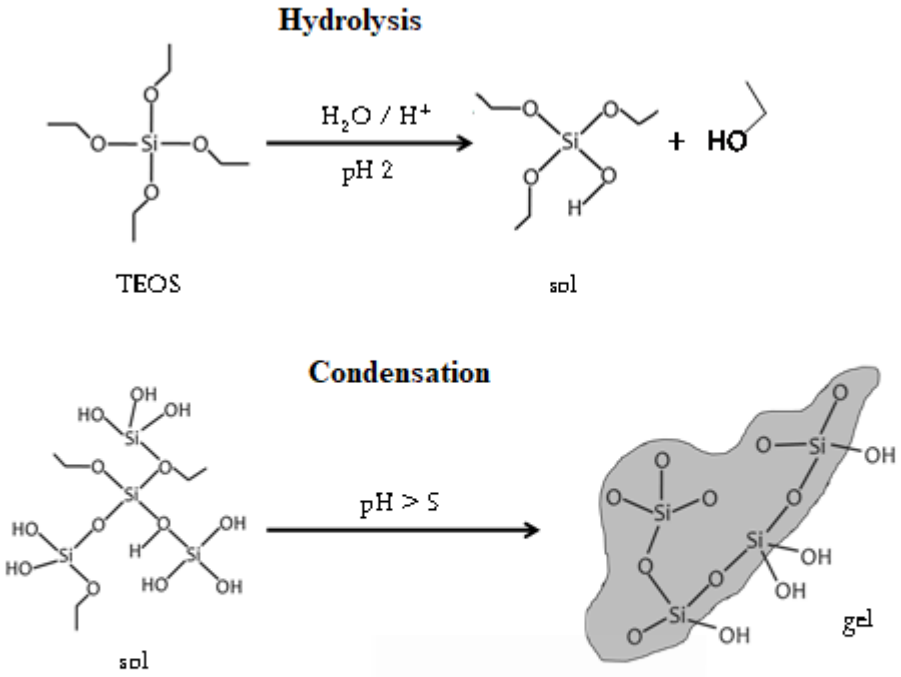

Figure 1.6. Steps of Sol-gel method for silica gel synthesis.

The hydrolysis step at acidic pH, figure 1.6, leads to a Meta stable colloidal solution (figure 1.7) at pH 2 known as sol. The second step, shown in figure 1.6, consists of the condensation by increasing the pH of the sol, thus obtaining the gel, by colloid aggregation.

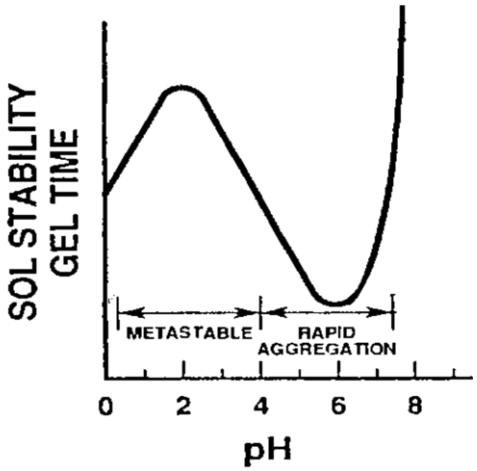

Figure 1.7. Effect of pH on the sol-gel colloidal system. [54].

A general flow chart for sol-gel process which leads to the production silica using silicon alkoxides ($Si(OR)_4$) is shown in (Figure 1.8). The general reactions of TEOS that leads to the formation of silica particles in the sol-gel process can be written as [48–50,54,58,59]:

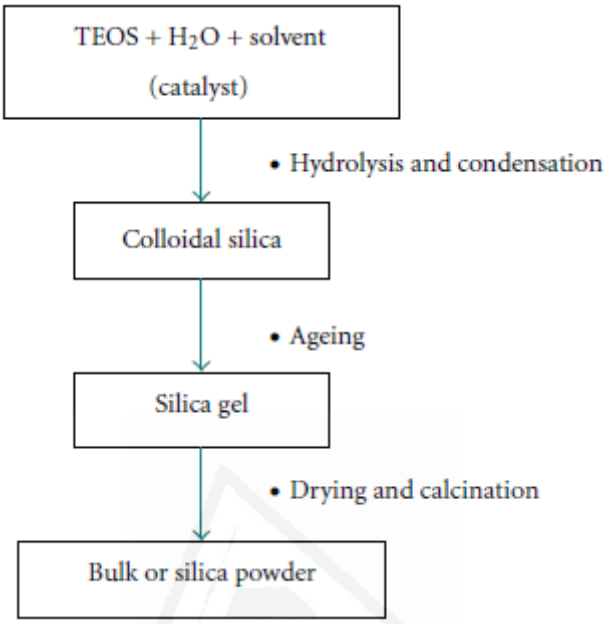

Figure 1.8. Flow chart of typical sol gel process.

In the hydrolysis step, the precursor, in this case TEOS, is mixed with water and ethanol, the latter acts as a co-solvent, and an acid catalyst, such as for example hydrochloric acid. During the formation of gel, the viscosity of the solution gradually increases as the sol, formed by a colloidal suspension of small particles (1-100 nm), interconnects with each other by poly-condensation reactions to form a rigid, porous network [54]. Depending on the conditions of the sol-gel process (Si: H_2O: EtOH ratio, type and concentration of catalyst, alkoxide precursors, etc.), gel formation can take place in seconds, minutes, even days or months. In addition, during drying, alcohol and water evaporate from the pores causing the gel to shrink, for that reason, xerogels, or totally dry gels, are significantly less porous than their hydrated counterparts. The formation of silica particles can be divided into two stages: nucleation and growth. Two models, monomer addition [49,50] and controlled aggregation [59,60], have been proposed to describe the growth mechanism of silica. The monomer addition model describes that, after an initial burst of nucleation, the particle growth occurs through the addition of hydrolyzed monomers, the (primary) particle surface. By contrast, the aggregation model elaborates that the nucleation occurs continuously throughout the reaction and the resulting

nuclei (primary particles) will aggregate together to form dimer, trimer, and larger particles (secondary particles). Both models lead to the formation of either spherical or gel network depending on the reaction conditions as shown in Figure 1.9 [60].

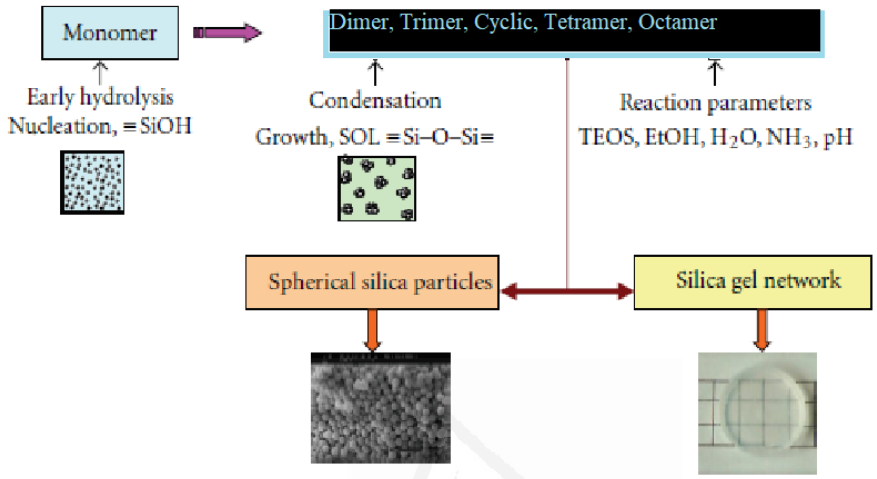

Figure 1.9. Silica formation by sol gel process[60].

The silica materials are chemically and photochemically stable. They are also optically transparent. As shown in (Figure 1.10A) [61], materials in various configurations can easily be obtained: films, fibers, monoliths, powders, etc. In addition, functional groups can be incorporated into the silica matrix, obtaining stable gels and modulating their properties in a simple manner. When the groups incorporated in the silica are organic in nature (Figure 1.10B), organically modified silica is obtained, and these compounds are known as ORMOSIL; ORganicallyMOdifiedSILica.

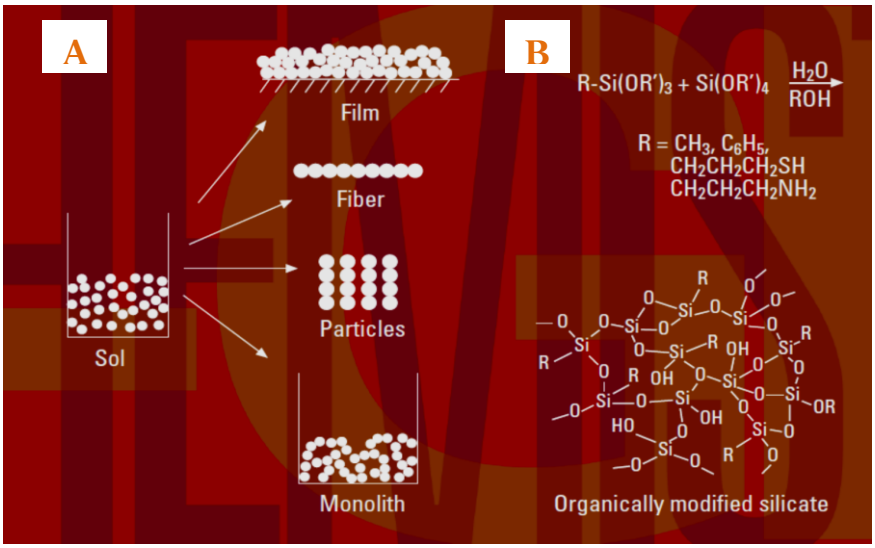

Figure 1.10. (A) Different forms of silica preparation. (B) Diagram of modification of silica with organic groups (ORMOSIL) [61].

In the mid-1980s, it was shown that there were molecules that could be trapped in the porous matrix, simply by doping the sol solution with these molecules, before their condensation (gelation) [62]. It was shown that the molecules retained by the gel retained the same properties as they were in dissolution [63]; that is when the application of sol-gel chemistry, in applications such as sensors, catalysis and electrochemical devices, shot up [52,63–69]. The sol-gel-based materials used in electrochemistry form a large family. They include inorganic inert materials, metal oxides with redox activity, organic-inorganic hybrids, and macro and microscopic compounds. Recent advances in the various fields and applications of sol-gel electrochemistry are described in two excellent review articles, respectively, by Lev et al [70], and by Alber and Cox [71]. Silica nanoparticles are widely applied as fillers in silica-polymer nanocomposites. The most commonly used route for synthesizing silica nanoparticles is sol-gel method due to its ability to produce monodispersed with narrow-size distribution nanoparticles at mild conditions [72].

1.3.2. Electrodes modified with silica

The field of silicon-modified electrodes began in the years 1989-1990 and has been increasing in recent years. Despite the extraordinary chemical characteristics offered by silica-based

materials, it is quite surprising that the electrochemical use of this material is so recent. Silica has many attractive properties (adsorption capacity, acid / base properties, thermal stability), which can be used in many applications. Furthermore, as mentioned above, silica can be modified with a wide variety of functional groups, which leads to considerable enrichment and control of its surface properties. For example, these properties have been exploited to a large extent in chromatography, designing new stationary phases. Also, the high surface area combined with the surface chemical properties makes silica an excellent material to be used as catalyst support. Despite all these attractive properties, the use of silica in electrochemical methods was not generalized. The silica gels prepared by the sol-gel chemistry are interesting materials for the modification of electrodes, and since they are not electroactive, they can be used as support for electroactive species, either by adsorption or entrapment during its formation, thus improving its amperometric detection [73–78]. But in the mid-90s, silica was used as support for enzymes without impeding their biological activity and also improving the coupling of the redox activity of the immobilized enzyme and the surface of the modified electrode [53,64]. In particular, the advances focused on the encapsulation of enzymes in silica materials synthesized at room temperature applying the sol-gel process.The use of silica as an electrode modified has demonstrated great versatility in the immobilization of different species, such as oxide films or other electroactive species. Much work in this direction has been done by Walcarius, Kubota, Gushiken and collaborators [79–84].

In summary, the most attractive properties of silica materials are that they have great capacity to accumulate various analytes by adsorption, silica can be modified with organic groups in a simple way and these modifications involve the development of a wide range of new materials. In addition, these materials serve as support for the immobilization of enzymes in the manufacture of biosensors. But the fundamental reason for the use of sol-gel materials in electrochemistry is the existence of multiple ways to combine the properties of inorganic materials with a wide variety of organic compounds through ORMOSIL.

1.3.3. Organically Modified Silica

They are composite materials or hybrid materials at the atomic scale that are easily produced by the sol-gel method, simply by the addition of molecular precursors that are capable of undergoing the same hydrolysis and condensation reactions as the metal alkoxide. In the sol-gel world, these materials are known by the term organosilica. Organosilica describes any siliceous material in which the silicon atoms (some or all) are covalently bound to at least one

carbon atom; for clarification, the term silica will be used to refer to materials that do not contain Si-C bonds at all and ORMOSIL will be used for organically modified silica-derived materials and which at least contains a Si-C bond. As seen above, a sol-gel silicate is formed in accordance with a polymerization reaction between alkoxysilanes and water (hydrolysis), followed by condensation. As can be seen in Figure 1.11, using precursors containing organic (R) functional groups directly attached to the Si atom of the sol-gel precursor, it is possible to prepare a wide variety of inorganic-organic hybrid materials [63] by varying the terminal group. ORMOSIL [85] has become an attractive field of study due to the variability and flexibility associated with its preparation method. They offer the possibility of being used in different areas: catalysis, protective coatings and ion exchange, separation techniques (chromatography), molecular printing, chemical sensors, among many other applications [86].

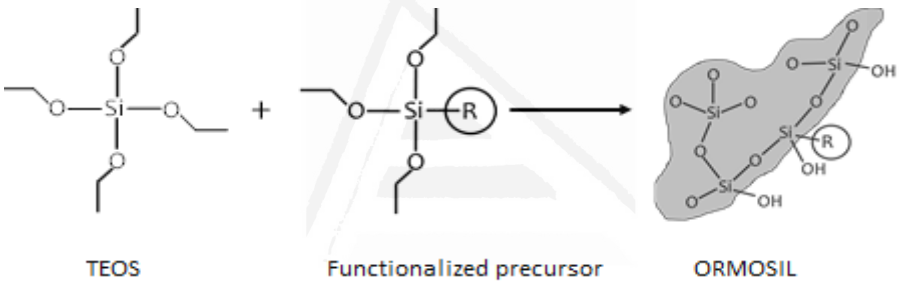

Figure 1.11. Reaction to obtain Organic Modified Silica (ORMOSIL).

Its use in chemical sensors offers a high versatility. With these hybrid materials it is easy to modify the sensor layers, for example, the pore size of the material, hydrophobicity, and flexibility can be altered or a specific functional group introduced into the matrix to improve sensor performance, including more specific and / or selective molecular recognition zones, improve the response time, the leaching rate, etc. [87]. One of the common problems encountered when modifying an electrode is that the reagent trapped in the sensor layer tends to leak, to leach to the solution. Using inorganic-organic hybrid materials has shown that these problems of unwanted diffusion have been solved [88,89].

With the inclusion of organic groups in the silica matrix the hydrophobicity of the material is also modulated, it is also a benefit for some applications, for example, an increase in the

hydrophobicity of the film can reduce the solubility of certain species in the matrix causing an increase in sensor performance [87].

On the other hand, by increasing the flexibility of the matrix, more coherent layers are achieved, avoiding cracks in the films [90]. These materials have also been used in the design of waveguide sensors for the detection of gases [91] and vapors [92].

1.3.4. Molecularly Imprinted Silica

Molecular recognition [93] is one of the basic processes found in nature. The preferred binding of a molecule to a receptor with high selectivity towards other structural analogue receptors can be designed. The earliest approaches are from the 1930s in the synthetic preparation of nanostructured materials for molecular recognition and thus explain the functioning of the human immune system, were inspired by the contributions of Mudd [94] and Pauling [95], in the decade of 1940. His basic assumptions were that in living systems, antibodies are constructed by the use of molecules such as finger prints or templates. The primary structure of any antibody would be the same, but the selectivity, that is, the difference in the conformation of the antibody would be induced by a template molecule. When the template molecule is removed, there remains a cavity with morphological and stereochemical characteristics related to those of the template and is maintained to give the antibody a preference to re-link the molecule. The description was very similar to the "key-lock" model, used to explain the action of enzymes in biochemical reactions. One of the great advantages of the sol-gel method is the facility to produce thin films of high quality. The advantage is obvious, since they are thin films, they have shorter diffusion lengths, which means that the binding kinetics of the molecule of interest and printed sites will be faster, improving the efficiency of the sensor.

1.3.5. Electro-assisted silica deposition

The two most common configurations in which we can find sol-gel materials are: monoliths and thin films. The monoliths are prepared by pouring the sol solution into a container, for example, in a cuvette; and let it gel slowly [96].These materials are electrical insulators, therefore, for their application in electrochemistry they require that the connection with the electrode surface be narrow. To integrate sol-gel matrices into the electrode surfaces, different

spin-coating [97,98]; dip-coating [99,100]; and spray coating, spraying [101,102] strategies are used. These methods are simple to apply, do not require the use of sophisticated instrumentation, and allow to control the thickness of deposited films. Normally, these techniques achieve thicknesses ranging from 100 nm to a few mm. However, they present some drawbacks, for example, the techniques of spin-coating and dip-coating can only be applied to flat surfaces, this would be solved by applying the spraying technique, which in general provides homogeneous coatings, but much thicker. The second limitation that these techniques have is the lack of selectivity, that is, the entire surface would be covered, so if what we want is to cover only some parts of the surface of the electrode we would have to make the coating in several stages by lithography, first coat with a layer that would later be removed and then cover the surface with the sol-gel film [103].

In 1999, Shacham and collaborators proposed an alternative [104] to help solve the afore mentioned drawbacks. The basic idea is to manipulate the two steps of the sol-gel method [54], controlling the pH electrochemically at the electrode / dissolution interface [105]. The hydrolyzed solution, the sol, is at a pH close to 2, at this pH value the condensation occurs very slowly. It is possible to accelerate the polycondensation by applying a negative potential in the electrode, for electrochemical generation of the basic catalyst (OH-), responsible for the poly-condensation, and thus generate a silica film on the conductive surface of the electrode. The formation of the sol-gel film by the local increase in pH resembles the electrolytic deposition of metal hydroxides, in which the reduction of H_2O is caused to increase the pH locally [106,107]. The characteristics of the film are affected by the applied potential, the electrodeposition time, the nature of the electrode, etc. so modulating these parameters can obtain different thicknesses, for example. The deposit is driven by the transfer of electrons, which occur in the vicinity of the surface of the electrode, forcing the reservoir to adapt to the surface. This allows the coating and filling of complex geometries [108]. This technique is, of course, limited to conductive surfaces. However, the formation of gels on the electrode does not involve electronic transfer processes, but rather acid-base reactions.The versatility of the electro-deposit technique has been demonstrated in previous work carried out in our research group, carrying out the modification of electrodes with silica-PSS, silica-SWCNT (single-walled carbon nanotubes), and silica-PANI for different applications [109].

1.4. Electrochemistry of silica gels

Electrochemical synthesis is a powerful technique for preparation of various compounds due to its capability in controlling both chemical and electrical parameters affecting the whole reaction [110]. Electrochemical methods can significantly contribute to the protection of the environment through the minimization of waste and toxic materials production. Therefore, electrochemistry is known as environmentally friendly method for synthetic attempts [111].

Electrochemistry plays an important role in sol–gel-based research [103,112–114]. In chemical sensor development, an electrode has often been used as the transducer to record the flow of electrons when an analyte or reagent gets oxidized/reduced. A well-known example is the preparation of a glucose sensor where glucose oxidase is trapped in a sol–gel-derived thin film. Glucose in solution diffuses into the film to react with entrapped glucose oxidase to generate hydrogen peroxide, which is then electrochemically oxidized[115]. The current flowing through the electrode relates to the concentration of glucose in solution.

Electrochemistry is also the driving force behind the development of alternative energy devices. A specific unique example involves the development of 3-D batteries by merging sol–gel chemistry, templating, and electrochemistry [116–118]. In the reverse case, sol–gel chemistry has been invaluable to electrochemists because it provides a simple means to fabricate stable, reusable electrodes for electroanalytical applications[119–121].

Sol–gel-derived materialshave been around for more than a century [54]. In the mid 1980s, it was shown that molecules can be entrapped in the porous framework by simply doping them into a sol prior to its gelation [62]. The retained molecule was shown to have many of the same properties that it did when it was in a solution [63]. Since this time, the field of sol–gel chemistry has exploded with numerous studies on understanding the structure and gelation of these porous hosts, as well as their applications in the areas of chemical sensors, catalysis, and solid-state electrochemical devices [52,63,66,68,69,122–124].

1.4.1. Electrodeposition of Silica-Based Films.

Silica thin films are traditionally formed via spin coating, dip coating, or spray coating a sol on a flat surface[54,99,125]. In 1999, Mandler and coworkers showed that it is possible to use electrodeposition to create sol–gel-based silica thin films on a conducting surface [104]. In this case, the film was prepared from a pre-hydrolyzed sol of methyltrimethoxysilane. Hydroxide ions were formed by application of a sufficiently negative potential to form methylated films ranging in thickness from nanometers to micrometers. In 2003, Collinson and coworkers used electrodeposition to create thin silica films on glassy carbon electrodes from sols prepared solely from tetramethoxysilane [96]. Since this time, a number of other papers have been published[126–130].

Films prepared by sols that contain a number of different alkoxysilanes including phenyltrimethoxysilane, 3-aminopropyltrimethoxysilane, mercaptopropyltrimethoxysilane, and a pyridine alkoxysilane precursor have been reported. Examples of conducting surfaces (electrodes) that have been used include glassy carbon, gold, indium tin oxide (ITO), and aluminum. To form adherent films on gold, a molecular "glue" must be used to attach the growing silica to the gold surface [126–130].

Another method for the polycondensation of hydrolyzed silica precursors has been proposed by Shacham et al. using the incorporation of electrochemistry into sol-gel treatment [104]. The purpose of electroplating is to facilitate the polycondensation of soil precursors by electrochemical pH control at the electrode / solution interface, thus allowing the kinetics associated with the sol-gel process. From a soil solution where the hydrolysis is optimal (pH 3) and the very slow condensation, electroplating by applying a negative potential to increase the pH at the electrode / solution interface (Figure 1.12), thus catalyzing the polycondensation on the electrode surfaces [130]. The thickness of the film deposited on the surface of the electrode is affected by the applied potential, the electroplating time and the nature of the electrode [131].

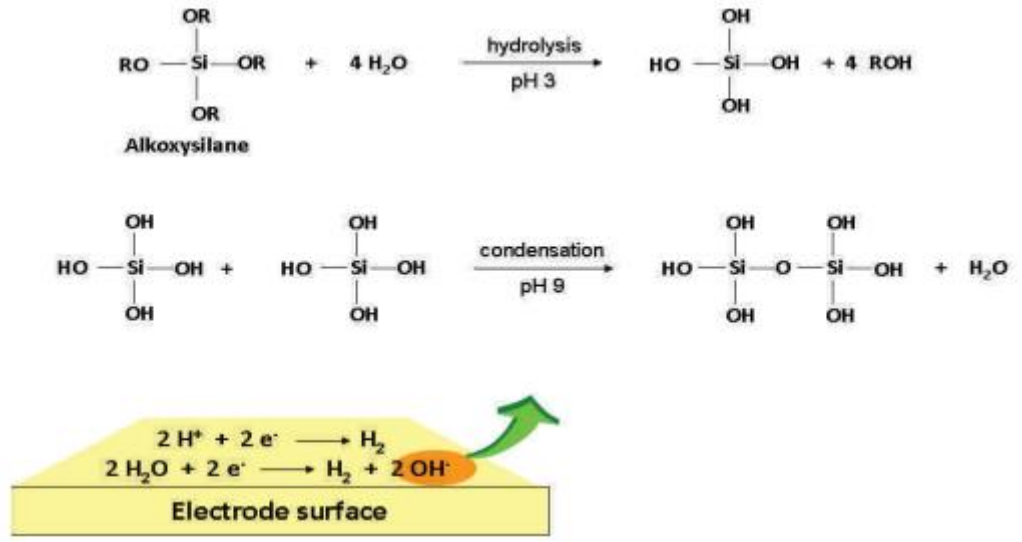

Figure 1.12. Principle of the electrochemical assisted generation of sol-gel at the surface of the electrode

Electrochemically assisted deposition is applied to precursors other than silica such as zirconia or Titania [132,133]. The electrochemically assisted deposition may be advantageously combined with the surfactant template process to generate a mesoporous sol-gel ordered with a single mesoporous orientation to the underlying support [134,135]. Organo-functional groups [134,136].

1.5. Ferrocene a typical transducer in biosensors

The discovery of ferrocene (Fc) brought a organometallic compound with excellent redox properties [137,138]. Ferrocene has good thermal stability and tolerance toward oxygen due to the interaction between the iron atom and the cyclopentadienyl ring. This interaction also facilitates the synthesis of various ferrocene derivatives [139]. Additionally, ferrocene has a lower oxidation potential to lose an electron on account of the oxidizability of its iron atom and two stable redox states (ferrocene and ferrocenium) (Figure 1.13)[140]. If they are properly designed, ferrocene derivatives and ferrocene based polymers [141], and dendrimers [142]. Which have a fast electron-transfer rate and exhibit excellent charge/discharged properties[143–145] can be applied in molecular recognition and as electrochemical sensors.

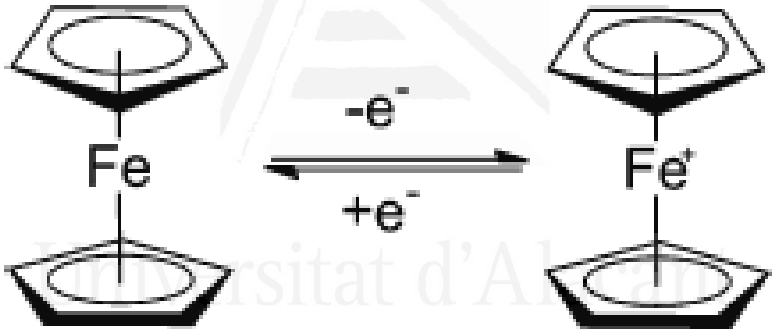

Figure 1.13. Reduced and oxidized states of ferrocene.

1.5.1. Applications of ferrocene

In the field of electrochemical detection, ferrocene has a promising application prospect in view of its impact as a component of molecular receptors and sensing materials. The description of the principle of ferrocene-based electrochemical detection and further discuss its design and performances. In particular, two forms of detection, molecular recognition and sensing systems, were specified. Ferrocene-based molecular receptors with all kinds of structures covering derivatives, polymers, and supramolecular receptors are presented. Benefits of their structures to the recognition behavior are compared and discussed.

In electrochemical sensors, the ferrocene containing component is used as a mediator or a label. The architectural design, enhancement effect of additives, and the structures of ferrocene-containing components in the corresponding sensors are discussed.

1.5.2. Examples of biosensors with ferrocene

An electrochemical reaction at the electrode / electrolyte interface is necessary to allow the electrochemical measurement. This reaction requires the presence of a redox molecule such as ferrocene [146], viologen [147] ormetalloporphyrin [148]; ferrocene is used as a redox mediator to shuttle electrons between the electrode and enzyme active site [149–151]. The use of ferrocene in the amperometric biosensor allows reversible redox reactions [152] and it has been used in this manner for many amperometric biosensors for the determination of phenolic acids with other enzymes [150,153]. Thus, Sulak et al. [149] used ferrocene as a mediator for the development of an amperometric phenol horse radish peroxidase (HRP) enzyme-based biosensor; to this is added the high cost of synthesis of certain polymers. All these problems have oriented research towards other more profitable and less costly matrices. Some recent examples of ferrocene based biosensing are reviewed below.

For example, Jiang et al. modified an electrode to facilitate electron transfer to glucose oxidase, the electrode was coated with a polyelectrolyte film for the quantitative detection of glucose. The polyelectrolyte with a ferrocenyl group were used as mediator between the redox center of glucose oxidase and the electrode. The electrodes have high operational stability and long-term storage stability [154].

Kaya et al. studied the application of an amperometric glucose sensor electrode;A graphite electrode coated with a PEDOT layer, was used as a transducer for the electrochemical deposition of the polymer of a novel ferrocene functionalized monomer.The use of a PEDOT layer as a working electrode has improved the location of the novel monomer on the transducer surface while improving the performance of the biosensor [155].

Jedrzak et al. has prepared an amperometric glucose biosensor from carbon paste electrode based on functional / silica-lignin system; For the immobilization of glucose oxidase. The electrode used ferrocene redox mediator[156].

Dervisevic et al. built ferrocene modified conducting polymer based amperometric urea biosensor. Based on functionalized aniline monomer on Pencil Graphite Electrode (PGE). The polymer-coated electrode surface was functionalized with di-amino-Ferrocene (DAFc) as the mediator, and Urease enzyme.The designed bio-electrode was tested with real human blood and urine samples where it showed excellent analytical performance with insignificant interference[157].

Zhou et al. developed a novel reagent-free glucose biosensor by immobilizing glucose oxidase by grafting a dendrimer with ferrocene covalently to the surface of a carbon nanotube-modified nanocomposite electrode. Due to the excellent electron transfer acceleration of the CNTs and the high-content loading of the biomolecules and ferrocene mediator on the electrode matrix, this biosensor showed excellent analytical performance such as fast response time less, wide linear range and low detection limit as well as satisfactory stability and reproducibility toward the amperometric glucose determination[158].

Godman et al. study the electrochemical characterization of layer-by-layer assembled ferrocene-modified linear poly(ethylenimine)/enzyme bioanodes. For biofuelcells ferrocenylhexyl- and ferrocenylpropyl-modified linear poly(ethylenimine) were used with glucose oxidase in the layer-by-layer assembly of enzymatic bioanodes on gold [159].

Finally, Feng et al. study the development of a novel cholesterol amperometric biosensor containing modified cholesterol oxidase and cholesterol esterase electrodes. The electrocatalytic behavior of cholesterol in the cholesterol biosensor was studied showing high selectivity, specificity and stability of the cholesterol sensor and applied to measure blood samples. [160].

1.6. Biosensors based on alkaline phosphatase

Alkaline phosphatase (ALP) is a vital hydrolysis enzyme in phosphate metabolism, which catalyzes the hydrolysis of phosphate ester groups in proteins, nucleic acids, and other small molecules. Meanwhile, a normal ALP expression is associated with occurrence and development of many diseases [161].

Alkaline phosphatase (ALP) is a hydrolase, which is responsible for the dephosphorylation process of nucleic acids, proteins, some other small molecules [162], and has been prevalently found in a variety of mammalian tissues, such as liver, bone, kidney, placenta, and intestine [163,164]. The enzyme of alkaline phosphatase has a role in the biomineralization process [165]. Alkaline phosphatases from several sources have been intensively studied at the air–water interface [166,167]. The normal concentration of ALP in adult serum is 20–160 U L^{-1}[168], According to previous reports, the aberrant expression of ALP is related to many diseases, such as liver dysfunction [169], bone diseases [170], diabetes [171], and prostatic cancer [172]. Moreover, it is also one of the most common markers in enzyme immunoassays, gene assays, histochemical staining, and related affinity sensing methods for monitoring proteins, nucleic acids, drugs, enzymes, and other analytes [173–177], that has been successfully applied for the ALP analysis in the real human serum [178]. In environmental biology field, ALP is widely used as an index parameter of phosphate anion (PO_4^{3-}) in phytoplankton phosphorus limitation. ALP also has regulation ability to phosphorus concentration for seasonal microorganism growth [179]. Therefore, a versatile, label-free, convenient and sensitive method for ALP activity assay is of great importance for diagnostic, analytical applications and environmental biological analysis [161].

1.6.1. The history of ALP

During the late 19th century and early years of the 20th century, researchers found that phosphorous existed in organic and inorganic forms in living animals. The conversion of organic to inorganic phosphate in biological systems was investigated under the coming years by several researchers [180]. They stated that phosphatases are a separate group of enzymes and extracted ALP from rice and wheat and referred to this enzyme as “phytase”. Plimmer[181] investigated how this “phytase” worked in animals and could draw the conclusion that organic phosphate was hydrolyzed to inorganic phosphate by a specific enzyme[181]. The first report that addressed the importance of ALP for skeletal mineralization was in 1923 by Robert

Robison [182]. Robison suggested that ALP increased the local concentration of phosphate by hydrolyzation of organic phosphate to inorganic phosphate. The liberated inorganic phosphate provides a substrate for mineralization that can be deposited together with calcium as HA. Robison found high activities of ALP in bone and cartilage of young rats and rabbits and hypothesized that hydrolysis of hexosephosphoric esters was necessary for mineralization. The hypothesis from this article is still cited today and the article was republished in 1991 [182]. In 1924, Robison and Soames observed that the pH optimum was alkaline in vitro [182]. Soon after Robison´s first report, this hypothesis was challenged when ALP was found in no calcifying tissues such as liver, placenta and intestine [180]. Today, the importance of ALP in skeletal mineralization is proven and verified by the discovery and characterization of hypophosphatasia (HPP) [183,184]. Measuring ALP activity in serum has been of significant clinical interest since the 1930s and high ALP activity indicates usually skeletal or hepatobiliary disease. Still, as of today, ALP is one of the most frequently used tests in routine clinical chemistry.

The importance of phosphate transfer reactions in biological systems is reflected by the ubiquity of phosphate compounds. Phosphate containing compounds fulfil biologically important multiple roles, such as being essential intermediary metabolites, genetic materials, energy sources and reservoirs of biochemical energy [185]. Due to the low reaction rates of phosphate ester hydrolyses the use of catalysts is required. The super-family of enzymes called phosphatase has a biochemical machinery enabling it to hydrolyse phosphor-esters rapidly under mild cellular conditions.

Alkaline Phosphatase catalysis hydrolysis of phosphate esters and transfer of free phosphate groups to supply biological systems with inorganic phosphate (Figure 1.14). It catalyses the cleavage of a phosphate groups from a variety of compounds, including Ribonucleic Acid (RNA) and DNA and the artificial substrates [186].

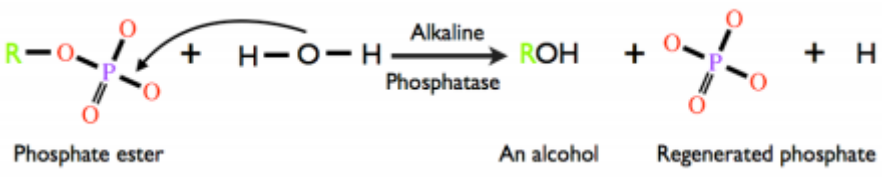

Figure 1.14. Schematic representation of the reaction mechanism of Alkaline Phosphatase.

1.7. *P*-Aminophenol transducer on ALP biosensor

Electrochemical detection of p-aminophenol

The detection of *p*-aminophenol in the development of immunosensors has been reported [187]. A particular advantage of *p*-AP is that it is electroactive, with an oxidation potential of 0.3V [187], while its precursor, *p*-aminophenyl phosphate is not electroactive at this potential.

A suitable enzyme label, e.g. Alkaline Phosphatase (ALP), is bound to the target DNA by a biotin molecule. We use *p*-aminophenyl phosphate (*p*-APP) as a substrate to start the redox process (Figure 1.15.a). The resulting species from the enzymatic reaction is para-aminophenol(*p*-AP). It has two electrochemically active groups at the benzene structure. Para-Aminophenol is oxidized to quinoneimine and reduced as depicted in the scheme in figure (1.15).

a) Process at the label

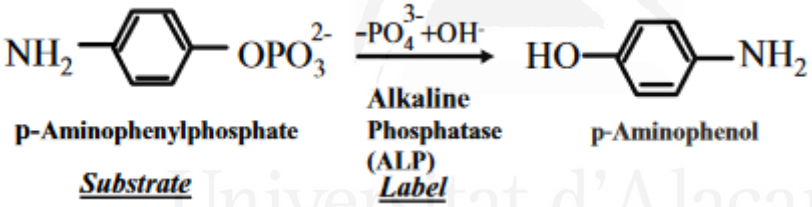

b) Redox process at the electrodes

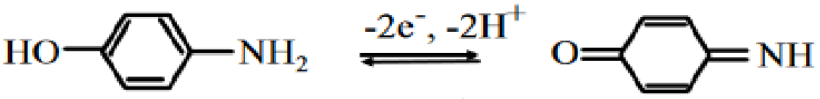

Figure1.15. Schematic plot of the electrochemical process at the label (a) and redox process at the electrodes (b).

In the redox reaction 2, electrons and 2 protons are involved. The electrons can be detected in the current flow between the electrodes, the protons are exchanged within the buffer solution. For electrochemical operation[188].

1.7.1. Examples of biosensors with *p*-aminophenol

Some recent examples of biosensing based on *p*-aminophenol detection formed on the literature are reviewed below.

Islam et al. developed an electrochemical microalgal bioassay for the determination of heavy metal toxicity in water on the basis of the alkaline phosphatase (ALP) enzyme inhibition of Chlamydomonas Reinhardtii. The ALP activity was inhibited using the phosphate starvation method, and the results were evaluated by measuring the electrochemical oxidation of *p*-aminophenol (*p*-AP) following the enzymatic conversion of *p*-aminophenyl phosphate (PAPP) as a substrate. Enzymatic activity over a *p*-APP substrate is affected by heavy metal ions, and this phenomenon decreased the chronoamperometric current signal [189].

Sharma et al. developed an electrochemical immunosensor based on the disposable screen-printed electrodes (SPEs) for the detection of Plasmodium falciparum histidine rich protein-2 (PfHRP-2) antigen. *p*-aminophenyl phosphate (*p*-APP) was used as substrate and the amperometric response was measured as a function of concentration of *p*-aminophenol in 0.1 M diethanolamine (DEA) buffer solution. The electrochemical immunosensor has higher sensitivity and faster than the standard spectrophotometric method[190].

Microfluidic immunosensor design for the quantification of interleukin-6 (IL-6) in human serum samples was developed by Messina et al. The detection of IL-6 was carried out using a sandwich immunoassay method based on the use of anti-IL-6 monoclonal antibodies, immobilized on a 3-aminopropyl-modified controlled-pore glass. The IL-6 in the serum sample is allowed to react with the immobilized anti-IL-6 and biotin-labeled secondary antibodies specific to IL-6.The *p*-aminophenol formed by alkaline phosphatase was quantified on a gold electrode at 0.10 V. Compared with the traditional IL-6 sensing method, the integrated microfluidic immunosensor required smaller amounts of sample to perform faster detection[191].

Screen-printed immunosensor for quantification of human serum immunoglobulin G(IgG) antibodies to Helicobacter pylori. The bound antibodies are quantified by alkaline phosphatase (ALP) enzyme-labeled second any antibodies specific to human IgG. *p*-aminophenyl phosphate (*p*-APP) was converted to *p*-aminophenol (*p*-AP), and quantified by square wave voltammetry. The electrochemical immunosensor showed higher sensitivity and lower time consumed than

the standard spectrophotometric detection ELISA method, demonstrate its potential usefulness for early assessment of human serum immunoglobulinG (IgG) antibodies to H. pylori[192].

Electrochemical immunosensor for progesterone analysis in milk was developed by Kreuzer et al. A disposable electrochemical biosensor, based on a screen-printed carbon electrode (SPE) coated with a progesterone-prog-BSA conjugate, was prepared and evaluated. Differential pulse voltammetry (DPV) and amperometry were used as electrochemical means to detect the product of the enzymatic reaction [*p*-aminophenol(*p*-AP)]. The use of DPV improved the accuracy of our measurements over conventional amperometric detection by electrode background correction[193].

Finally, a novel electrochemical immunosensors for seafood toxin analysis was described by Kreuzer et al. on a screen-printed electrode (SPE) system for measurement of a variety of seafood toxins, such as okadaic acid, brevetoxin, domoic acid and tetrodotoxin. A disposable screen-printed carbon electrode coupled with amperometric detection of *p*-aminophenol, produced by the label, alkaline phosphatase, was used for signal measurement [194].

2. Experimental techniques

2.1. Introduction

This chapter presents the different techniques, reagents and materials used during this PhD thesis work. It also describes the functionalization techniques used for the preparation of the new materials. Nevertheless, the specific experimental conditions will be explained in detail in each chapter.

2.2. Characterization techniques

2.2.1. Electrochemical techniques

There exist a large number of electrochemical techniques which are available for characterization.

In order to perform the electrochemical measurements that are shown in this work, a standard three electrode cell was used. The cell is filled with an electrolyte in order to ensure sufficient conductivity, it consists of a reference electrode (RE); working electrode (WE), which corresponds to the material to be measured; and a counter electrode (CE) which is an inert material with high surface area.

Electrochemical techniques allow the analysis of the processes that occur on the surface of an electrode (working electrode, WE) submerged in an electrolyte. The fundamental information of this technique is given by the amount of electrical current (i) that passes through the electrode in response to a stimulus, at a certain time scale.

The stimulus referred to is a potential difference (ΔE) applied with respect to another electrode (non-polarizable electrode, reference electrode, RE). The current measured on the electrode has a double origin, since it can come from either i) the migration of ions to compensate fixed charges on the surface of the electrode (capacitive phenomena), or ii) molecules that experience; an oxidation-reduction reaction as a result of the applied electrochemical potential (faradic phenomena).

2.2.1.1. Electrochemical cell with three electrodes

Besides the working electrode electrochemical measurements require the use of two auxiliary electrodes in addition to the electrode to be characterized. These are carefully selected to achieve optimal analysis conditions:

- To circulate current, a second electrode submerged in the solution is required (counter-electrode, CE). A complementary reaction to the WE takes place that closes the transit of charges through the system. Generally it is an inert material whose electrochemical reactivity does not involve the dissolution of metal ions, being the Pt, the Au and the inert carbonaceous materials common candidates to perform this function.

- For a suitable control of the potential applied to the WE, a third electrode (reference electrode, RE) is necessary. Although it is true that to apply a potential difference only the presence of two electrodes in a solution is necessary, the control over the electrochemical potential experienced by a particular electrode (WE) can only be established with precision when on the second electrode (RE)) no current flows.

Among the most common reference electrodes are the reference electrodes of H_2 (g) in which H_2 is bubbled over a Pt electrode immersed in a solution with electrolyte support (Normal Hydrogen Electrode, NHE, for pH = 0 and Reversible Hydrogen Electrode, RHE for pH equal to that of the working solution); second-species electrodes such as Ag / AgCl and calomel (Hg / Hg_2Cl_2) generally submerged in concentrated solutions of NaCl or KCl; and finally the electrodes called pseudo-references for having a sensitive potential to working conditions, the most typical being an Ag wire which is directly immersed in the working electrolyte.

Figure 2.1. Electrochemical cell of three electrodes.

As can be seen in figure 2.1, in addition to the three electrodes already described, a gas pin is used to eliminate oxygen dissolved in solution by purging N_2 (g). This is usually done through a constant bubbling for at least 10 minutes before starting the experiment, and then it is passed to keep the internal environment of the cell purged with N_2, with the aim of maintaining an inert atmosphere during the electrochemical measurements.

Another common accessory is the Luggin capillary equipped with a key that allows the reference electrode to be kept in a small compartment saturated with H_2 (g) and oblivious to possible changes in the composition of the solution. The use of a Pt wire as part of the reference system suggests filling the Luggin with a solution that only contains the supporting electrolyte and is free of any species that can react on the surface of the metal. This accessory is dispensable if Ag / AgCl, calomel or pseudoreference electrodes are used.

2.2.1.2. Cyclic voltammetry (CV)

Cyclic voltammetry is a very useful technique for assessing the electrochemical behavior of an electrode. It is possible to get information about electrochemical reactions, thermodynamics of redox processes, and kinetics of electron-transfer reactions, capacitive currents, and adsorption processes, among others.

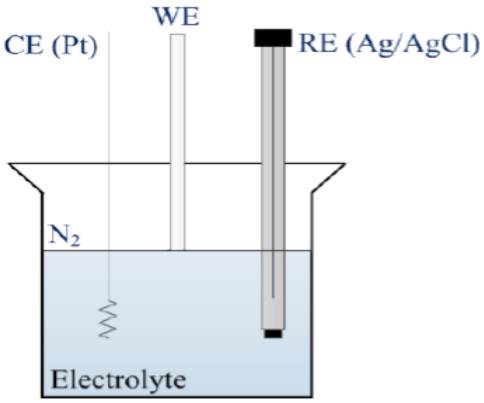

Figure 2.2. Scheme of a three electrochemical cell.

Cyclic voltammetry experiments consist in a linear scanning of the potential of a working electrode. In the experiment, the current flowing through the WE is measured during a potential change with time using a constant potential scan rate [195]. The applied potential to the WE is measured against the RE and the CE closes the electrical circuit for the current to flow. At the beginning, the WE is held at an initial potential *Ei*, where no reaction occurs, usually at the open circuit potential. During the measurement, the potential of the WE is changed linearly at a specific scan rate *v* between two potential limits (*E1* and *E2*) and in reverse order using the same conditions. The current passing from the WE to the CE is recorded as function of the potential. Figure 2.3 shows the theoretical cyclic voltammetry measurements of potential vs. time and current vs. potential (cyclic voltammogram).

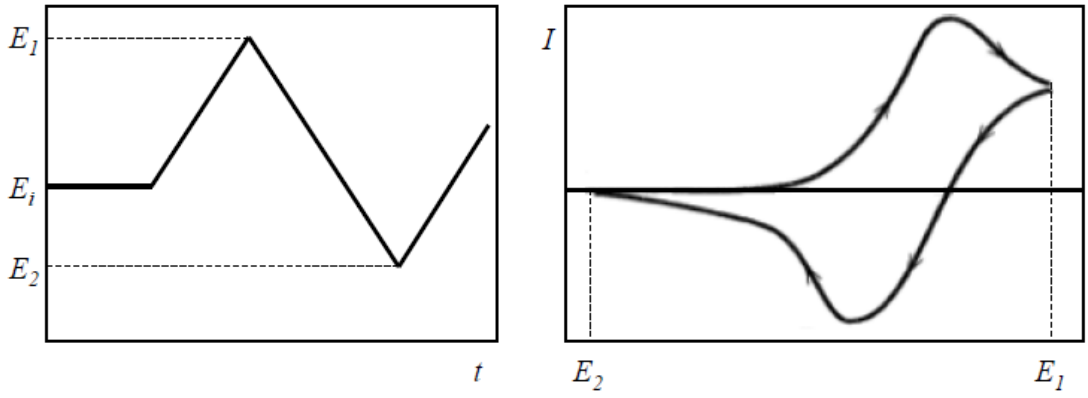

Figure 2.3. Cyclic potential sweep (left) and the resulting cyclic voltammogram (right).

The response of each material is different and depends on the combined action of capacitive currents delivered during the formation of the electrical double layer over the surface of the electrode and possible redox reactions (it can also imply the modification of the electro-activity of the electrode) that can occur on the electrode surface.

2.2.1.3. Chronoamperometry (CA)

Chronoamperometry is very useful for the quantitative analysis of different capacitive and redox processes. Figure 2.4 shows a schematic chronoamperometric experiment of potential vs. time and current vs. time. Chronoamperometry usually involves stepping the potential of the working electrode from the initial potential *Ei* to a potential *E1* at which usually a faradic reaction is occurring. Then, the response of current with time reflects the change in the reaction rate occurring at the surface of the working electrode. It is important to note that capacitive currents related to the formation or modification of the double layer will appear at the beginning of the potential step, being the main contribution at short times. After such time, the faradic current will be the most important contribution to current.

Chronoamperometry is widely used in sensors application in order to correlate the measured current and the amount of an analyte dissolved in the electrolyte when a potential is applied to the electrode [196]. If a steady state can be established, the final current will correspond to a specific concentration. When a known amount of analyte is added to the electrolyte, it will be

possible to make a calibration curve where steady state currents are plotted versus different concentrations of the analyte.

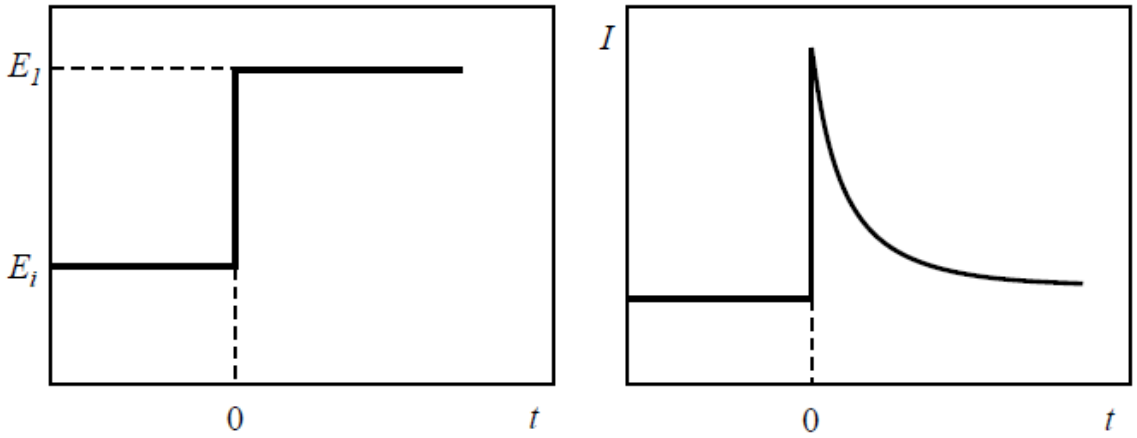

Figure 2.4. Chronoamperometry experiment. Potential- time profile (left) and the resulting response of the current as a function of time (right).

2.2.2. Spectroscopic techniques

2.2.2.1. X-ray photoelectron spectroscopy (XPS)

The X-ray photoelectron spectroscopy is a quantitative detection technique useful for determining the elemental composition, the chemical species and their oxidation states on the surface of a material. This technique is considered as a surface characterization technique due to its low penetration power (1-3 nm) [197].

The technique consists in the determination of the kinetic energy of the emitted electrons when the samples are irradiated with a monochromatic X-ray beam. The irradiation can produce the emission of valence or inner layers electrons from the sample atoms. The electron emission has a specific kinetic energy which is related to the electron configuration of the elements and consequently to the binding energy of the ejected electron. The binding energy can be calculated from the energy of the X-ray source by subtracting to the energy of the incident radiation, the kinetic energy of the emitted electron and the work function, which is a characteristic of the apparatus and the sample [198]. The obtained spectrum shows the number of counts or intensity recorded in a range of binding energies. Generally, the binding energy increases for the higher

oxidation states of the elements, and these changes can be seen as a shift of the binding energy of the intensity peak.

The experimental setup has an X-ray source, an electron detector and the energy analyzer. All the experiments are performed at ultrahigh vacuum (5 x 10^{-7} Pa) in order to avoid the collision between the ejected electrons and residual molecules, which can affect the signal quality.

The surface composition and oxidation states of the species in the materials were studied using a VG-Microtech Mutilab 3000 spectrometer and Mg Ka radiation (1253.6 eV). The C1s peak position was set at 284.6 eV and used as reference to shift the position of the whole spectrum. Deconvolution of the XPS N1s spectra was done by least squares fitting, using Gaussian-Lorentzian curves, while a Shirley line was used for the background determination. The deconvoluted N1s peaks were assigned to different surface groups and the oxidation states of nitrogen according to those described in previous works [199].

2.2.2.2. Fourier transformed infrared spectroscopy (FTIR)

In infrared spectroscopy the vibrational spectrum of a compound is obtained by exposing the sample to infrared radiation and recording the variation of absorption with frequency. FTIR spectroscopy uses a Michelson Interferometer that produces an interferogram from the splitted beam, which contains information about the whole range of IR frequencies coming from the source. The analysis of the interferogram resulting from the interaction with the sample permits to obtain the IR spectrum. To do this, the interferograms in the time domain are mathematically treated using the Fourier Transform in order to determine the absorption of the sample at each wavelength [200].

In the experiment, after the signal is processed, the spectrum of the absorbed/transmitted IR radiation fraction as a function of the frequency or wavenumber is obtained. Bands will appear at certain wavelengths where the sample has absorbed IR radiation. This absorption of IR radiation is related to the excitation of the different vibrational modes of a molecule and different bands will appear depending on the specific chemical bonds in the sample, which allows to identify the species in the material.

In this work, the equipment used in the characterization of silica materials was a Nicolet 5700 spectrophotometer with deuterated triglycine sulfate detector (DTGS) and Fourier transform.

2.2.3. Microscopic techniques

2.2.3.1. Transmission electron microscopy (TEM)

In transmission electron microscopy (TEM), a thin sample is irradiated with an electron beam of uniform current density, whose energy is within the range of 100 to 200 keV. Part of these electrons are transmitted, another part is scattered and another part gives rise to interactions that produce different phenomenon such as light emission, secondary electrons and Auger, X-rays, etc. The transmission electron microscope uses the transmission / dispersion of the electrons to form images [201] the diffraction of the electrons to obtain information about the crystalline structure; and the emission of characteristic X-rays to know the elemental composition of the sample (chemical composition, phases or mixture of phases).

A condition for the transmission of electrons through the sample is that it is thin, that is, transparent to electrons. It is recommended not to use samples of more than 10 nm in thickness since the smaller the thickness of the sample, the better the quality of the images obtained.

The simplest electron microscopes consist of two imaging lenses much like conventional optical microscopes. The illumination comes from cannon of electrons emitted by a filament of W or LaB6. The electrons are accelerated by applying a negative potential (100 - 100 kV) and focused by two condensing lenses on a thin sample, transparent to the electrons.

After passing through the sample the electrons are picked up and focused by the objective lens within an enlarged intermediate image. The image is further enlarged thanks to the projecting lenses, which control the magnification of the image on the fluorescent screen. The final image is projected on a fluorescent screen or a photographic film.

The preparation of the samples consists in the dispersion of the latter in ethanol. Subsequently, the dispersion is deposited on a carbon or metal grid and is introduced directly into the microscope.

In the present work we used the JEOL 120 kV transmission electron microscope model JEM-1400 Plus. The source of electrons used consists of a hot filament of tungsten that, by thermionic effect, emits electrons, which are accelerated by a potential of 100 to 200 kV. A resolution between lines of 0.2 nm and between points of 0.38 nm is obtained. The camera of acquisition of images is of the brand GATAN model ORIUS SC600. It is mounted on axis with the microscope at the bottom and is integrated into the image acquisition and treatment program

GATANDigitalMicrograph 1.80.70 for GMS 1.8.0. The equipment used is installed in Technical Research Services of the University of Alicante.

2.2.3.2. Scanning electron microscopy (SEM)

Scanning electron microscopy is a technique that allows the visualization of the morphology of solid samples on the physical limit of the optics, allowing a resolution of a few thousand Å, depending on the nature of the sample [202]. The technique employs a source of electron emission, usually tungsten or lanthanum, and an accelerated electron beam of between 5 and 30 keV. This consists, mainly, in sending a beam of electrons to the surface of the sample and, by means of an appropriate detector, to register the secondary electrons and backscattered. The beam moves on the sample by scanning in the X and Y directions, so that the intensity of the image varies at each point with the intensity of the electron beam generated on the surface.

The electrons torn from the atoms of the sample, product of the bombardment of electrons of the primary beam, are called secondary electrons. These provide information about the surface topography and it is the signal with which an image of the sample is obtained. Due to the low energy of the secondary electrons (less than 50 eV), in their trip towards the outside of the sample they lose energy by different interactions, so that only those that are very close to the surface have some probability of escaping the material and get to the detector. Therefore, the signal of the secondary electrons comes from the same surface and from a very small area below it, around a few nanometers (of the order of 5 to 10 nm).

On the other hand, being low energy electrons, they can be easily deviated from their initial emergent trajectory, and information can be obtained from areas that are not in view of the detector. This particularity is fundamental to grant this signal the possibility of providing information "of relief".

Electrons that bounce elastically on the surface are called backscattered electrons. Its energy is greater than 50 eV and the depth of the site from which they come (of the order of hundreds of nanometers) is greater than that of the secondary electrons. The intensity of the signal of backscattered electrons, for a given energy of the beam, depends on the atomic number of the atoms of the material. This fact allows, from differences in intensity, distinguish phases of material of different chemical composition, although there is no difference in topography

between them. The zones with the highest atomic number (Z) will be darker than the zones with the smallest atomic number. This is the main application of the backscattered electron signal.

Samples that are to be analyzed by scanning electron microscopy must be dried before being introduced into the microscope; otherwise the low pressure in the microscope will cause water (and other volatile liquids) to evaporate, violently leaving the sample, altering the structure of it. When it is desired to visualize a sample in a scanning electron microscope, it must be conductive since, if not, it is charged during the irradiation by a load accumulation that diverts the electronic beam and, as a consequence, distortions appear in the image. One solution to this problem is to coat the sample with a conductive film, with a thickness between 10 and 25 nm.

The choice of the material with which the sample is to be coated depends mainly on the study that is going to be carried out. Thus, for the observation of secondary electron images, gold and gold-palladium are the materials that offer the best results; being heavy elements, they produce more emission. When it is intended to perform a micro analytical study, it is advisable to use carbon. The low atomic number of this element makes it practically transparent to the X rays emitted by the sample. Aluminium, chromium, etc. are also sometimes used. It is also important that the sample is not covered with a material that is part of it.

The scanning electron microscope used in this work is of the brand JEOL JSM-840, installed in Technical Services of Investigation of the University of Alicante. This equipment consists of a detector of secondary electrons type scintillate photomultiplier with resolution of 4 to 3.5 nm and a backscattered electron detector type Si P-N with resolution of 10 to 5 nm.

2.2.3.3. Scanning electron microscopy of field emission (FESEM)

The field emission scanning electron microscope (FESEM) is an instrument that, like the SEM microscope, is capable of offering a wide variety of information from the sample surface, but with higher resolution and a range of energy. Much older the operation is the same as that of a conventional SEM; an electron beam is swept on the surface of the sample while on a monitor the information that interests us is displayed based on the available detectors.

The biggest difference between FESEM and SEM lies in the electron generation system. The FESEM microscope uses as a source of electrons a field emission cannon that provides much focused high and low energy electron beams, which greatly improves the spatial resolution and allows working at very low potentials, from 0.02 to 30 kV, allowing us to observe electron

beam sensitive samples without damaging them and minimizing loading effects. Another very remarkable feature of the FESEM microscopes is the use of detectors inside the lens. These detectors are optimized to work at high resolution and very low acceleration potential, which is why they are fundamental to obtain maximum performance from the equipment.

The equipment installed in Technical Services of Investigation of the University of Alicante and used in this thesis is a scanning electron microscope of emission of field (FESEM) mark ZEISS model Merlin VP Compact equipped with a system of microanalysis by EDX brand BRUKER model Quantax 400 The resolution it reaches is 0.8 nm at 15 kV and 1.6 nm at 1 kV.

2.2.3.4. Thermogravimetric techniques

Thermogravimetry (TG) is defined as the technique in which the weight of a sample is measured against time or temperature while the sample is subjected to a temperature controlled program in a specific atmosphere [203].

The temperature program can be kept at a constant temperature (isothermal), heating at a constant speed (the most usual next to the isotherm), cooling or any combination of them. The usual thing is that there is a loss of weight but it is also possible that there is a gain of it. The atmosphere can be static or dynamic at a given flow rate (reduced pressure conditions are also used) and the most common gases are N_2, air, Ar, CO_2, H_2, Cl_2, or SO_2 are also used.

A fundamental characteristic of the TG is that it only allows to detect processes in which there is a variation of weight such as decompositions, sublimations, reduction, desorption, absorption, etc. while it does not allow studying processes such as mergers, phase transitions, etc.

Thermal methods often require complementary analysis by other techniques for a complete understanding of the processes that are occurring, even the simplest ones. The thermal methods most used simultaneously with TG are differential thermal analysis (DTA) and differential scanning calorimetry (DSC), giving rise to TG-DTA and TG-DSC techniques. On the other hand, the products released in a thermogravimetric analysis can be analyzed by any analytical method: the gases can be separated by means of a gas chromatographic column; they can be analyzed by infrared spectroscopy (TG-IR) or by mass spectrometry (TG-MS). In this thesis the different samples of silica were analyzed using thermogravimetry coupled to a mass spectrometer.

2.2.3.5. Thermogravimetry coupled to mass spectrometry (TG-MS)

Mass spectrometry is a great technique for the identification of gases and vapors. If a gaseous sample is introduced into a mass spectrometer under high vacuum conditions (of the order of 10-6 mbar) the molecules can be ionized in different ways, for example by impacts with high-energy electrons accelerated by a difference of potential of the order of 70 V:

$$M + e^- \rightarrow M^{\cdot +} + 2e^-$$

The species $M^{\cdot +}$is the molecular ion, usually a radical cation with an unpaired electron. With such high energy, there is a high probability that the molecular ion will split into an ion fragment of smaller mass and a neutral fragment. The fragmentation pattern is characteristic of the molecule studied and can be used as a kind of fingerprint [204].

The equipment used is the one that is in Technical Services of Investigation in the University of Alicante, treats of a team of TG-DTA of the mark METTLER TOLEDO model TGA / SDTA851e / LF / 1600, able to work between room temperature and 1600 ° C. As for the Mass Spectrometer, it is a quadrupole team of the brand PFEIFFER VACUUM model THERMOSTAR GSD301T with a mass range of up to 300 amu, with a SEM detector (electronic multiplier).

2.3. Experimental methods

2.3.1. Cleaning of glass material

In cyclic voltammetry the cleaning of the glass material that is in contact with the solutions is quite important. The cleaning protocol is as follows:

The glass material is immersed in a concentrated acid solution of $KMnO_4$ for about 12 hours. The recipe for preparing the oxidant solution is the following: 30 g of $KMnO_4$ + 5 mL H_2SO_4 (98%) in 2 L of H_2O. In this way it is possible to oxidize the organic matter present to simpler species to be eliminated.

The glass material is then removed from the oxidant mixture and rinsed with an acidic H_2O_2 solution. With this solution, the remains of MnO_4- that have not reacted are reduced. Then the material is washed with abundant ultrapure water (18.2 MΩ • cm) to eliminate salts, residues and oxidation products.

After the washing, the glassware is boiled repeatedly in heating plates or in microwaves with ultrapure water, thus eliminating substances that may still be adhered to the walls of the material. Finally, the material is rinsed with ultrapure water and it is ready to be used.

2.3.2. Pre-treatment of electrodes

Another important aspect in voltammetry is the conditioning of the electrode surface. Specular finishing surfaces are generally desired in both metallic and carbonaceous electrodes, in order to minimize the real area and with it the contribution of the double capacitive layer in the voltammograms. Polishing is therefore the classic pre-treatment for disco electrodes.

The polishing protocol comprises a series of steps consisting of the use of diamond or alumina suspensions of progressively smaller particle size. It is usual to start with suspensions with a grain size of 1 μm, to later refine with finer particles of the order of 0.5 or 0.25 μm. The last polishing will be followed by a thorough sonication of the electrode (5-10 minutes) to detach those Adhered residues during polishing.

In the case of polishing with alumina, said ultrasonic washing is carried out in an alkaline solution (0.01 M NaOH) to favor the solubilization of possible embedded grains. In the case of vitreous carbon electrodes, if the material is very porous as it happens with certain batches, the polishing is not enough to regenerate a clean surface after a previous use. In this case it is preferable to use wet grinding with fine sandpaper (grain 400 or 1000). Occasionally, it is possible to use pliers to remove the outer portion of the rod, after which it is essential to use sandpaper to generate a new smooth surface.

2.3.3. Solutions, reagents and electrodes

The water used for the preparation of all solutions was obtained from an *ELGA Lab Water Purelab* system with a resistivity of 18.2 MΩ • cm measured at 25 ° C. The electrolytes used were solutions of sulfuric acid (H_2SO_4, 98%) supplied by *Merck*, and solutions buffered at pH= 7 prepared with potassium dihydrogen phosphate (KH_2PO_4, 99.5%) and dipotassium hydrogen phosphate (K_2HPO_4, 99.8%), reagents supplied by *Merck and Sigma-Aldrich*, respectively.

The working solutions were deoxygenated before the beginning of the experiments by bubbling, for about 15 minutes, nitrogen gas (99.999%) supplied by *Air Liquide*.

The reagents used were: tetraethoxysilane (98%), methyl triethoxysilane (MTES, 99%), n-propyl-triethoxysilane (PrTES, 98%), octyltrimethoxysilane (OTMS, 96%), phenyl-triethoxysilane (PhTES , 98%), ethanol (99.95%), supplied by *Sigma-Aldrich*; potassium chloride (KCl, 99%), and hydrochloric acid (HCl, 37%) supplied by *Merck*, potassium permanganate (KMnO4, 99%), hydrogen peroxide (H_2O_2, 20%) supplied by *VWR International*, *P*ara-aminophenol-hydrochloride, $Fe(CN)_6^{-4/-3}$, Ferrocenium hexafluoro-phosphate supplied by *Sigma-Aldrich*.

For the polymerization of poly (3,4-ethylenedioxythiophene) (PEDOT) were: the monomer 3,4-ethylenedioxythiophene (EDOT, 97%) which was subsequently dissolved in a dispersion of sodium polystyrenesulfonate (PSSNa), both supplied by *Sigma- Aldrich*.

The reagents necessary for the preparation of the silica used in the electrodeposition weretetraethoxysilane (TEOS, 98%) ethanol (EtOH, 99.95%), supplied by *Sigma-Aldrich*,potassium chloride (KCl, 99%), and hydrochloric acid (HCl, 37%) supplied by *Merck*.

The working electrodes used were a platinum polycrystalline electrode, vitreous carbon rods (geometric area = 0.07 cm^2) supplied by Carbone Lorraine, model V-25. As auxiliary electrode a platinum wire was used and as a reference electrode a reversible hydrogen electrode (RHE), bubbling hydrogen gas (99.999%) supplied by *Air Liquide*.

3. Modulation of the electrocatalytic performance of PEDOT-PSS by reactive insertion into a sol-gel silica matrix

3.1. Introduction

Electrode surface modification with accurate control of the building blocks is able to produce integrated molecular systems with extended applications in electroanalysis [205–207]. The use of these modified materials spread out during the last years and, particularly, the sol-gel route offered the opportunity of preparing ceramic-like films under rather mild conditions [61,208]. This soft-chemistry synthesis enhanced the possibility of incorporating temperature sensitive biomolecules, such as enzymes to the silica host layer, resulting in very stable hybrid materials useful for bioanalytical purposes [209].

The surface modification with silica gels is typically performed by coating the electrode with thin films obtained from a sol, which is obtained by the hydrolysis of metal alkoxyde precursors in water/alcohol solutions by conventional techniques such as spin or dip coating or, even, by electro-assisted deposition [210,211]. In this latter method, electrogenerated hydroxide ions trigger the polycondensation of the hydrolysed precursors producing films with very controlled properties, including mesoporous assemblies or compact molecularly imprinted structures, which are useful for the encapsulation of electrocatalytic species [103,211–213]. Silica is an intrinsic dielectric material whose weak electrochemical properties (electroactivity, electron conductivity) can be enhanced by the incorporation of chemical modifiers such as carbon nanomaterials, metal nanoparticles or conducting polymers giving rise to the so-called hybrid silica materials [214,215]. Particularly, conducting polymers are very interesting components for several applications because of their tuneable properties. For example, polyaniline can be grown through porous sol–gel silica films by electrochemical reactive insertion. Silica favours the fast growth of polymer due to confinement effects of oligomeric species formed upon oxidation [216]. These silica–PANI hybrids show enhanced electrochemical capacitance, since silica matrix avoids the electric collapse between vicinal conducting fibres but allow the diffusion of ionic species in contact with the conjugated polymer [210]. The modulated permselectivity of silica for electroactive species turns into an ability to discern between positively and negatively charged species and, accordingly, this material can be used as preconcentration agent in electrochemical sensing [217]. The improved electrochemical properties of silica-conducting polymer hybrids were used to develop electrodes for direct electrochemistry of cytochrome c, cyt c, encapsulated within a silica film. The electrochemical insertion of poly(3,4-ethylenedioxythiophene) doped with poly-(styrenesulfonate), PEDOT–

PSS, through the silica pores connects electrically protein molecules, giving rise to a 3-fold enhancement in the cyt c electrochemical reduction rate [213]. This material has been also employed in sensor devices because of its outstanding properties. For example, organic PEDOT-based electrochemical transistors were used for the simultaneous detection of glucose and lactate [218] and voltammetric sensors based on the same material were used to determine neurotransmitters [219] glucose [220] or cytochrome c [221] in aqueous medium.

PEDOT-PSS is commercially available in the form of suspensions for a straight forward surface modification. However, it can be deposited on suitable electrodes by electrochemical polymerization for a better control of the film properties (morphology, thickness, etc.). Since the solubility in water of EDOT monomer is rather low, the addition of a surfactant is usually required. We will make use of PSS, which acting also as a polyelectrolyte, provides sufficient ionic conductivity to the aqueous solution. After electrochemical deposition, PSS remains within the structure of polymeric PEDOT as the doping agent [222].

PEDOT can be applied as the transducer element of biosensors where oxygen-containing species, such as peroxides, can act as mediators for the charge transfer from redox enzymes [223,224]. Additionally, this polymer has been used to develop second-generation biosensors that incorporate redox species as mediators (quinones, ruthenium complexes, ferrocene, ferricyanide, etc.) to perform the electron transfer.

Among the available redox mediators, ferrocene derivatives received attention. Ferrocene is commonly classified as an outer-sphere redox probe, which is considered to lack any adsorption step and to show low reorganization energies upon redox transitions [225]. For those reasons, ferrocene has been used routinely to investigate electron transfer kinetics in chemically modified electrodes [226,227]. Besides, ferrocene has been employed in the development of efficient biosensors [228,229] and also to induce electron transfer from PEDOT films to glucose oxidase or horseradish peroxidase, among other enzymes [230,231].

The present work focuses on the electrochemical synthesis of modified electrodes containing PEDOT-PSS films and their application to the study of ferrocene redox reactions. In this way, the electrocatalytic performance of PEDOT-PSS modified electrodes will be tuned by inserting this conducting polymer within electrodeposited silica matrices and, afterwards, the electrochemical performance of the hybrid material will be explored for ferrocene redox

processes. All the electrode modifications will be performed, exclusively, by electrochemical methods.

3.2. Experimental part

Reagents used in this work were tetraethyl orthosilicate (TEOS, Sigma-Aldrich, reagent grade), ethanol (EtOH) (Sigma-Aldrich, p.a.), potassium chloride (Merck, p.a.), hydrochloric acid (Merck, reagent grade), sulfuric acid (Merck, p.a.), 3,4-ethylendioxythiophene (EDOT) (Sigma-Aldrich 97%), poly(sodium 4-styrenesulfonate) (PSS) (Sigma- Aldrich p.a.) and ferrocene (Sigma-Aldrich, p.a.).

All solutions were prepared with purified water obtained from an ELGA Lab Water Purelab system (18.2MΩ cm). Electrochemical experiments were performed in conventional electrochemical glass cells. The working electrode was a glassy carbon rod (GC, geometric area=0.07 cm2, Carbone Lorraine, model V-25). The current densities expressed are referred to that geometric area. The GC electrode was carefully polished with emery paper and subsequently rinsed with ultrapure water. A platinum wire was employed as counter electrode, and a reversible hydrogen electrode introduced in the same electrolyte solution placed in Luggin capillary was used as reference electrode. Electrochemical experiments were performed with an eDAQ Potentiostat (EA163 model) coupled to a EG&G Parc Model 175 wave generator and the data acquisition was performed with a eDAQ e-corder 410 unit (Chart and Scope Software).

EDOT electropolymerization was carried out in aqueous medium prepared by dissolving 1.46 g PSS in 10.0 mL ultrapure water, 53 μL EDOT monomer were then added and the resulting solution was stirred in an ultrasonic bath for 30 min.

The precursor solution to synthesize silica was 6 mL of TEOS (0.0269 mol), 8.2 mL of EtOH and 5.8 mL of a solution 0.01M HCl+0.46M KCl (this salt was added to provide conductivity to the solution). This mixture was stirred for one hour in a close vial. The silica was obtained by electrochemical methods on glassy carbon (GC) rods. The electrode was immersed in that solution and connected to the negative terminal of a power source. A constant current of −2.5 mA cm^{-2} was applied to trigger the reduction of water and an increase in the pH near the electrode, causing the transition of silica to gel. This current was applied for 1 min. A Pt wire was used as the anode in this set-up. After silica deposition on GC, the electrode was rinsed with ultrapure water and kept humid (in hydrogel state).

The surface morphology of modified glassy carbon electrodes was studied by field-effect scanning electron microscopy (FESEM, ZEISS model Merlin VP Compact). X-ray photoelectron spectroscopy (XPS, KALPHA, Thermo Scientific) was used to analyse the surface composition. All spectra were collected using Al K radiation (1486.6 eV), monochromatized by a twin crystal monochromator, yielding a focused X-ray spot (elliptical in shape with a major axis length of 400 μm) at 3 mA×12 kV. The alpha hemispherical analyser was operated in the constant energy mode with survey scan pass energies of 200 eV to measure the whole energy band and 50 eV in a narrow scan to selectively measure individual elements. XPS data were analysed with Avantage software. A smart background function was used to approximate the experimental backgrounds, and surface elemental compositions were calculated from background-subtracted peak areas. Charge compensation was achieved with the system flood gun that provides low-energy electrons and low-energy argon ions from a single source. The experimental curves were adjusted using a combination of Lorentz (30%) and Gaussian (70%) functions.

3.3. Results and discussion

3.3.1. Electrochemical synthesis of PEDOT-PSS films

Figure3.1 shows cyclic voltammograms recorded for a glassy carbon (GC) electrode in the course of EDOT monomer oxidation in aqueous solution containing PSS as the electrolyte.

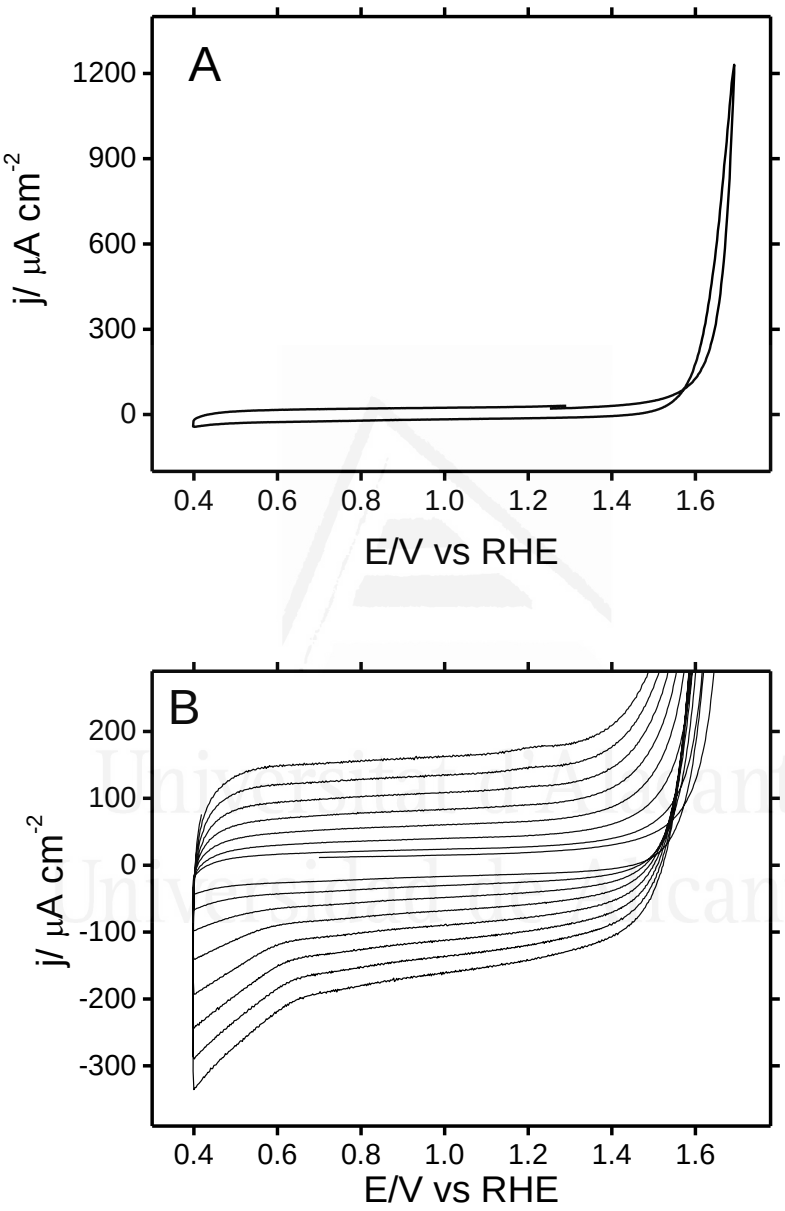

Figure3.1.(A) First cyclic voltammogram (B) Successive cyclic voltammograms obtained for a GC electrode in EDOT aqueous solution containing PSS. Scan rate50 mVs^{-1}.

During the first forward scan, the current density is almost zero within the potential region comprised between 0.4 and 1.5 V. The monomer oxidation starts at around 1.6 V and proceeds with fast electrochemical kinetics, as deduced from the high slope of the *j-E* curve.

In successive potential cycles, the progress of a current plateau between 0.4 V and 1.5 V reveals the capacitance-like response of the deposited PEDOT-PSS film, while the polymer mass can be readily determined at any time from its double-layer charge, assuming a value of 70 F g^{-1} for the specific capacitance [213,232].

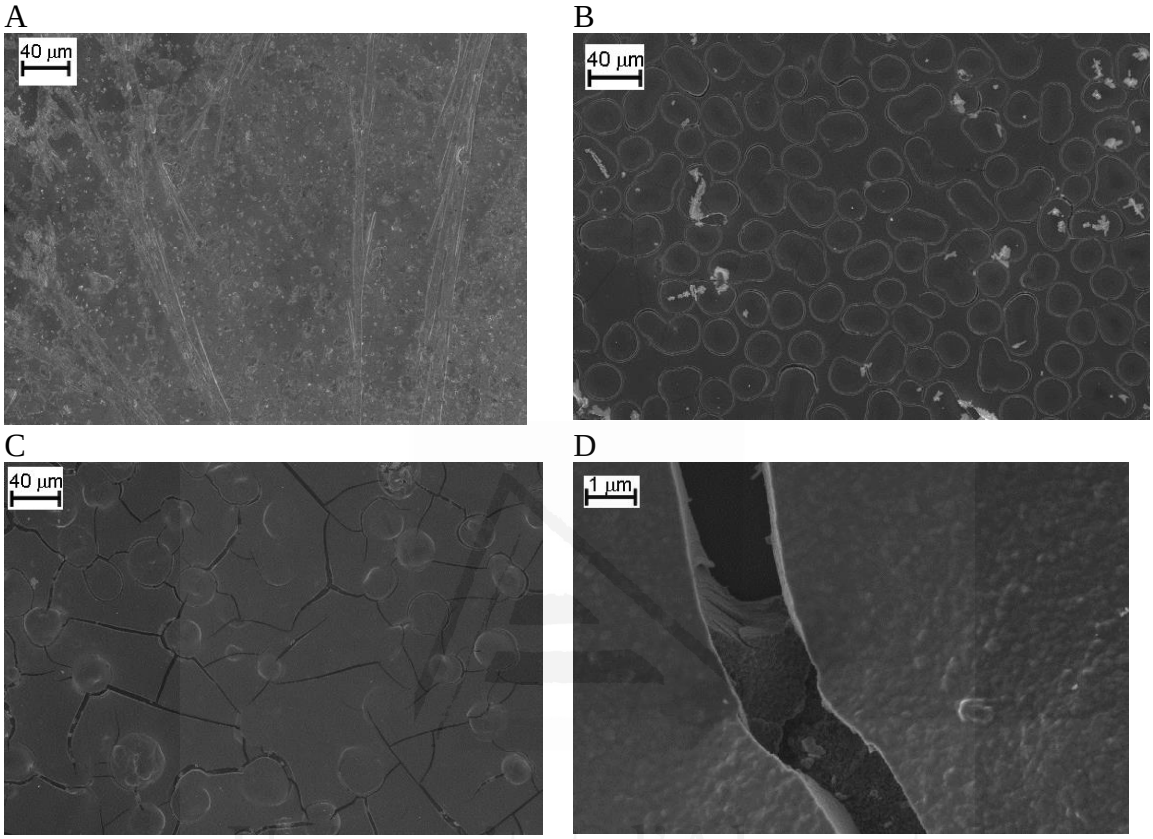

Figure 3.2. FESEM images of PEDOT-PSS films deposited on GC electrodes. Mass of polymer: (A) 46.5µgcm^{-2}; (B) 202µgcm^{-2}; (C)and(D)815µgcm^{-2}

The surface morphology of deposited PEDOT-PSS films was examined with the aid of a field emission SEM device. Figure 3.2 shows micrographs obtained for different electrodes with increasing mass of deposited polymer ranging between 46.5 and 815 µg cm^{-2}. All films cover uniformly the whole surface of the GC substrates, although they can be observed more clearly when larger amounts of polymeric material are deposited (Fig. 2B–D). Some crack-like defects, particularly those appearing in Figure3. 2C and D, are generated by the drying process. It is worth mentioning that the surface homogeneity of these PEDOT-PSS films contrasts with some literature data. For example, it was reported either a granular aspect when the material is deposited from organic solvents[233] or an aggregated, cauliflower-like, structure when it was deposited from aqueous solutions on gold substrates [234]. The favourable interaction between

carbon support and polymer layer seems at the origin of the smoother morphology shown by our samples.

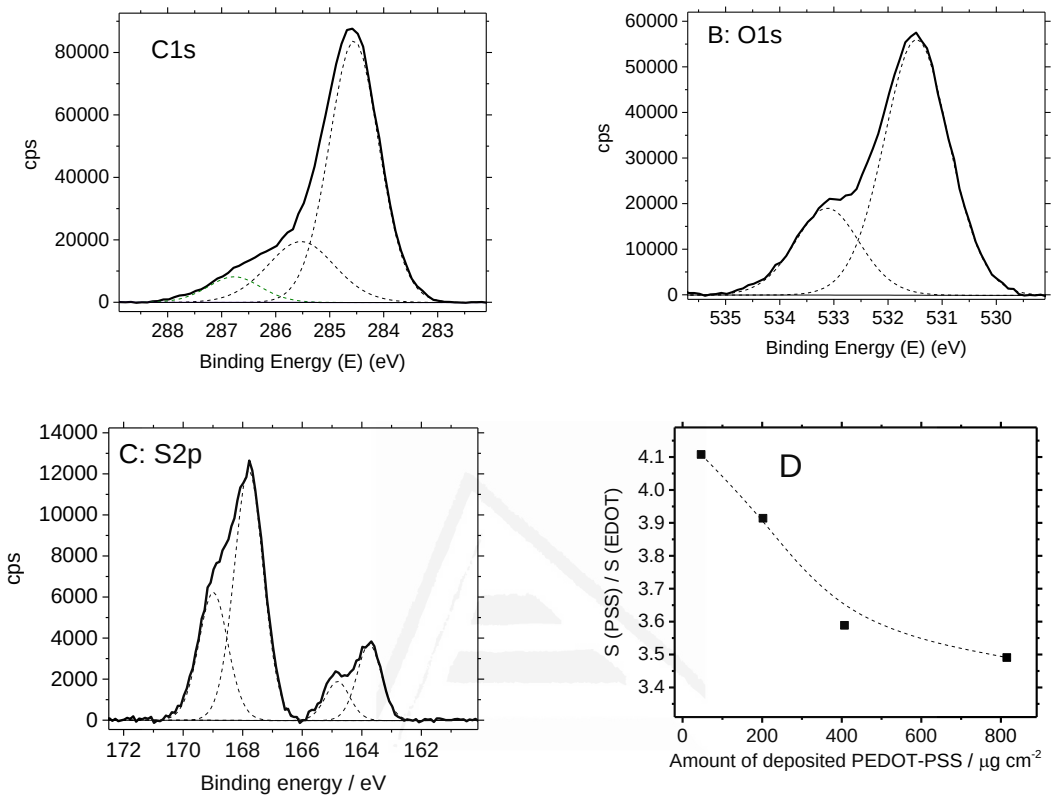

Figure3.3. High resolution XPS spectra acquired for: (A) C1s region; (B) O 1s region and (C) S 2p region of a PEDOT-PSS film (202μgcm^{-2}) deposited on GC. (D) Sulfonate-to-EDOT ratio obtained from the S $2p_{3/2}$ signals for electrodes covered with different amounts of deposited PEDOT-PSS.

High resolution X-ray photoelectron spectroscopy (XPS) has been employed to characterize the chemical structure of PEDOT-PSS coatings. A glassy carbon electrode covered with a mass of deposited polymer close to 202 μg cm^{-2} (as in Fig. 3.2B) was transferred to the UHV chamber, where C, O and S spectral regions were analysed. The recorded C 1s core level spectrum is depicted in Figure 3.3A, where three main contributions at 284.5, 285.5 and 286.8 eV can be clearly distinguished. The peak at lower binding energy corresponds to carbon located either in

the aromatic backbone of PEDOT or at the phenyl moieties of PSS. Besides, the contribution at 285.5 eV is originated from C atoms directly bound to S atoms, as those present in both EDOT and PSS units. Finally, the high energy element at 286.8 eV can be assigned to C-O-C structures present at EDOT moieties [235–237].

Regarding the O 1s signal (Figure 3.3B), it can be deconvoluted into two major contributions at 531.5 and 533.1 eV. The peak at lower binding energy is consistent with the presence of PSS sulfonate groups [236], whereas the 533.1 eV peak relates to those oxygen atoms present at the dioxyethylene bridge in EDOT units and also to a high binding energy contribution of PSS [238].

Finally, the S 2p region of the photoelectronic spectrum is shown in Figure 3.3C. It is characterized by the presence of two major bands corresponding to sulphur species with different oxidation states. Both signals can be deconvoluted into two contributions, showing a characteristic separation between the $2p_{3/2}$ and $2p_{1/2}$ spin-split doublets of 1.18 eV. The low-energy signal, with an S $2p_{3/2}$ contribution at 163.8 eV, is assigned to sulphur atoms located at the thiophene rings in EDOT monomers. Besides, the S $2p_{3/2}$ contribution to the higher binding energy signal (167.9 eV) is attributed to sulphur in a higher oxidation state, which corresponds to those sulfonate groups contained in the PSS dopantanion[236,238,239].

From the ratio of both S2p signals, the sulfonate to thiophene proportion in any sample of electrodeposited polymer can be conveniently obtained. Such a proportion was calculated for a number of samples and plotted against the amount of deposited polymer in Figure 3.3D. The plot suggests an excess of PSS dopant content for extremely thin samples (up to 4.1 S atomic ratio) and the occurrence of a progressive depletion of polyelectrolyte ions for films with higher amount of deposited polymer.

3.3.2. Electrochemical behaviour of ferrocene at unmodified PEDOT-PSS films

We will examine first the electrocatalytic performance of pristine PEDOT-PSS films toward a typical redox mediator as ferrocene. For comparative purposes, the electrochemical activity of a bare glassy carbon electrode has also been included in the study (Figure3.4A). The electrochemical oxidation of the ferrocene redox centre, $Fe^{2+} \rightarrow Fe^{3+}$, at GC substrates is characterized by the presence of a reversible anodic peak centred at 0.515 V in acidic medium.

The faradic counter-process occurs at 0.385 V during the reverse scan. As a result, the peak separation between anodic and cathodic features, ΔE_P, is 130 mV under the experimental conditions employed.

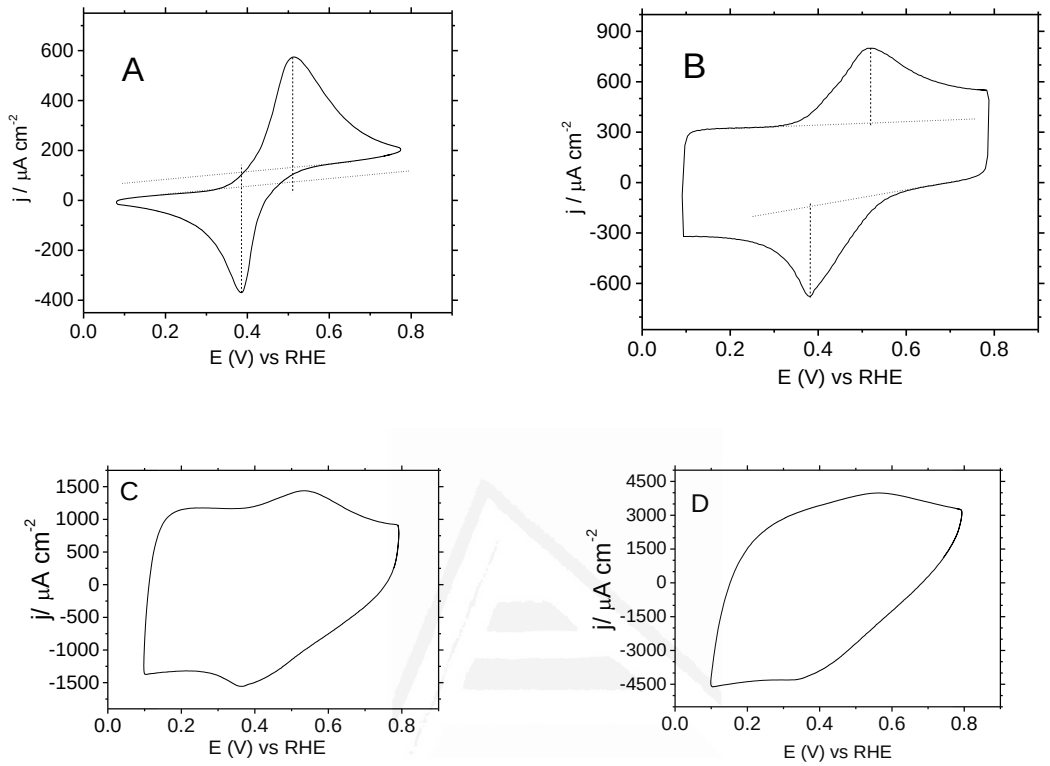

Figure 3.4. Steady-state cyclic voltammograms obtained in 1 mM ferrocene aqueous solution for a bare GC electrode (A) and for increasing amounts (46.5, 202 and 815 μgcm−2) of PEDOT-PSS deposited on GC substrates (B–D). Background electrolyte 0.5 M H_2SO_4 in all cases. Scan rate 100 mVs^{-1}.

The activity of PEDOT-PSS against the same redox probe can be observed in Figure3.4B–D. A current plateau whose shape resembles a double-layer charging current appears between 0.1 V and 0.3 V on the CV of the 46.5 μg cm^{-2} PEDOT-PSS film (Figure 3.4B). This featureless potential region is followed by the onset of ferrocene oxidation at 0.3 V and then by the associated anodic peak centred at 0.518 V. In the reverse scan, the faradaic counter-process appears at 0.382 V giving rise to a peak separation close to 136 mV. Figure 3.4C and D shows similar experiments performed for higher amount of deposited polymer. Current densities coming from PEDOT-PSS, below 0.3 V, increase at increasing amounts of deposited polymer.

However, the redox peaks related to electron transfer from ferrocene seem progressively hindered, suggesting that PEDOT-PSS is a poor electrocatalytic material for this redox probe.

Further analysis was performed over the voltammetric results to evaluate the kinetics of the electron transfer across the polymer. The kinetic reversibility of the electrochemical reaction was evaluated from peak separation of the redox process of the cyclic voltammetry experiments by applying either the method of Nicholson [240] (see the annex to chapter 3 and Ref. [217] for more details). In such experiments, stabilized cyclic voltammograms for bare GC electrodes and PEDOT-PSS films immersed in test solutions containing ferrocene were obtained at different scan rates ranging from 10 to 200 mV s^{-1}. The values of peak separation for a scan rate of 100 mV s^{-1} are shown in Figure 3.5A.

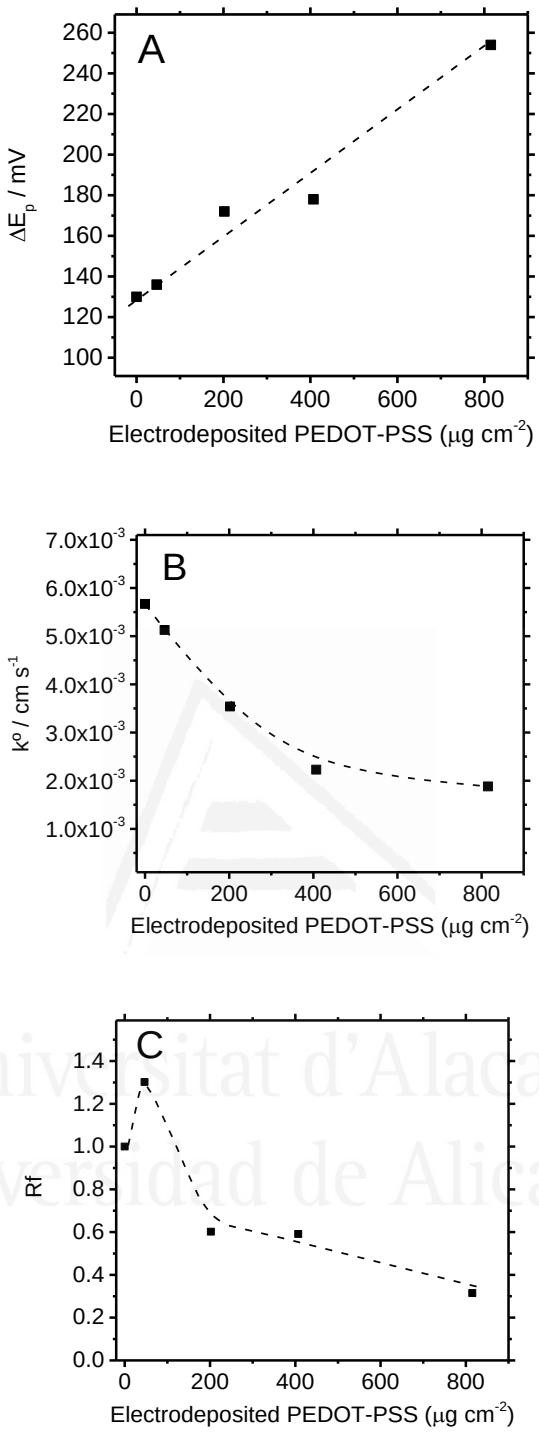

Figure 3.5. (A) Voltammetric peak separation, (B) heterogeneous rate constant for the electron transfer to ferrocene, ko, at bare GC electrodes and at PEDOT-PSS films (C) roughness factor, Rf, obtained from the ratio between the electroactive area for the electron transfer and the surface geometric area (Data obtained from the kinetic study presented in the annex to chapter 3).

From the kinetic study it is derived that the standard heterogeneous rate constant for the charge transfer to ferrocene is $k° = 5.67 \times 10^{-3}$ cm s^{-1} for bare GC electrodes, while for PEDOT-PSS films are presented in Fig. 3.5B. The trend is that the rate of electron transfer decays at higher amounts of deposited PEDOT-PSS films up to a value close to $k° = 2 \times 10^{-3}$ cm s^{-1}. This result confirms that unmodified PEDOT-PSS is a poor electrocatalyst to oxidize ferrocene. Another relevant parameter that can be obtained from Randles-Sevcik plots is the true active area available for the electron transfer to the redox probe. Such a parameter can be evaluated through the roughness factor of the electrode, R_f, which represents the ratio of electroactive area that transfers charge effectively to the redox probe to the geometric area [217,241]. Figure 3.5C shows R_f factors calculated for the reaction of interest at each electrode. As observed, an extremely thin PEDOT-PSS film shows even higher electroactive area than bare GC surfaces. However, increasing the amount of polymer results in a gradual loss of the active area up to values below a half of the geometric area.

These results can be explained in the light of FESEM and XPS characterizations performed above. On the one hand, the surface of electrodeposited polymer films appeared very smooth which implies a low roughness factor. This is probably due to the plasticizer effect induced by PSS in addition to the soft conditions used for the synthesis (potentiodynamic polymerization at moderate scan rate). On the other hand, XPS results have shown that the relative content of PSS anionic dopant, and consequently the doping level, is influenced by the mass of electrodeposited polymer. The higher the amount of deposited polymer, the lower the doping level. This trend means that films with higher amount of polymer show probably less conductivity, which could disturb their electrocatalytic performance against the redox probe.

3.3.3. Electrochemical behaviour of ferrocene at hybrid silica PEDOT-PSS electrodes

It is known that chemically modified, porous SiO_2 matrices possess the ability of improving the kinetics of several electrochemical reactions [212,217,242]. This effect is achieved thanks to the particular environment provided by silica pores, which can rearrange electroactive molecules, change their diffusion transport properties and even stimulate favourable, or adverse, electrostatic interactions. In this section, we will try to modify the activity of PEDOT-PSS toward the oxidation of ferrocene by inserting the polymer through a three-dimensional silica matrix deposited previously on the GC surface [212].

After silica was deposited on GC, the electrode was rinsed with ultrapure water and kept humid (in hydrogel state) to be immersed in an aqueous solution containing both EDOT and PSS under experimental conditions similar to those in Figure 3.1. The polymer was deposited potentiodynamically until a capacitance of 14.1 mF cm^{-2} was reached. On a flat GC surface such a capacitance value corresponds to a PEDOT-PSS mass density close to 202 μg cm^{-2}. [232] However, when the polymer is grown within the silica template, those 14.1 mF cm^{-2} means that equivalent amounts of electroactive material have been deposited.

We should focus first on the morphology of such electrochemically deposited SiO_2 layer, which is shown in Figure 3.6A and B at different magnifications. The deposit looks homogeneous all over the surface, with randomly distributed pores showing an approximate diameter of around 2 μm. The granular structure that can be distinguished in the magnified micrograph (B) comes from the aggregation of silica colloids upon deposition.

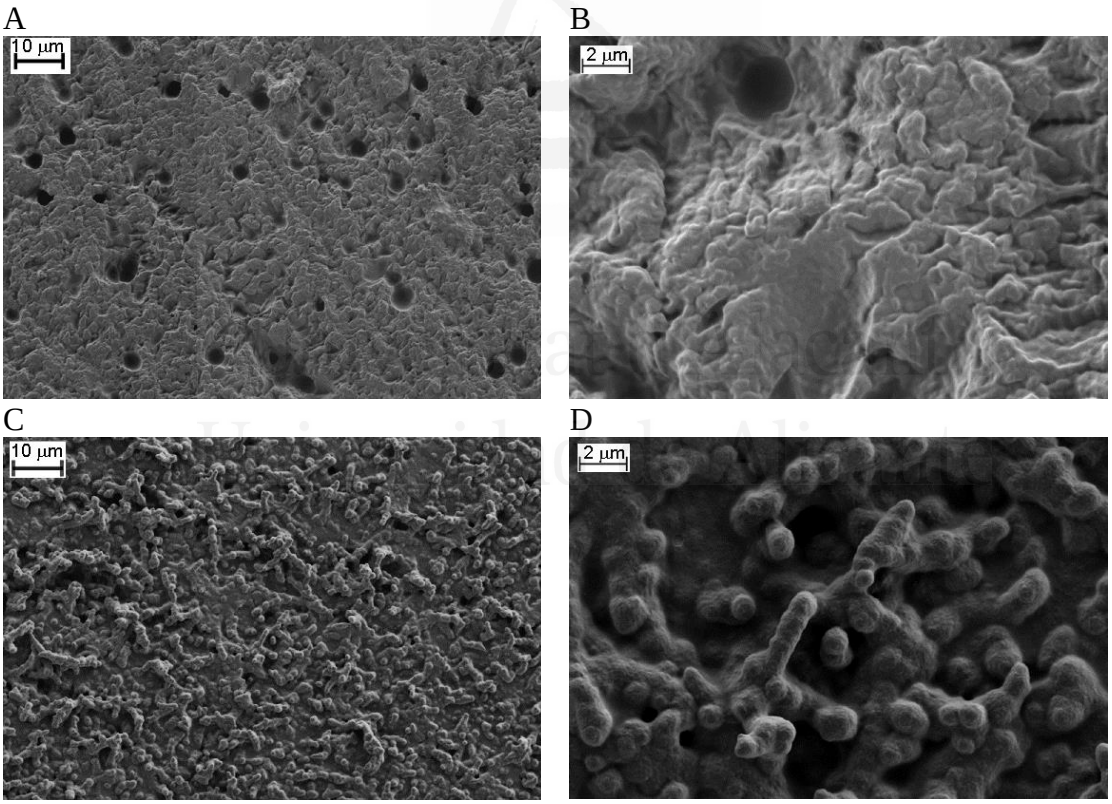

Figure3.6.A and B: FESEM images of silica-modified electrodes prepared by electrodeposition. C and D: Hybrid silica-PEDOT-PSS modified electrodes.

Figure 3.6C and D were obtained after the electrochemical polymerization of EDOT through the silica pores shown in the previous images. The resulting hybrid silica-PEDOT-PSS electrode shows rounded edge, broad (near one micron) dendritic structures, which provide the modified sample with an aspect quite different to the smoother, unmodified polymer films shown in Figure 3.2. These striking architectures are formed by PEDOT-PSS emerging from the silica material (which can be discerned as a flat surface behind the dendrites) and their particular shape is a consequence of the patterned growth of the polymer forced by the three-dimensional hollow structure of SiO_2. The hybrid material was also characterized by XPS spectroscopy and the results are shown in Figure 3.7.

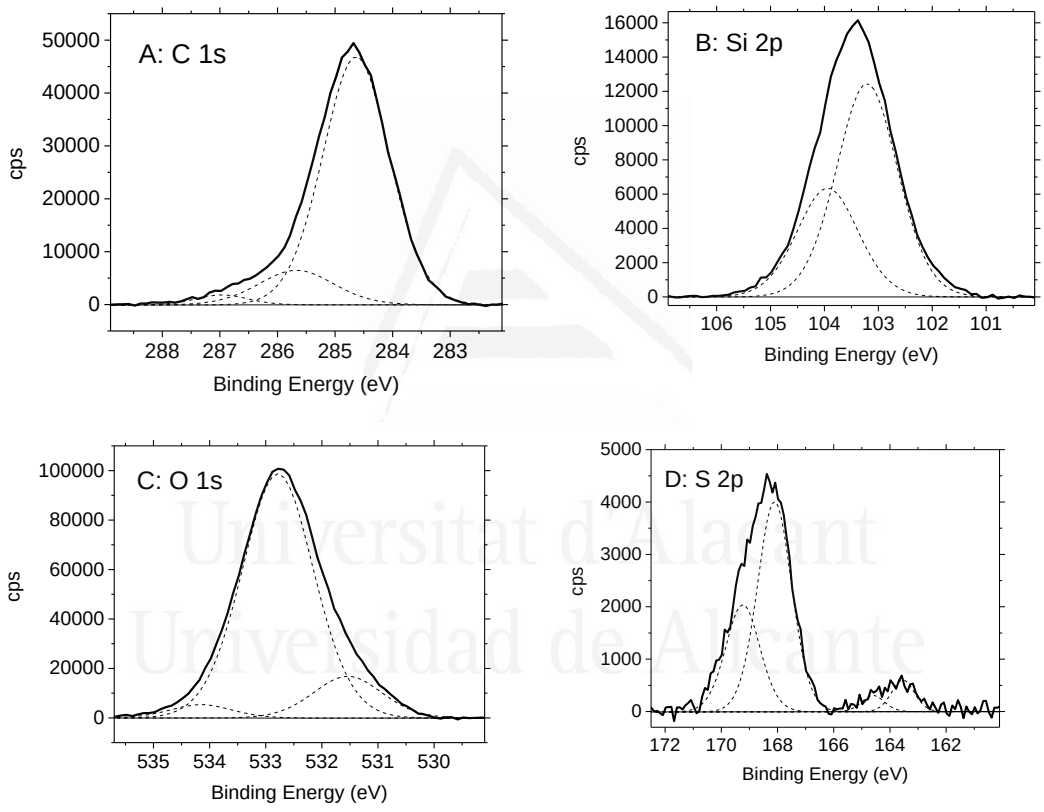

Figure3.7. High-resolution XPS spectra obtained for: (A) C 1s region; (B) Si 2p region; (C) O 1s region and (D) S 2p region of hybrid silica-PEDOT-PSS film (14.1 mF cm^{-2}) deposited on a glassy carbon substrate.

The C1s core level spectrum shown in Figure 3.7A presents the three main features at 284.5, 285.5 and 286.8 eV already observed for unmodified PEDOT-PSS films in Figure 3.3A. They are assigned, respectively, to aromatic carbon in both PEDOT and PSS, C atoms bound to S

atoms and C-O in EDOT units. Figure 3.7B shows the binding energy region at around 103 eV, which reveals the presence of oxidized silicon atoms on the surface, SiO_x ($x > 1.8$) [243–245]. The presence of both C and Si signals in the outer surface (with a C/Si atomic ratio close to 2.7) supports the occurrence of an interpenetrating hybrid material. The O 1s region in Figure 3.7C shows three major contributions at 531.5, 532.8 and 534.2 eV. The peak at lower binding energy corresponds to the sulfonate groups of PSS [236], while the main feature at 532.8 is attributed to inorganic O bound to Si atoms of the silica matrix [246,247]. The higher binding energy peak corresponds to both, oxygen in the dioxyethylene bridge of EDOT units and the high binding energy contribution of PSS [238].

The chemical composition of a PEDOT-PSS polymer grown across the silica matrix can be investigated by exploring the S 2p region in Figure 3.7D. The presence of two major signals corresponding to different sulphur species allows the doping level of the polymer to be quantified, as it was done in Figure 3.3C. The low energy signal comes from sulphur atoms located at EDOT centres while the higher binding energy peak is attributed to sulphur in PSS. In this case, the atomic ratio of sulphur in PSS to sulphur in EDOT is 10.0. Such a large value reveals that the doping level of this polymer is significantly higher than any of the films deposited on bare GC surfaces. Therefore, it is necessary to establish whether or not a higher doping level means in practice better electrocatalytic performance to transfer charge to ferrocene.

According to such strategy, Figure 3.8 shows two cyclic voltammograms recorded in 1 mM ferrocene solution. The dotted line was obtained for a 202 μg cm^{-2} PEDOT-PSS film deposited straight on the bare GC surface while the solid line was recorded with a silica-PEDOT-PSS hybrid material containing the same amount of electroactive polymer inserted within the SiO_2 pores.

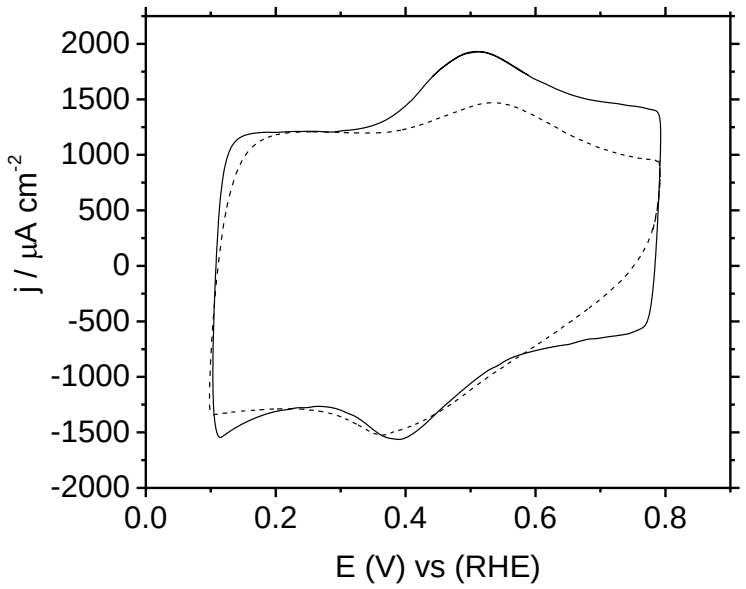

Figure 3.8. Steady-state cyclic voltammograms recorded in 1 mM ferrocene with two different electrodes. Solid line: a hybrid material silica-PEDOT-PSS obtained by electropolymerization of EDOT on a GC previously modified with a layer of silica. Dotted line: an unmodified PEDOT-PSSfilm deposited on bare GC. The same amount of electroactive PEDOT-PSS was incorporated at both electrodes. Background electrolyte 0.5 M H_2SO_4. Scan rate 100 mV/s.

Since the amount of electroactive PEDOT-PSS sites is the same, both CVs present similar pseudo-capacitive currents below 0.3 V. However, the major difference arises in the potential region for the electron transfer to the redox probe. The anodic peak associated to ferrocene oxidation appears at 0.514 V for the hybrid material. Since the faradic counter-process is centred at 0.388 V, the peak separation becomes $\Delta E_P = 126$ mV. Such a value is significantly lower than those 172 mV obtained for the polymer deposited on bare GC (dotted line). According to the procedure described in the annex to chapter 3, it was determined that the standard rate constant for the charge transfer at the hybrid electrode was $k° = 6.02 \times 10^{-3}$ cm s^{-1}. This figure means that the electron transfer rate almost doubles that measured in the absence of a silica matrix, which according to Figure 3.5A approaches to $k° = 3.6 \times 10^{-3}$ cm s^{-1}. Apart from the improvement in the charge transfer kinetics, it deserves also attention the alteration of the electroactive area in PEDOT-PSS caused by the silica matrix. Making use of the Randles-Sevcik equations at different scan rates the electroactive area for ferrocene oxidation on a

modified polymer gives a value close to $R_f = 2.31$, which is almost four times that obtained for a pristine PEDOT-PSS (Figure 3.5B).

3.4. Conclusions

PEDOT-PSS can be electrodeposited on bare GC surfaces from aqueous solutions containing EDOT monomer in the presence of PSS anions. After electropolymerization, XPS revealed an excess of PSS dopant for extremely thin samples and a progressive depletion of these polyelectrolyte ions as the amount of deposited polymer increases. The unmodified PEDOT-PSS material is a poor electrocatalyst toward the oxidation of ferrocene. Indeed, it has been found that the electron transfer rate decays progressively as the amount of polymer deposited increases.

The modest electrochemical performance of pristine PEDOT-PSS films can be overcome by growing the polymer through a silica matrix deposited previously on the GC surface. Contrary to the smooth surface of unmodified PEDOT-PSS films, the organic-inorganic hybrid material exhibits three-dimensional structures, as a result of the patterned growth. The electron transfer constant for ferrocene oxidation almost doubles when the electrochemical reaction takes place on this modified polymer and, in addition, the doping level of PEDOT multiplies by a factor of three those found for films of similar electroactive mass deposited on bare GC surfaces. Such an effect is accompanied by a significant increase in the true active area available for the electron transfer to the redox probe.

3.5 Annex to chapter 3

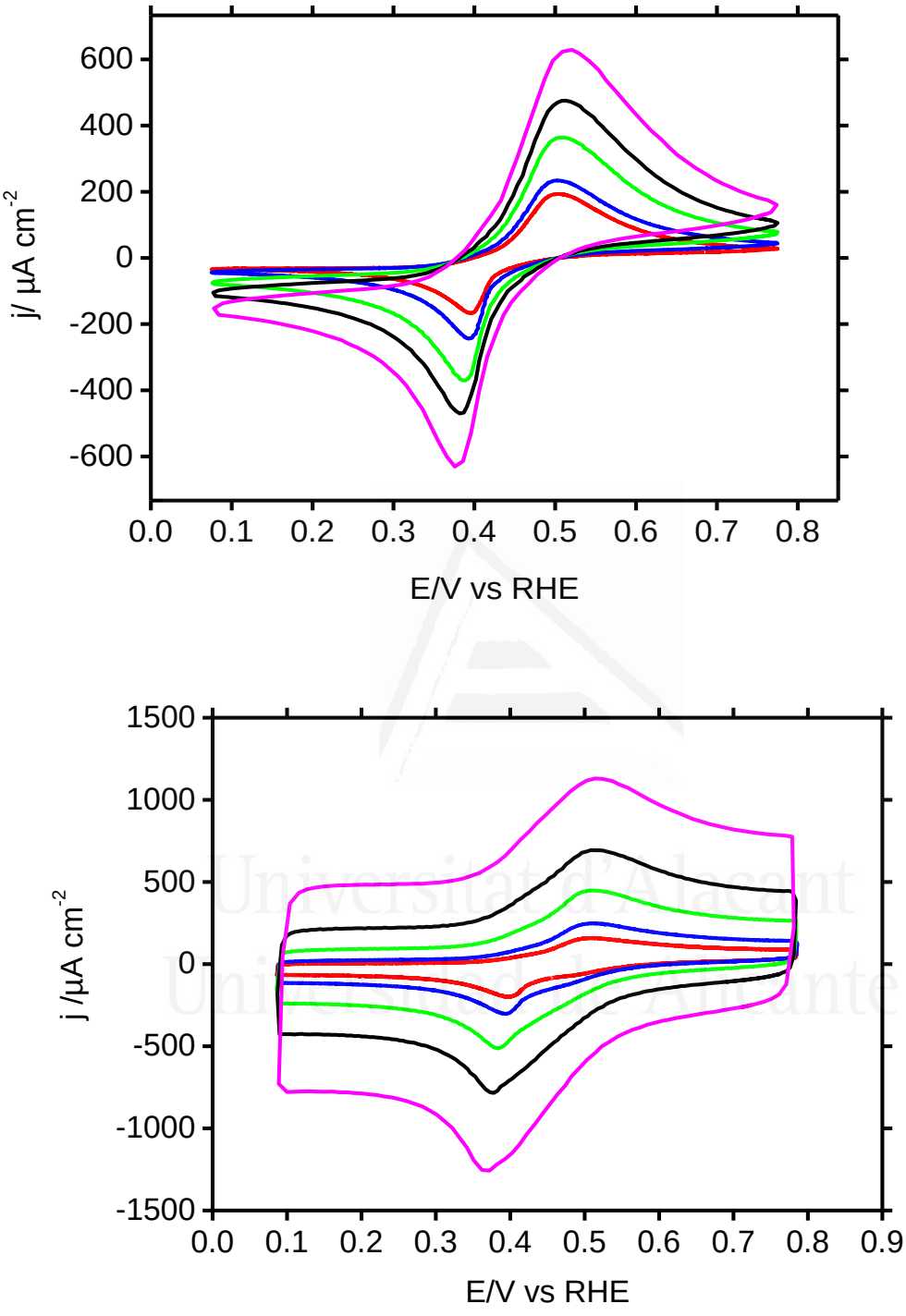

Figure S1: Stabilized cyclic voltammograms of a test solution containing ferrocene (1 mM) at different scan rates: 10, 20, 50, 100 and 200 mV s^{-1}. (A) Bare GC (B)PEDOT-PSS (46.5 µg cm^{-2}) modified electrode.

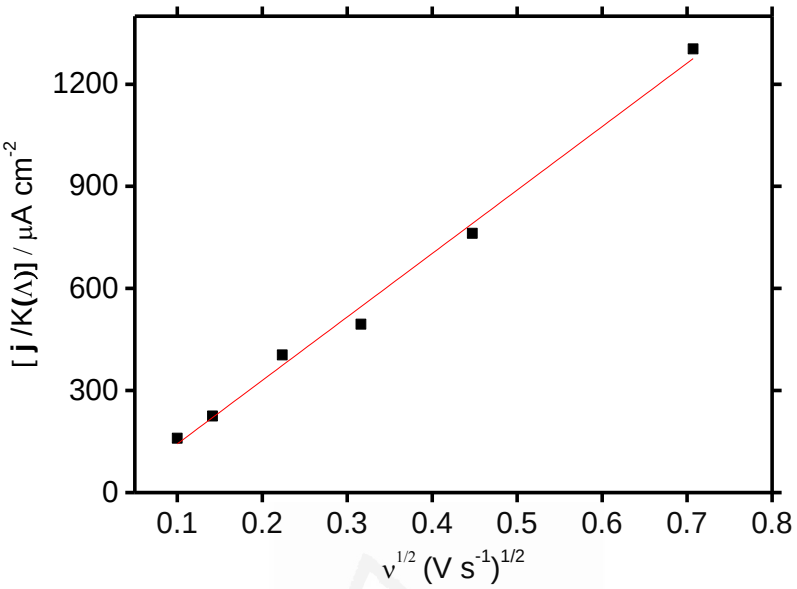

Figure S2: Randles–Sevcik plot obtained with the corrected value of current from sets of CV recorded at different scan rates for the redox probe ferrocene. (A) for bare glassy carbon electrode; (B) GC/PEDOT-PSS (4.65×10^{-5} g cm^{-2}) electrode

Voltammetric data were analyzed assuming that: i) both the oxidized and the reduced forms of ferrocene show similar diffusion coefficients, and ii) the energy barriers for the electron transfer are symmetrical, which means $\alpha \sim 0.5$.

The kinetic reversibility of the electrochemical reaction can be evaluated from cyclic voltammetry experiments through the dimensionless parameter ψ, which is obtained from ΔE_P by applying either the method of Nicholson [1,2] or the approach of Mahé et al. [3]. The reversibility of an electrochemical system can also be characterized by means of the so-called equivalent parameter, Λ, which depends linearly on ψ in the following way [4]:

$$\Lambda = \psi\sqrt{\pi} \qquad (1)$$

Particular values of Λ for the oxidation of ferrocene on bare GC at different scan rates are presented in Figure S3.

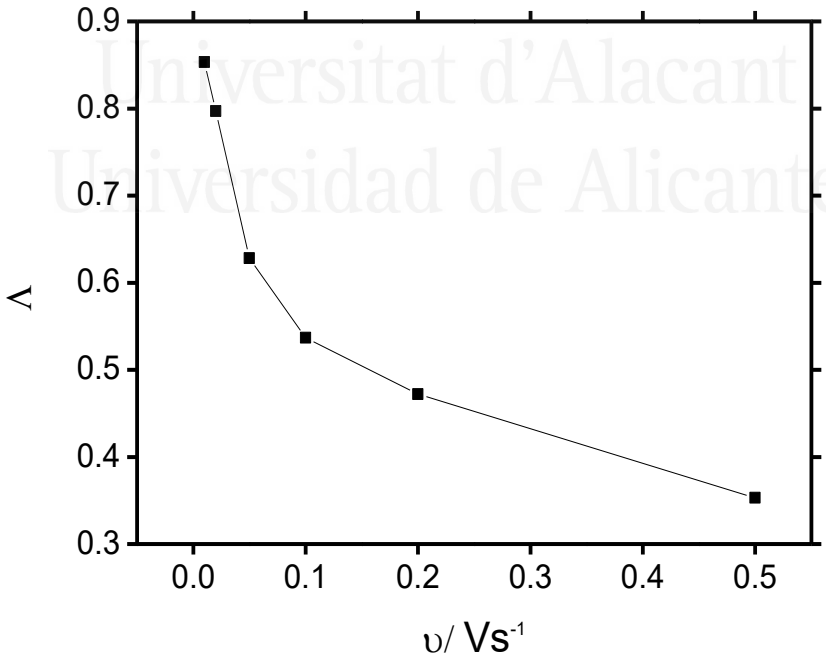

Figure S3: Values of Λ at different scan rate for ferrocene redox probe with a GC electrode.

They range between 0.85 and 0.35, which means the electrochemical reaction is kinetically quasireversible for the scan rates investigated. Usually, the standard rate constant for the electron transfer, k^o, is derived from Λ according to the following expression:

$$\Lambda = k^0 \left(\frac{RT}{nFDv}\right)^{1/2} \qquad (2)$$

where the diffusion coefficientof ferrocene, *D*, must be known. Fortunately, it can be evaluated from Randles-Sevcik plots (Figure S2B):

$$I_p(rev) = 2.687 \times 10^5 ACn^{3/2}(Dv)^{1/2} \qquad (3)$$

In this relation, $I_p(rev)$ is the current for a reversible redox process, *A* is the electrode area (0.070 cm^2), *C* the concentration of ferrocene (10^{-3}mol cm^{-3}), *n* the electrons transferred (1) and υ the scan rate (in V s^{-1}). It is worth mentioning that the application of Eq. 3 to non-reversible systems can be done provided that the experimental peak current (I_p) has been transformed using the dimensionless parameter $k(\Lambda)$:

$$I_p(rev) = \frac{I_p}{k(\Lambda)} \qquad (4)$$

$k(\Lambda)$ values for the reaction of interest have been plotted against the scan rate in Figure S4. Ferrocene diffusion coefficient was calculated from the slope of the linear fit (D= 2.87×10^{-5} cm^2s^{-1}) and then used to quantify k^o from Eq.2

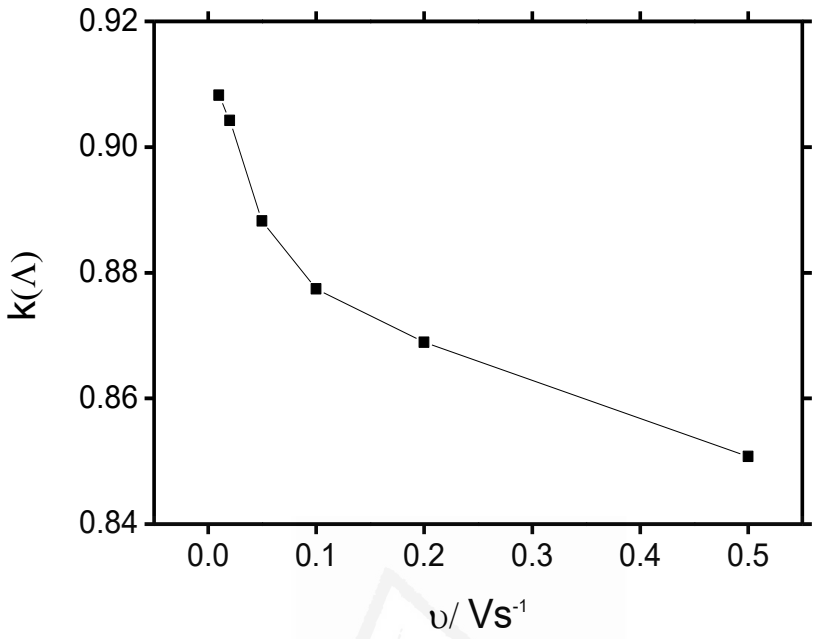

Figure S4: Values of *k(Λ)* at different scan rate for ferrocene redox probe with a GC electrode.

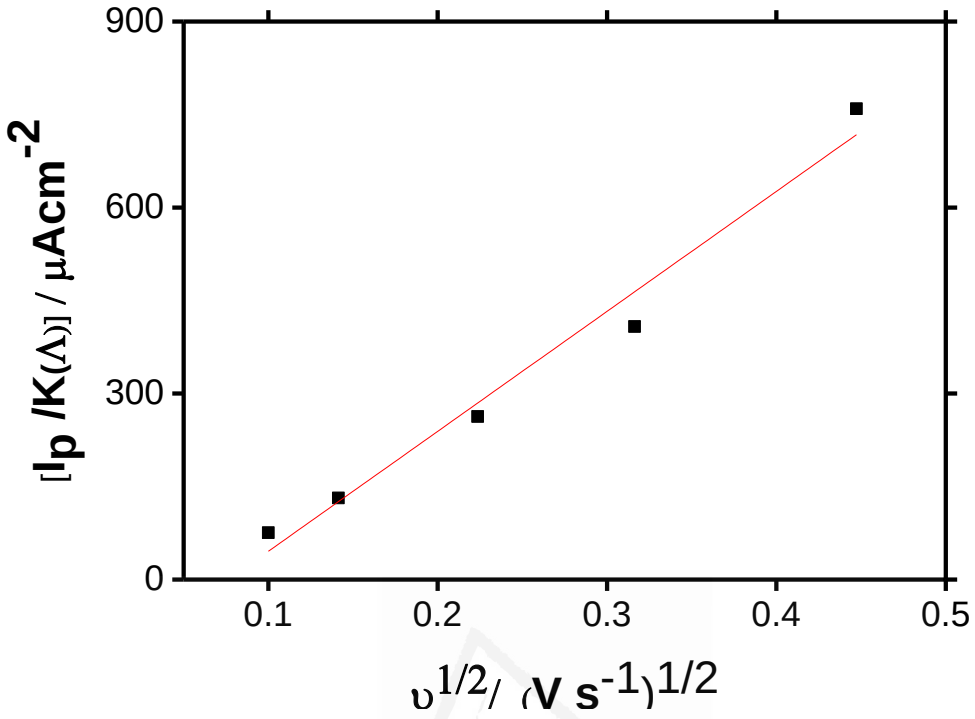

Figure S5: Randles–Sevcik plot obtained with the corrected value of current density for bare glassy carbon modified with silica (150mCcm^{-2}) and 4.65×10^{-5}g cm^{-2} of PEDOT-PSS deposited immersed in a test solution containing ferrocene (in 0.5M sulfuric acid solution) at scan rate 100mV/s.

References for annex

[1] A.J. Bard, L.R. Faulkner, Electrochemical Methods: Fundamentals and Applications, Wiley, New York, 1980.

[2] T.J. Smith, K.J. Stevenson, C.G. Zoski, Handbook of Electrochemistry, First Edit, Elsevier, Amsterdam, 2007.

[3] E. Mahe, D. Devilliers, C. Comninellis, Electrochim. Acta 50 (2005) 2263–2277.

[4] H. Matsuda, Y. Ayabe, Zeitschrift Fur Elektrochemie 59 (1955) 494–503.

4. Electrochemical behavior of redox probes encapsulated in silica monoliths sol-gel: Platform for biosensor development

4.1. Introduction

We have synthesized monoliths of silica using sol-gel methodology. Two redox probes were encapsulated in the monoliths. The monolithic hydrogel has been used as electrolytic medium for an electrochemical cell, in contact with a screen-printed carbon electrode. This allowed the study of the electrochemical behavior of encapsulated ferro / ferricyanide and *p*-aminophenol probes. The electrochemical response of these probes in solution was compared with that obtained in the hydrogel.

The chemical character of silica was modulated by introducing organic functionalities (methyl, propyl, octyl and phenyl groups). The probe *p*-aminophenol was studied in these systems since this specie is the product generated by the enzyme alkaline phosphatase, which will allow us to develop biosensors based on this protein and its substrate (*p*-aminophenylphosphate). It has been shown that these proteins may be included within sol-gel matrices of silica and retain their activity within the monolith [248].

4.2. Experimental part

Reagents used in this work were tetraethyl orthosilicate (TEOS, 98%), ethanol (EtOH, 99.95%, *p*-aminophenol,ferro / ferricyanide $Fe(CN)_6^{-4/-3}$, trizma, methyl-triethoxlysilane (MTES, 99%), n-propyl-triethoxysilane (PrTES, 98%), octyl-trimethoxysilane (OTMS, 96%) andPhenyl-trimethoxysilane (PhTES, 98%), supplied all by Sigma-Aldrich.Hydrochloric acid (HCl, 37%) were supplied by Merck, reagent grade.

All solutions were prepared with purified water obtained from an ELGA Lab Water Purelab system (18.2MΩ cm).

As supporting electrolyte buffered solutions at pH 7 were used prepared with trizma (55mM).

Electrochemical experiments were performed with an eDAQ Potentiostat (EA163 model) and the data acquisition was performed with a eDAQ e-corder 410 unit (Chart and Scope Software).

As explained in chapter 2 to synthesize silica by the sol-gel method, two reactions were carried out, the first of which consists in the acid hydrolysis of the precursors. In the case of conventional silica (SC), 5.6 mL of TEOS (0.0251 mol), 7.6 mL of EtOH and 5.7 mL of a 0.01 M HCl solution are mixed and stirred for one hour with magnetic stirring in a close vial. EtOH acts as a co-solvent, and HCl as an acid catalyst. Once the hydrolysis was done, we have a metastable solution, known as sol, formed by silica colloids.

The hydrogel is formed between 10 and 20 seconds by while mixing half of precursor solution and half of redox probe solution, the redox probes encapsulated in silica monoliths sol-gel.

In addition to conventional silica, we can also synthesize organically modified silica (ORMOSIL). The precursor solutions of the different ORMOSIL were prepared following the same procedure used for conventional silica, but replacing part of the TEOS precursor with different concentration (1% -5% -10% and 20%) of the corresponding precursors modified with organic groups (trialkoxysilanes): methyl triethoxysilane (MTES), n-propyl-triethoxysilane (PrTES), octyl-trimethoxysilane (OTMS) and phenyl-triethoxysilane (PhTES). The total moles of silicon precursor were kept constant (0.0251 moles).

The enzyme ALP used, from Sigma-Aldrich, was in the form of lyophilized powder and came from bovine intestinal mucosa (Mw = 160 KDa). It was dissolved in Tris for later use.

The substrate used in the enzymatic reaction was *p*-aminophenylphosphate (10mM), from Sigma-Aldrich. It was dissolved also in Tris for later use.

For preparation of hydrolyzed TEOS, in a vial, a silica solution was prepared at room temperature, mixing TEOS (5.6 mL) with ETHANOL (7.6 mL) and 2.7 M HCl (0.01M). The solution, with two clearly differentiated phases, was vigorously stirred for approximately one

hour, time necessary for the TEOS to hydrolyze. The appearance of a single phase was used as a visual indicator to know that the hydrolysis had ended.

Rotation of the hydrolyzed TEOS, the objective of this phase was the complete elimination of the residual ethanol generated during the hydrolysis process, since it can negatively interfere with the immobilized biomolecules and in the proteins, induce a total or partial unfolding of their native conformation. The vial was then weighed with the solution on a scale and then subjected to vacuum roto-evaporation in the Rotavapor. After approximately 30 minutes the rotation was stopped and the vial was reweighed, in order to check if all the ethanol had been eliminated.

Manufacture of monoliths using the sol-gel technique, fall the existing enzymatic immobilization methods, the sol-gel process is one of the most used because of the many advantages it possesses. The monoliths obtained with it present, among other benefits, thermal and chemical stability, possibility of varying the number and size of its pores, stability of the biomolecules encapsulated in their interior, and resistance to the loss and desorption thereof.

Preparation of matrices with the ALP enzyme and the *p*-APP, once the rotated TEOS was obtained, 1 ml of this latter with 1 ml of solution of ALP and 1ml of solution of *p*-APP have been mixed, the mixture was stirred several times but carefully so as not to form bubbles. Following this protocol, gel formation occurred in approximately 15 minutes at room temperature and pressure.

Table 4.1: Molar fraction (expressed as moles of organic silicon precursor) divided by the total moles of silicon precursor in the organically modified precursor solutions, xR (total moles of silicon = 0.0251), theoretical composition of the gels, and acronym used in the present thesis.

Molar fraction $R–Si(EtO)_3$/total moles Si	Theoretical composition of the gel	Acronym
0	SiO_2	SC
0.01	$SiO_{1.995}R_{0.01}$	1R
0.05	$SiO_{1.975}R_{0.05}$	5R
0.10	$SiO_{1.95}R_{0.1}$	10R
0.20	$SiO_{1.9}R_{0.2}$	20R

To carry out the thermogravimetric analysis coupled to mass spectrometry (TG / MS) and infrared spectroscopy with Fourier Transform Transmission (FTIR) the silica was obtained by synthesizing in a cuvette, the silica was milled and dried overnight using a vacuum oven at 65 ° C to remove moisture; subsequently, 20 mg of sample was used in an alumina crucible. The thermogravimetric analyzes were carried out under the following conditions:

-Atmosphere N_2: O_2 in relation 4: 1
-Flow: 100 mL • min^{-1}
-Isothermal stage at 25ºC for 120 minutes
-Temperature ramp of 10ºC • min^{-1} up to 700ºC
- Mass spectrometer in SIM mode (Single-Ion monitoring) following the following m / z signals: 28, 29, 31, 32, 35, 44, 45

These analyses were carried out with the equipment Technical Services of Research in the University of Alicante. (METTLER TOLEDO model TGA / SDTA851e / LF / 1600). As for the mass spectrometer, it is a quadrupole equipment of the brand PFEIFFER VACUUM model THERMOSTAR GSD301T with a mass range of up to 300 amu and SEM detector (electronic multiplier).

For the characterization by infrared Fourier transform spectroscopy (FTIR) in transmission mode, the silica was dried overnight using a vacuum oven at 65 ° C to remove moisture. The silica powder was ground with KBr with a concentration of 0.2% weight (400 mg of KBr and 1 mg of silica). 150 mg of this mixture was weighed and pressed by applying 3.5 Tn for 15

minutes using a mold to obtain a tablet. The spectra were obtained by acquiring 100 interferograms with a resolution of 8 cm^{-1}, in transmission mode. The equipment used was a Nicolet 5700 spectrophotometer with a deuterated triglycine sulfate detector (DTGS).

4.3. Results

4.3.1. Characterization by thermogravimetric analysis

Thermogravimetry is a thermal analysis technique that consists of measuring the mass variation of a sample as a function of time for a given temperature or temperature profile.
First, a series of samples, specifically conventional silica and different XR silicas, have been analyzed in order to know in detail the interaction between the organic group (R) and silica. Figure 4.1 shows thermogravimetric curve of a sample of conventional silica (SC).

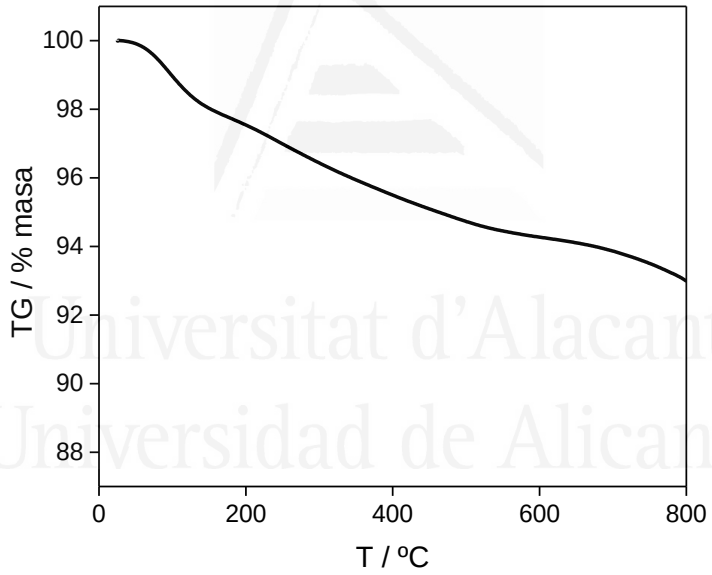

Figure 4.1. Thermogravimetric curve of a sample of conventional silica (SC).

For conventional silica (SC), in figure 4.1 the thermogram is shown, as observed, with the increase in temperature a mass loss between 200 and 800 ºC is produced. This mass loss may be due to the presence of EtO^-groups without hydrolyzing, that is, TEOS precursor, partially hydrolyzed.

Figure 4.2 shows the first derivative (DTG), a peak around 100 ° C is observed.

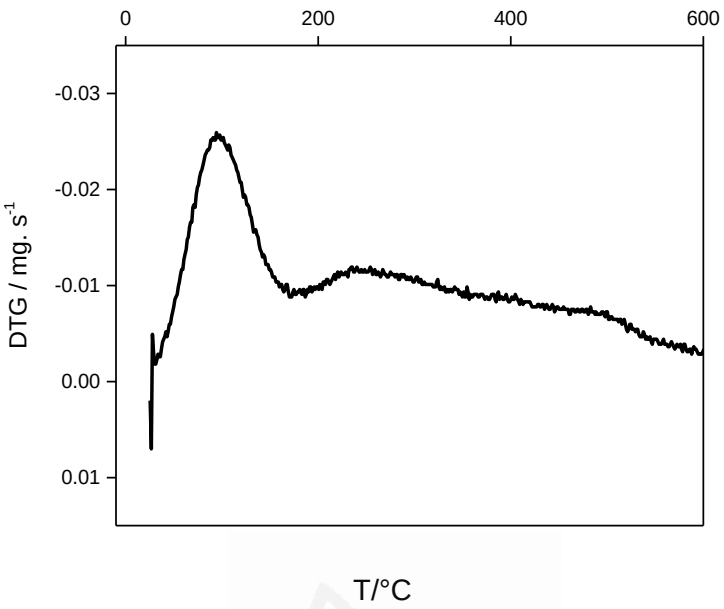

Figure 4.2. Thermogravimetric curve ofthe first derivative (DTG).

In this figure we see that the mass of the sample begins to descend to a temperature close to 100ºC, reaching a constant mass value at 600ºC. The DTG curve shows the speed of mass change, in this case loss of mass, with increasing temperature. Around 100ºC we observe a peak that can be related to the loss of water contained in the gel.

Figure 4.3 shows the signal obtained by mass spectrometry for m/z 44 (CO_2) for a sample of conventional silica (SC).

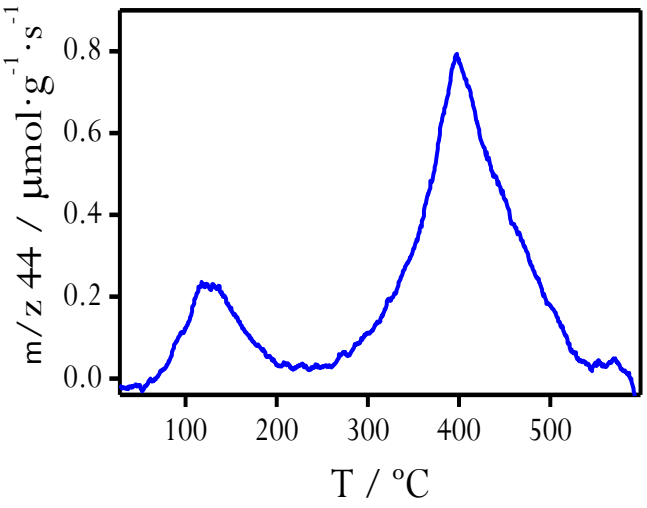

Figure 4.3. Signal obtained by mass spectrometry for m / z 44 (CO_2) for a sample of conventional silica (SC).

The loss of mass occurring at 100 ° C is concomitant with the emission of CO_2 from the sample, it indicates the presence of ETOH molecules that could have remained in the pores of the silica.

At 400 ° C a CO_2 peak is observed, due to ethoxy residues in the gel, probably unhydrolyzed ethoxide groups bonded to silicon [249].

Figure 4.4 shows the thermograms for modified silica with different concentrations of methyl triethoxysilane (MTES) in the precursor solution (xM): 1% (1M), 5% (5M), 10% (10M) and 20% (20M).

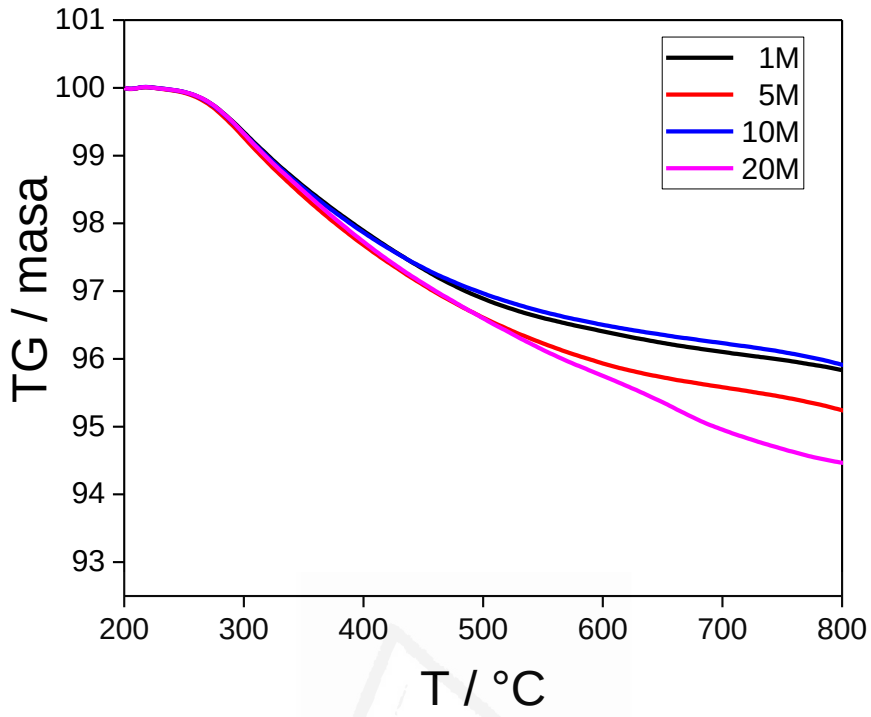

Figure 4.4. Thermogravimetric curves of different samples of silica modified with methyl groups (xM) synthesized chemically: 1M (black), 5M (red), 10M(blue) y 20M (purple).

It is observed that when increasing the temperature the loss of mass for the silica xM is quite similar, the mass loss oscillates between 3 and 5% in all cases.

Table 4.2 shows the results of the thermogravimetric analysis for silica samples modified with different concentrations of methyl groups (xM) in the precursor dissolution, molar % of methyl groups (M), theoretical formula (obtained from the precursor solution) and formula measured by TG.

Table 4.2: Molar percentage of organic group calculated from TG measurements (Molar %), Theoretical formula obtained from the precursor solution (TF), and measured formula obtained by TG (MF).

Sample	Molar %	TF	MF
1M	38.1	$SiO_{1.995}(CH_3)_{0.01}$	$SiO_{1.809}(CH_3)_{0.381}$
5M	46.1	$SiO_{1.975}(CH_3)_{0.05}$	$SiO_{1.791}(CH_3)_{0.416}$
10M	35.3	$SiO_{1.95}(CH_3)_{0.1}$	$SiO_{1.823}(CH_3)_{0.353}$
20M	48.5	$SiO_{1.9}(CH_3)_{0.2}$	$SiO_{1.757}(CH_3)_{0.485}$

It is observed, in all cases that between 38 and 49% of methyl groups have been incorporated independently of the concentration of precursor used in the precursor solution. Similar results were obtained by Porcel-Valenzuela on silica gel obtained by electrochemical deposition[250].

Figure 4.5 shows the thermograms for silica xP, that is, modified using different concentrations of n-propyl triethoxysilane (PrTES) in the precursor solution.

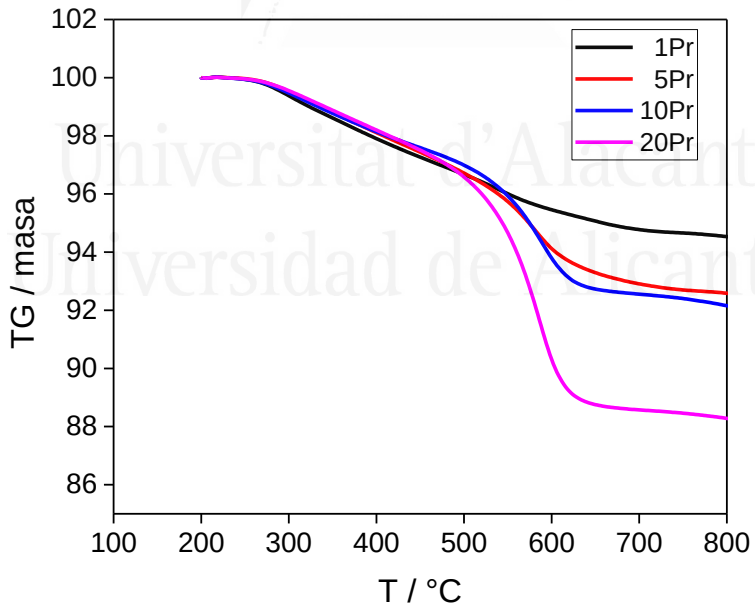

Figure 4.5. Thermogravimetric curves of different samples of silica modified with propyl groups (xP) synthesized chemically: 1P (black). 5P (red), 10P (blue) y 20P (purple).

Figure 4.5 shows the thermograms for silica xP, modified using different concentrations of n-propyl-triethoxysilane (PrTES) in the precursor solution, as can be seen in table 4.3. It is observed that the loss of mass, with the increase in temperature, becomes greater when the concentration of propyl group in the gel increases. This mass loss can be used to determine the concentration of organic groups in the gel.

Table4.3 shows the results of the thermogravimetric analysis for silica samples modified with different concentrations of propyl groups (xP) in the precursor solution. Molar % of propyl groups (P), theoretical formula (obtained from the precursor solution) and formula measured by TG.

Table 4.3: Molar percentage of organic group calculated from TG measurements (Molar %), Theoretical formula obtained from the precursor solution (TF), and measured formula obtained by TG (MF).

Sample	Molar %	TF	MF
1P	9.5	$SiO_{1.995}(C_3H_7)_{0.01}$	$SiO_{1.952}(C_3H_7)_{0.095}$
5P	13.0	$SiO_{1.975}(C_3H_7)_{0.05}$	$SiO_{1.934}(C_3H_7)_{0.130}$
10P	14.2	$SiO_{1.95}(C_3H_7)_{0.1}$	$SiO_{1.928}(C_3H_7)_{0.142}$
20P	22.4	$SiO_{1.9}(C_3H_7)_{0.2}$	$SiO_{1.888}(C_3H_7)_{0.224}$

It is noted that the amount of propyl groups incorporated into the gel increases with increasing amount of propyl groups in the precursor solution. In general terms, the concentration of groups incorporated on silica is higher than on the precursor solution.

For the silica modified with propyl groups the decomposition of the organic matter takes place at temperatures between 550 and 750ºC. Decomposition occurs at lower temperature values as the amount of organic group in the silica increases, i.e., more thermally stable gels are obtained using lower concentrations of organic precursor.

Figure 4.6 shows modified silica thermograms with different concentrations of octyl-trimethoxysilane (OTMS) in the precursor solution (xO).

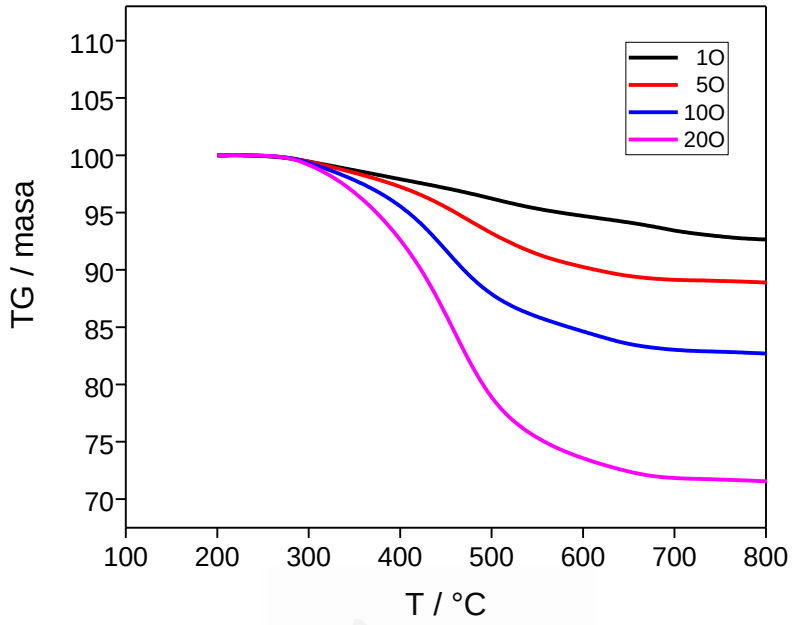

Figure 4.6. Thermogravimetric curves of different samples of silica modified with octyl groups (xO) synthesized chemically: 1O (black), 5O (red), 10O (blue) y 20O (purple).

It is observed that as the temperature increases, increasing mass losses occur as the concentration of octyl group increases in the gel and a very definite mass loss process appears at temperatures above 300 ° C.

Table 4.4 shows the molar % organic group values calculated by thermogravimetric analysis for modified silica with different concentration of octyltrimethoxysilane (OTMS) in the precursor solution (xO): 1%, 5%, 10% and 20%.

Table 4.4: Molar percentage of organic group calculated from TG measurements(Molar %), Theoretical formula obtained from the precursor solution (TF), and measured formula obtained by TG (MF).

Sample	Molar %	TF	MF
1O	4.9	$SiO_{1.995}(C_8H_{17})_{0.01}$	$SiO_{1.975}(C_8H_{17})_{0.049}$
5O	7.7	$SiO_{1.975}(C_8H_{17})_{0.05}$	$SiO_{1.961}(C_8H_{17})_{0.077}$
10O	12.8	$SiO_{1.95}(C_8H_{17})_{0.1}$	$SiO_{1.935}(C_8H_{17})_{0.128}$
20O	24.0	$SiO_{1.9}(C_8H_{17})_{0.2}$	$SiO_{1.879}(C_8H_{17})_{0.240}$

Table 4.4 shows results of the thermogravimetric analysis for silica samples modified with different concentration of octyl group (xO) in the precursor solution. Molar % of octyl groups (O), theoretical formula (obtained from the precursor solution) and formula measured by TG.

It is observed that the molar % values calculated by thermogravimetric analysis increase with the increase of the octyl group concentration, in the end of the OTMS in the precursor solution. As in the previous results the concentration of organic groups on the gels is higher than the concentration on the precursor solution.

It is also observed that as the concentration of organic group in the gel increases, the temperature at which decomposition of organic matter takes place is lower. Therefore, more thermally unstable gels are obtained by increasing the concentration of organic matter in the silica matrix.

Figure 4.7 shows thermograms for modified silica with different concentrations of phenyl-triethoxysilane (PhTES) in the precursor solution (xPh).

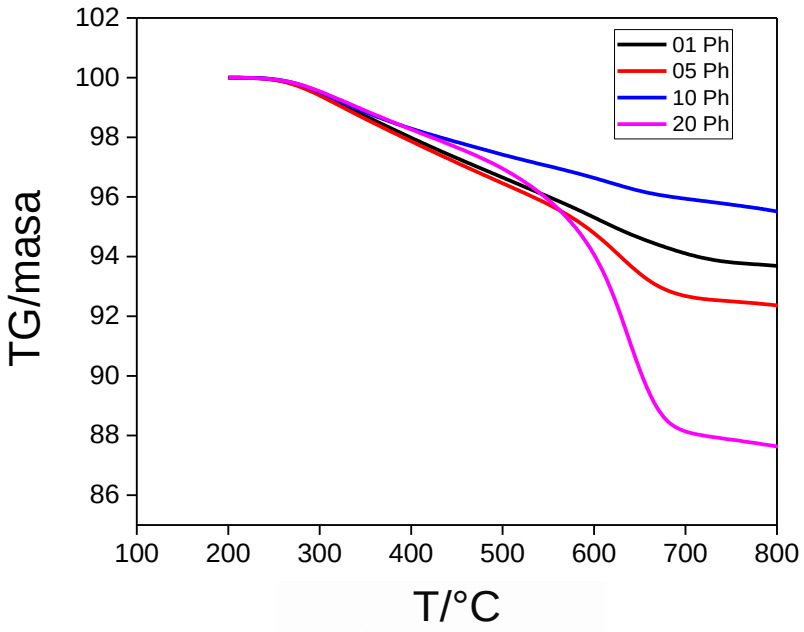

Figure 4.7. Thermogravimetric curves of different samples of silica modified with Phenyl groups (xPh) synthesized chemically: 1Ph (black), 5Ph (red), 10 Ph (blue) y 20Ph (purple).

Figure 4.7 shows thermograms for modified silica with different concentrations of phenyl-triethoxysilane (PhTES) in the precursor solution. It is observed that as the temperature increases, mass losses occur which increase as the concentration of the phenyl group increases in the gel precursor solution.

Table 4.5 shows the molar % values of the organic group calculated by thermogravimetric analysis for modified silica with different concentration of phenyltriethoxysilane (PhTES) in the precursor solution (xO): 1%, 5%, 10% and 20%.

Table 4.5: Molar percentage of organic group calculated from TG measurements (Molar %), Theoretical formula obtained from the precursor solution (TF), and measured formula obtained by TG (FM).

Samples	Molar %	FT	FM
1Ph	5.5	$SiO_{1.995}(Ph)_{0.01}$	$SiO_{1.972}(Ph)_{0.055}$
5 Ph	7.0	$SiO_{1.975}(Ph)_{0.05}$	$SiO_{1.964}(Ph)_{0.070}$
10 Ph	4.3	$SiO_{1.95}(Ph)_{0.1}$	$SiO_{1.978}(Ph)_{0.043}$
20 Ph	13.2	$SiO_{1.9}(Ph)_{0.2}$	$SiO_{1.933}(Ph)_{0.132}$

Table 4.5 shows results of the thermogravimetric analysis for silica samples modified with different concentration of phenyl group (xPh) in the precursor solution. Molar % of phenyl groups (Ph), theoretical formula (obtained from the precursor solution) and formula measured by TG.

It can be seen that the molar % values calculated by thermogravimetric analysis increase with increasing phenyl group concentration except at 10%, a similar result were obtained by Porcel-Valenzuela [250].

It is remarkable that on contrast with the previous results, Ph groups concentration in the gel is lower than the concentration on the precursor solution.

4.3.2. Characterization by infrared spectroscopy in transmission mode

Fourier Transform Infrared (FTIR) spectroscopy is a technique used to determine the energy of the vibrations of bonds in the solid silica network [251], and also qualitative and quantitative features of IR-active molecules in organic or inorganic solid, liquid or gas samples. It is a rapid and relatively inexpensive method for the analysis of solids, which allows us to better understand the behavior of silica in different environments.

Conventional silica precursors contain four identical alkoxide groups that are hydrolysable (Si-O bonds), usually ethoxide groups; while to obtain organically modified silica, precursors containing non-hydrolyzable alkyl groups (Si-C bonds) are used: methyl (M), n-propyl (P), octyl (O), and phenyl (Ph). The use of infrared spectroscopy reveals the existence of chemically different and comparable films according to the nature of the precursors used.

The analyzed samples were synthesized as described in the experimental part of this chapter. Figure 4.8 shows the FTIR spectrum synthesized chemically and modified with different concentration of (Methyl) groups.

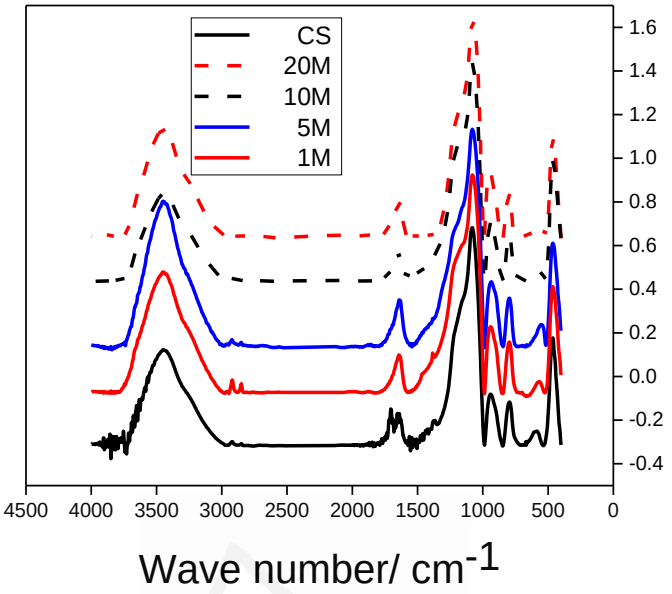

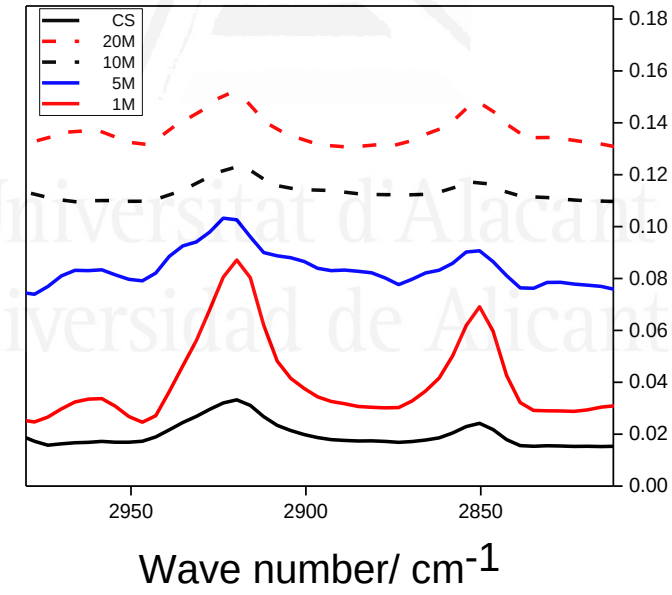

Figure 4.8. FTIR spectrum synthesized chemically and modified with different concentration of Organic-MOdifed-SILica groups (Methyl).

In the high frequency area (4000 cm-1 to 2500 cm-1), we observed that all samples had a broad band centered around 3470-3450 cm^{-1} which corresponds to the overlap of the vibrating tension bands, "stretching", in the O-H bond of the H_2O molecules (H-O-H…H) and the bands of the same type due to the O-H bonds of the silanol groups of the silica (SiO-H…H_2O) [252]. Approximately 2900-2800 cm^{-1} of the vibration bands appear in most samples corresponding to the symmetrical and anti-symmetric tension bands of the C-H bonds of the aliphatic groups, $-CH_2$ and $-CH_3$.

We observe the spectrum area for frequency values between 1800 cm^{-1} and 400 cm^{-1}. The bands corresponding to the deformation vibrations, "bending", of adsorbed H_2O molecules appear around 1653-1634 cm^{-1}[253]. The adsorption of water molecules on the surface of the silica is due to the existence of superficial silanol groups and therefore to the hydrophilic nature of these materials. The vibrations corresponding to the covalent Si-O bonds occur mainly in the range between 1200 and 1000 cm^{-1}. It can be observed that a very intense and wide band appears, for all the samples, between 1095 and 1089 cm^{-1}, assigned to the antisymmetric tension vibration (stretching) of the Si-O-Si structure. About 930-950 cm^{-1}, there is one shoulder in the anterior band that is attributed to EtO- without hydrolyzing [254]. This confirms that what was previously seen by TG-MS, which starts from organic matter in conventional silica, is due to EtO- without hydrolyzing groups. On the other hand, the symmetrical (stretching) vibrations corresponding to the Si-O-Si structure appear at 800 cm^{-1}[252]. Between 469 and 470 cm^{-1}, a band is observed that corresponds to the vibration of deformation (bending) in the plane by rocking, "rocking" of the Si-O-Si structure [255]. The band that is observed around 560 cm^{-1} is assigned to defects by tension, "stretching", in the SiO_2 network [252].

From figure 4.8, by varying the concentration of organic group in the precursor solution, it is observed that the intensity of the vibration bands varies depending on the concentration of the methyl group, but there is no direct relationship between the concentration of the organic group and the intensity of the bands, we saw the same thing with TG analyzes.

Figure 4.9 shows the FTIR spectrum synthesized chemically and modified with different concentration of ORMOSIL (Propyl).

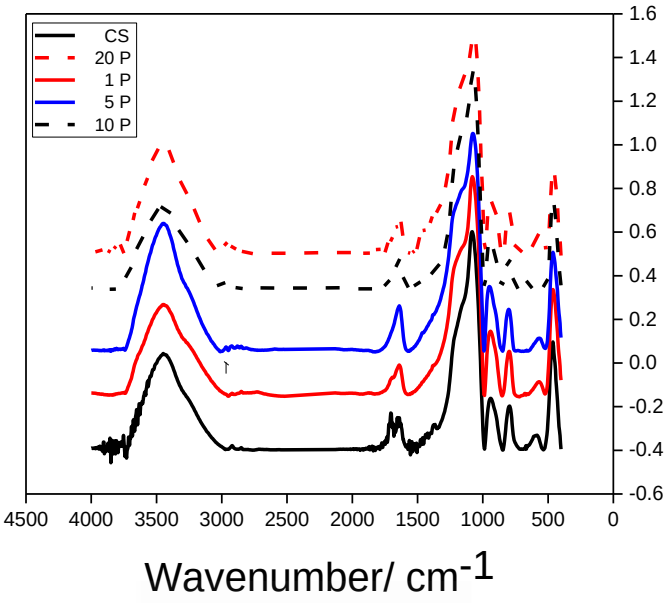

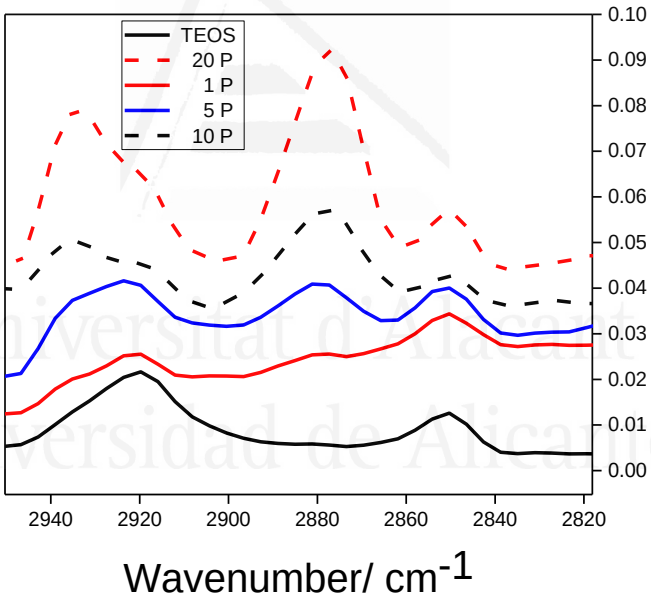

Figure 4.9. FTIR spectrum synthesized chemically and modified with different concentration of Organic-MOdifed-SILica groups (Propyl).

By varying the concentration of organic group in the precursor solution the intensity of the vibration bands that appear around 2900-2800 cm^{-1}, assigned to symmetric and anti-symmetric stretching of the CH bonds of aliphatic groups(CH_2 ,CH_3), increased with the concentration of organic group in the precursor solution.

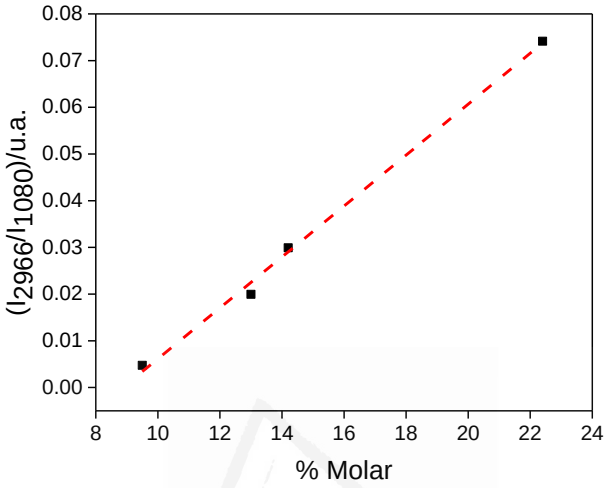

Figure4.10. Ratio of intensity ν_sC-H (2966 cm^{-1}) / ν_s Si-O-Si (1080cm^{-1}) depending on the concentration of propyl groups calculated by TG.

Figure 4.10 shows the relationship between the value of the intensity of the absorbance bands at 2966 cm^{-1} corresponding to the symmetric vibration of the C-H bond and the symmetric vibration band of the Si-O-Si bond observed around 1080 cm^{-1}as a function of the concentration of propyl groups calculated by thermogravimetric analysis (table 4.3).

It is observed that there is a linear relationship of this relationship with the concentration of propyl group in the precursor solution. For adjustment parameters for the relationship between the quotient of intensities of the bands measured by FTIR and the concentration of the propyl group calculated by thermogravimetric analysis, the value of the slope is 5×10^{-3} and R^2 is 0.996. A similar result were obtained by Porcel Valenzuela[250].

Figure 4.11shows the FTIR spectra modified octyl groups.

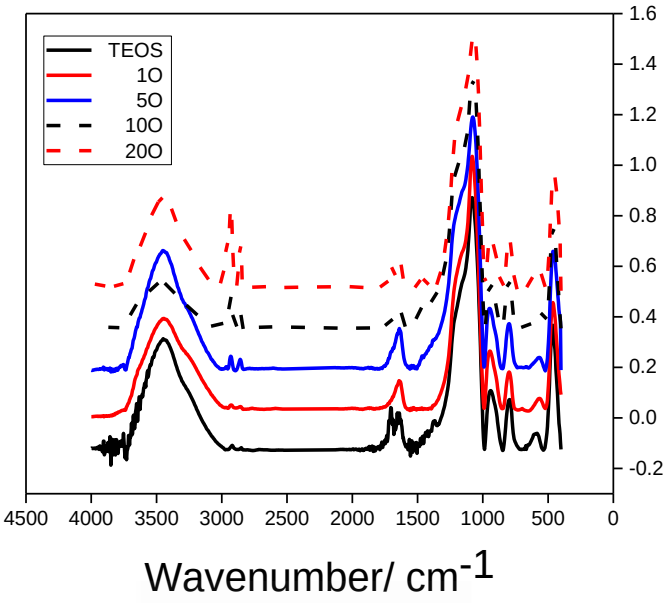

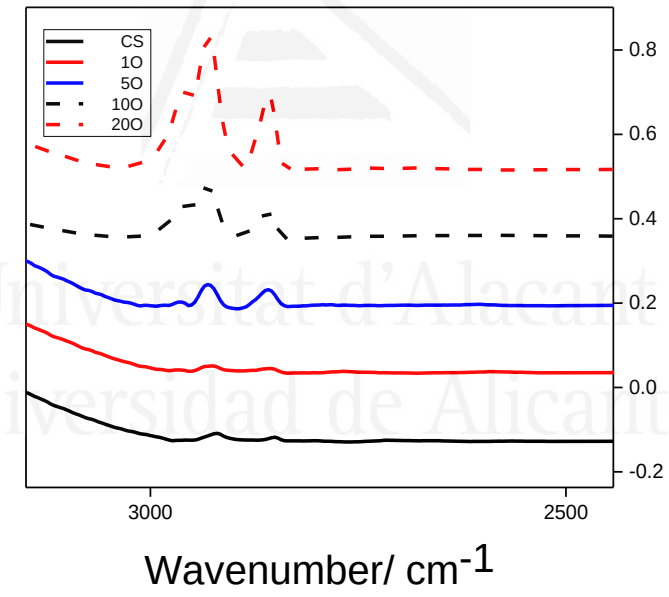

Figure 4.11. FTIR spectra of silica synthesized chemically and modified with different concentration of ormosils groups (Octyl).

Figure 4.11 shows the FTIR spectrum for modified silica with different concentration of octyl groups, it is observed that when increasing the concentration of the organic group in the gel precursor solution, the intensity of the vibration bands observed between 2800 and 2900 cm^{-1}, corresponding to the vibration of symmetric and anti-symmetric tension of bonds between aliphatic groups, increases .

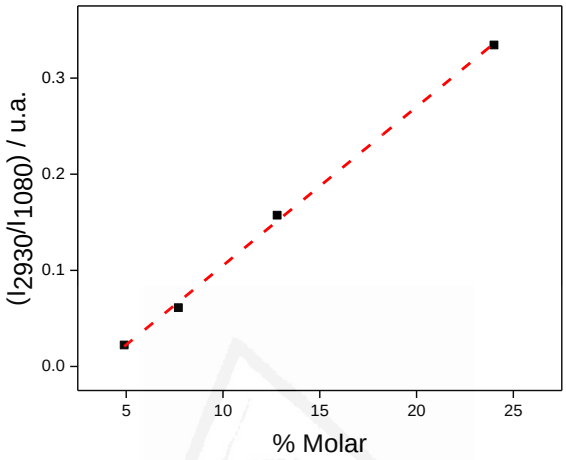

Figure 4.12: Ratio of intensity ν_sC-H (2930 cm^{-1}) / ν_s Si-O-Si (1080cm^{-1}) depending on the concentration of octyl groups calculated by TG.

Figure 4.12 shows the relationship between the value of the intensity of the bands at 2930 cm^{-1} corresponding to the symmetric vibration of the C-H bond and the symmetric vibration band of the Si-O-Si bond observed around 1080 cm^{-1} depending on the concentration of octyl groups calculated by thermogravimetric analysis (table 4.4). It is observed that the intensity increases by increasing the concentration of octyl group in the precursor solution. The same results are also obtained for the ratio of intensities with bands that appear at 2850 cm^{-1}. A similar results were obtained by Porcel-Valenzuela [250].

Figure 4.13 shows the FTIR spectrum synthesized chemically and modified with different concentration of ORganic-MOdifed-SILica groups (Phenyl).

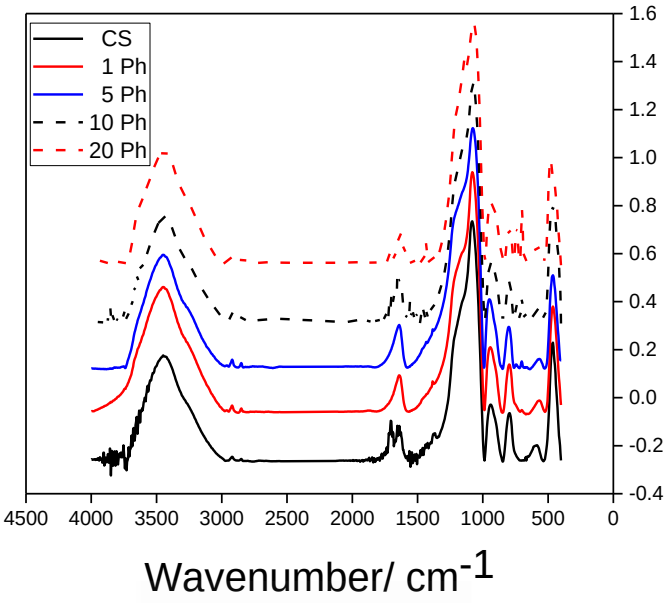

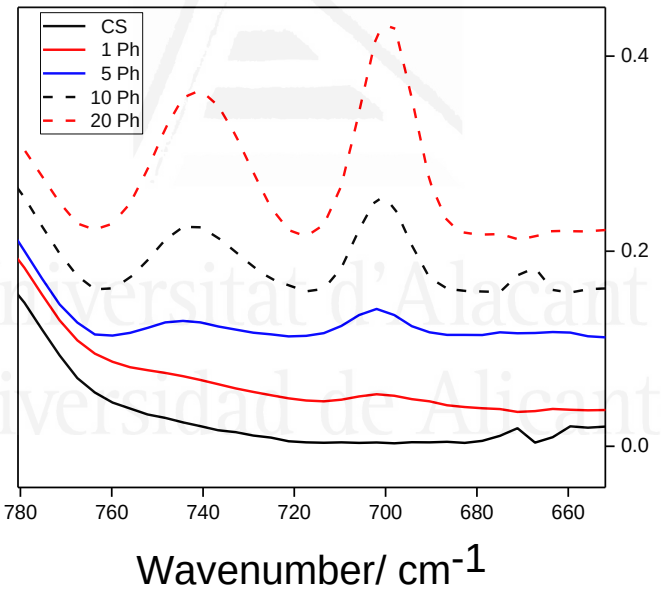

Figure4.13. FTIR spectrum synthesized chemically and modified with different concentration of ORMOSIL groups (Phenyl).

The FTIR spectrum for modified silica with different concentration of phenyl groups, it is observed that the intensity of the vibration bands varies depending on the concentration of the organic group.

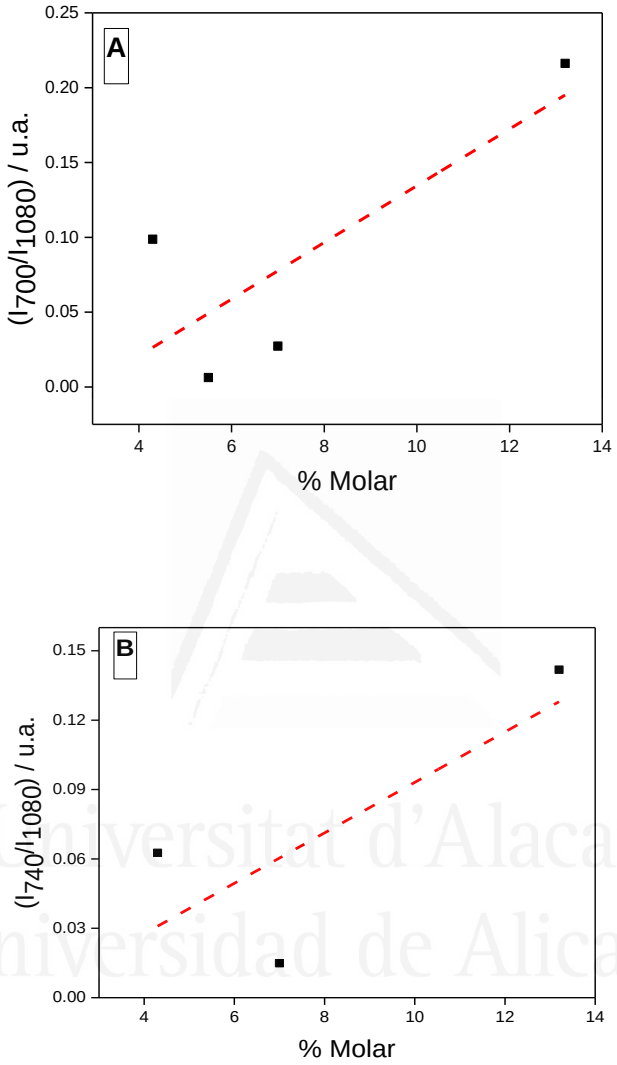

Figure 4.14. (A) Ratio of intensities ΦC-H (700 cm-1) / νsSi-O-Si (1080cm^{-1}) and (B) ωδ, γC-H (740 cm^{-1}) / νsSi-O-Si (1080cm^{-1}) as a function of the concentration of phenyl groups calculated by thermogravimetric analysis.

Figure 4.14.A shows the relationship between the intensity value of the deformation vibration band of the aromatic ring outside the plane for the C-H bonds, which appears at 700 cm^{-1} and the symmetric vibration band of the Si-O-Si bond that is observed at 1080 cm^{-1} depending on the concentration of phenyl group calculated by thermogravimetric analysis (table 4.5). Figure 4.14.B shows the relationship between the transmission value of the quotient of two vibration bands: the one related to the deformation of the C-H bond outside the plane in pitch mode (740 cm^{-1}) and the corresponding one with vibration symmetric of the Si-O-Si link (1080 cm^{-1}).

It is observed that there is no good linear relationship between the transmission of those vibration bands and the concentration of phenyl groups calculated by thermogravimetric analysis. A similar results were obtained by Porcel Valenzuela [250].

4.3.3. Electrochemical behavior of *p*-aminophenol in solution and in silica

The electrochemical activity of a carbon electrode against the *p*-aminophenol redox probe is shown. Figure 4.15 shows the stabilized cyclic voltammogram immersed in a test solution containing *p*-aminophenol (10 mM) at scan rate 100mVs^{-1}.

The voltammogram shows in the scan to positive potential an anodic peak centred at 0.418V, which is related with the oxidationof (*p*-aminophenol). In the reverse scan, the faradic counter-process occurs at -0.400V. The peak separation between anodic and cathodic features (ΔE_P) is 818 mV.

For these probes we determined the equilibrium potential (Eq) of the redox probe and after we deduce the over potential $\eta=E-E_q$.

The overpotential is the potential difference (voltage) between the thermodynamically determined reduction potential of a half-reaction and the potential at which the redox event is observed experimentally.

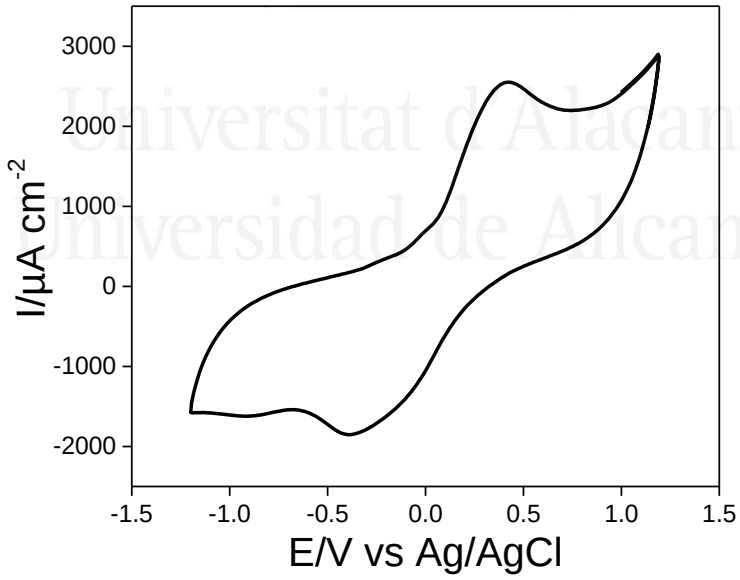

Figure 4.15. Stabilised cyclic voltammogram of carbon electrode immersed in a test solution (10mM) containing *p*-aminophenol at scan rate 100 mV s^{-1}.

We have synthesized monoliths of silica using sol-gel methodology as indicated in the experimental section. This allowed the study of the electrochemical behavior of encapsulated *p*-aminophenol.

Figure 4.16 shows stabilised cyclic voltammogram of the carbon electrode immersed in monolith of silica containing *p*-aminophenol compared with the stabilised cyclic voltammogram of a test solution at scan rate 100 mV s^{-1}.

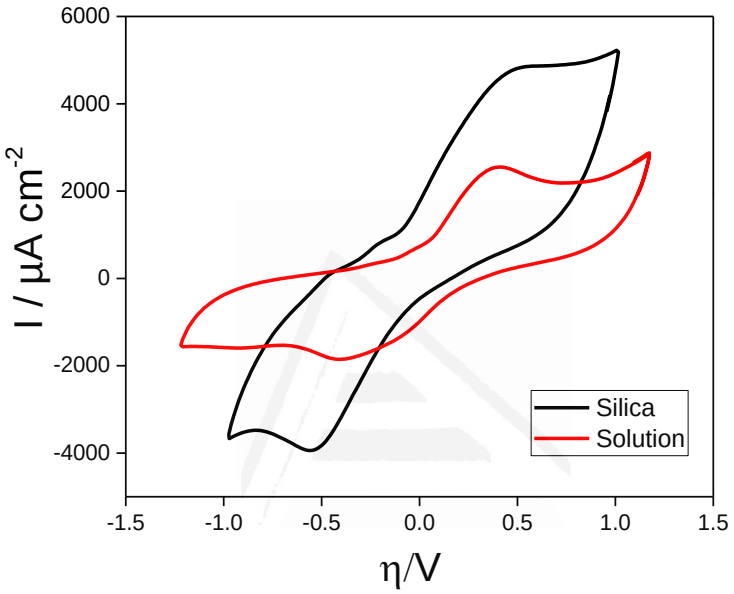

Figure 4.16. Stabilised cyclic voltammogram of carbon electrode immersed in monolith of silica containing *p*-aminophenol compared with the stabilised cyclic voltammogram a test solution at scan rate 100 mV s^{-1}.

The voltammogram of the silica monolith shows in the scan to positive potential an anodic peak centred at 0.547V. In the reverse scan, the faradic counter-process occurs at -0.547V. The peak separation between anodic and cathodic features (ΔE_P) is 1094 mV.

Figure 4.17 shows the evolution of the peak separation at different scan rate immersed in solution and silica monolith containing *p*-aminophenol.

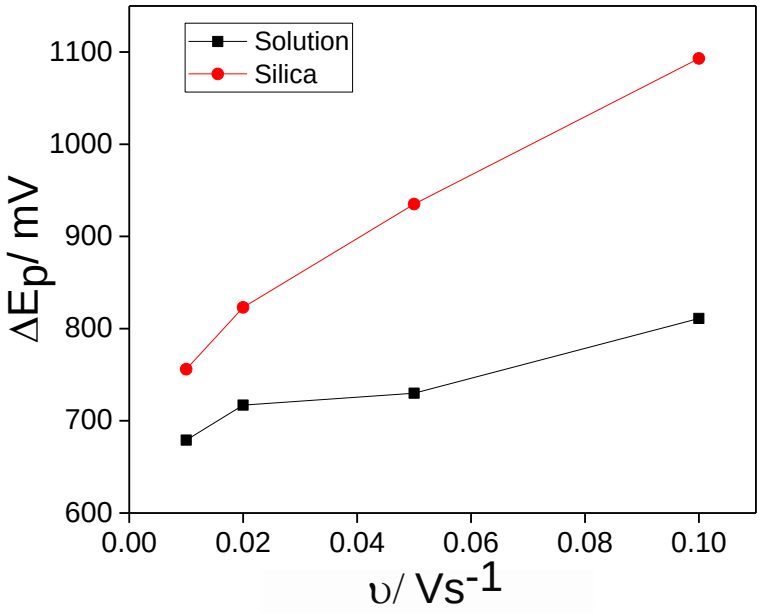

Figure 4.17: Evolution of the peak separation vs the scan rate immersed in solution and silica monolith containing *p*-aminophenol.

As observed in figure 4.17 at low scan rate (10 mV s^{-1}) the peak separation amounts 679 mV in a test solution and amounts 756 mV for the monolith of silica. When the scan rate is increased, the peak separation increases up to 811 mV in a test solution and 1094 mV for the monolith of silica at scan rate (100 mVs^{-1}).

In order to classify this redox process as kinetically reversible, quasi-reversible or irreversible the peak separations were analysed.The kinetic reversibility of an electrochemical reaction can be evaluated from cyclic voltammetry experiments thanks to a dimensionless parameter Ψ, which is derived from the voltammetric peak-to-peak separation (ΔE_P), as determined by the Nicholson's method[256]. The numerical values of Ψ can be obtained either from the original Nicholson's paper for the quasi-reversible reactions or from the numerical approach developed by Mahé et al[257]. Alternatively, the system reversibility can be evaluated by means of an equivalent parameter,Λ, which was defined by Matsuda and Ayabe[195,258]as :

$$\Lambda = \psi\sqrt{\pi} \qquad \text{(Eq. 1)}$$

It is usually assumed that an electrode process will be kinetically reversible for Λ>15, quasi-reversible for 15 ≥ Λ ≥ 0.001 and irreversible for Λ values lower than 0.001. The values of Λ at different scan rates are collected in figure 4.18 for the electrode immersed in test solution of *p*-aminophenol.

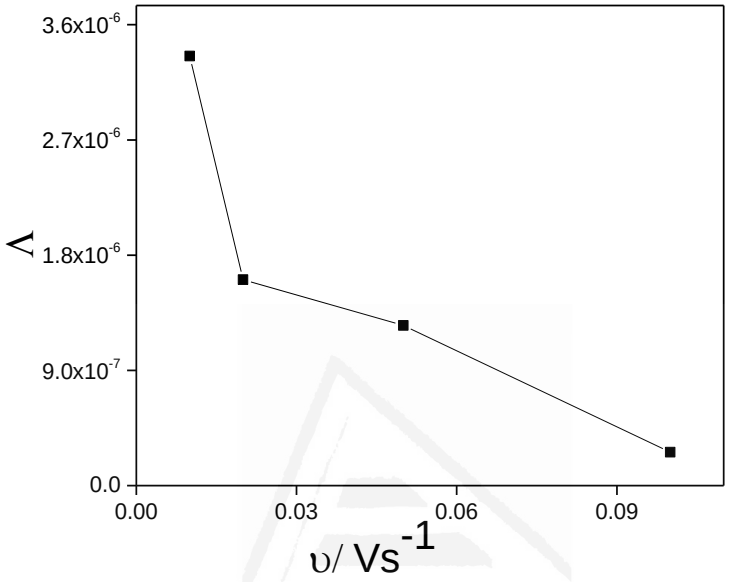

Figure 4.18. Values of Λ at different scan rate for *p*-aminophenolredox probe with a carbon electrode.

As observed in figure 4.18 at low scan rate (10 mV s^{-1}) the value of Λ is $3.35\times10^{-6}$and when the scan rate is increased, the value of Λ decreases to 2.60×10^{-7} at scan rate (100 mVs^{-1}).According to those data the redox probe can be classified kinetically as irreversible in the whole range of scan rates.

The relationship between the standard rate constant, k^0, for the electron transfer of the electrochemical reaction and the Λ parameter was shown by Matsuda [258].

$$\Lambda = k^0 \left(\frac{RT}{nFD\upsilon}\right)^{1/2} \qquad \text{(Eq. 2)}$$

According to this equation, two factors govern the value of Λ at constant temperature: the diffusion coefficient (D) and the standard rate constant for the charge transfer (k^0).

The diffusion coefficient of the redox probe can be determined from the Randles-Sevcik plot (see figure 4.19). Despite the linearity of that plot, the classical Randles-Sevcik equation can be only applied to reversible systems:

$$I_p(rev) = 2.687\ x10^5 ACn^{3/2}(Dv)^{1/2} \qquad \text{(Eq. 3)}$$

Where $I_p(rev)$ is the current for a reversible redox process (A), A is the electrode area (cm^2), C the concentration of the redox probe (in mol cm^{-3}), n the number of electrons transferred, D the diffusion coefficient ($cm^2\ s^{-1}$) of the redox probes and υ is the scan rate ($V\ s^{-1}$).The application of this equation to both quasireversible and irreversible systems is only possible after the correction of the experimental peak current (I_p):

$$I_p(rev) = \frac{I_p}{k(\Lambda)} \qquad \text{(Eq. 4)}$$

Where $k(\Lambda)$is an adimensional parameter defined by Matsuda and Ayabe [258], that accounts for the kinetic factor governing the peak current.

Figure 4.19 shows the evolution of the current of the oxidation peak as a function of the square root of the scan rate of *p*-aminophenol in solution.

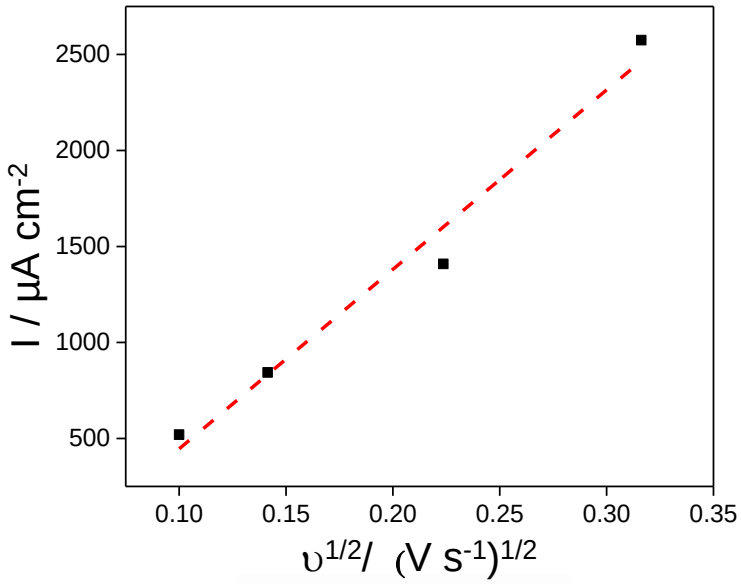

Figure 4.19. The evolution of the current of the oxidation peak as a function of the square root of the scan rate of *p*-aminophenol in solution.

As observed in figure 4.19 when the scan rate increased, the current of the oxidation peak increases linearly. Since the redox process is highly irreversible the peak current must be corrected by *k(Λ)*.With the values of *k(Λ)*the experimental values of current at each scan rate can be corrected to apply the Randles-Sevcik expression.

Figure 4.20 shows the evolution of the corrected peak currents vs the scan rate of *p*-aminophenol in solution.

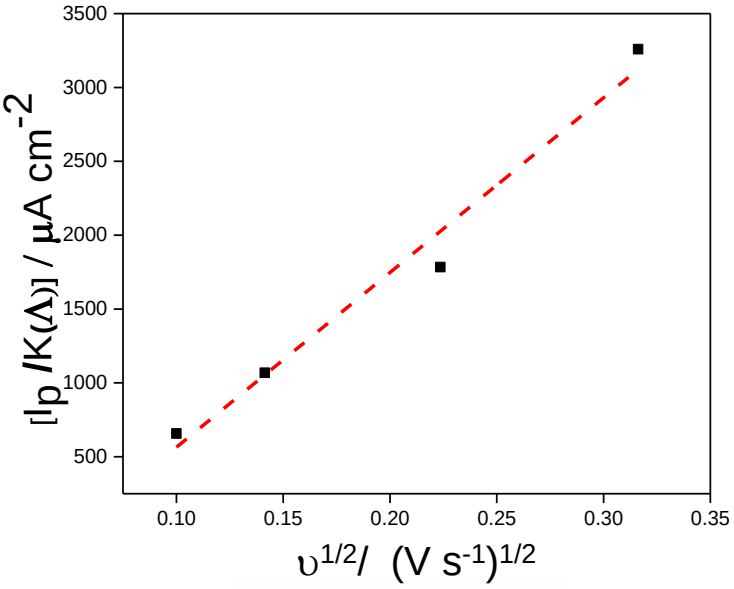

Figure 4.20. Randles–Sevcik plot obtained with the corrected value of current at different scan rates for the redox probe *p*-amino phenol.

The diffusion coefficient for solution of *p*-aminophenol in solution were calculated from the value of the slope linear fit in figure 4.20, it is of value $D=2.42\times10^{-6}cm^2\cdot s^{-1}$. A similar results were obtained by other authors [259].

Once the diffusion coefficient has been calculated, we can deduce the charge transfer rate constant k° from (Eq. 2).

Figure 4.21 shows the evolution of the standard rate constant for the charge transfer k° at different scan rate for *p*-aminophenol solution.

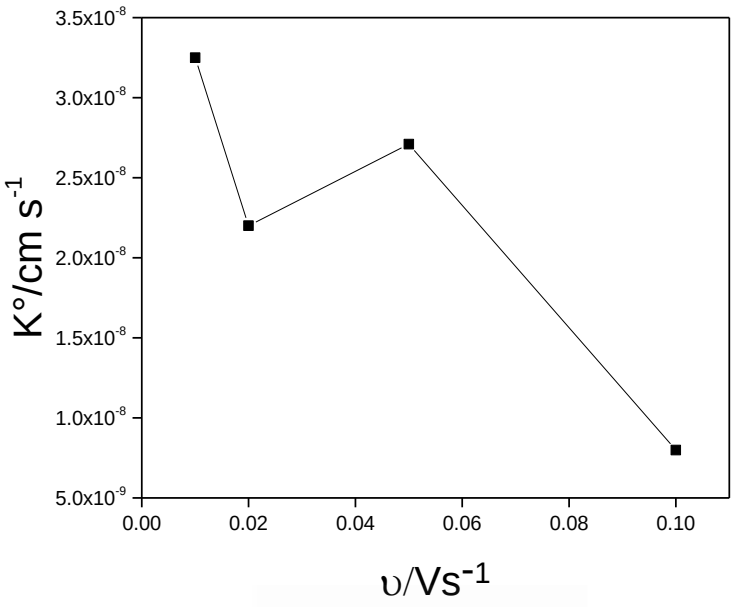

Figure 4.21. Evolution of the standard rate constant for the charge transfer k° at different scan rate for *p*-aminophenol solution.

As observed in figure 4.21 at low scan rate (10 mV s^{-1}) the value of k° is 3.25×10^{-8} cm $s^{-1}$and when the scan rate is increased, the value decreases up to 7.99×10^{-9} cm s^{-1} at 100 mVs^{-1}.

Similar analysis was performed with *p*-aminophenol encapsulated in silica. Figure 4.22 shows the evolution of the corrected peak currents vs the scan rate of *p*-aminophenol in silica.

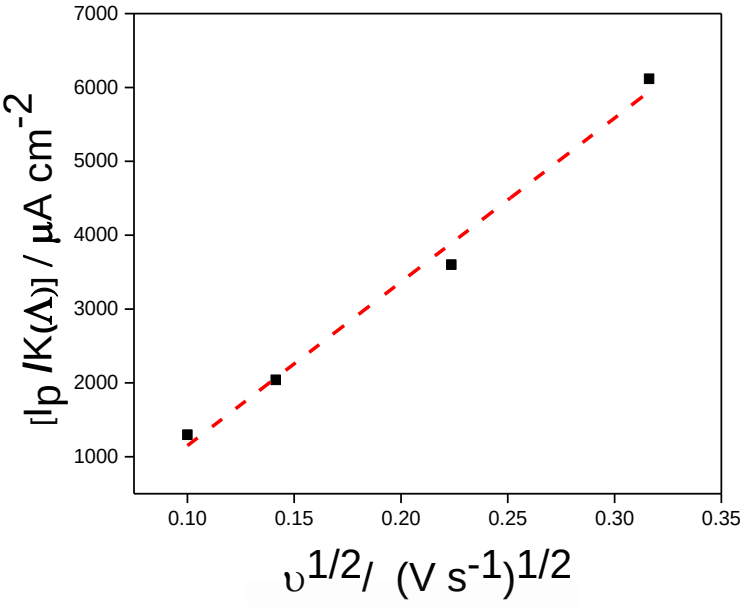

Figure 4.22. The evolution of the corrected peak currents vs the scan rate of *p*-aminophenol in silica.

The diffusion coefficient for solution of *p*-aminophenol in silica were calculated from the value of the slope linear fit in figure 4.22, it is of value $D=8.51\times10^{-6}cm^2\cdot s^{-1}$. This value is near four times higher than the diffusion coefficient in solution.

4.3.4. Electrochemical behavior of $Fe(CN)_6^{-4/-3}$ in solution and in silica

The electrochemical response of $Fe(CN)_6^{-4/-3}$redox couple is shown in figure 4.23. The stabilized cyclic voltammogram of a test solution containing $K_4Fe(CN)_6$ (1mM)+ $K_3Fe(CN)_6$ (1 mM) at scan rate 100mVs^{-1} shows in the scan to positive potential an anodic peak centred at 0.186V. In the reverse scan, the faradic counter-process occurs at -0.186V. The peak separation between anodic and cathodic features (ΔE_P) is 372 mV.

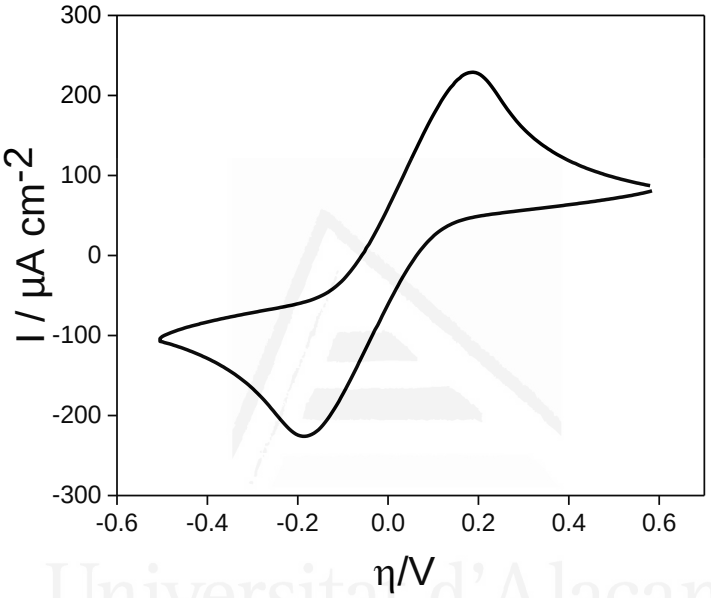

Figure 4.23. Stabilised cyclic voltammogram of a test solution containing $K_4Fe(CN)_6$ (1mM)+ $K_3Fe(CN)_6$(1 mM) at scan rate 100 mV s^{-1}.

We study the electrochemical behavior of silica encapsulated $Fe(CN)_6^{-4/-3}$probe. Figure 4.24 shows stabilised cyclic voltammogram of the carbon electrode immersed in monolith of silica containing $K_4Fe(CN)_6$(1mM)+$K_3Fe(CN)_6$(1 mM) compared with the stabilised cyclic voltammogram of a test solution at scan rate 100 mV s^{-1}.

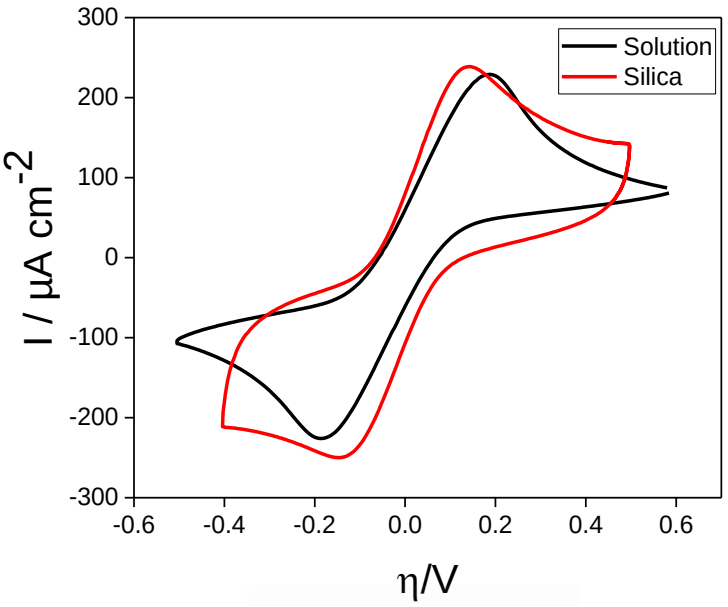

Figure 4.24. Stabilised cyclic voltammogram of the carbon electrode immersed in monolith of silica containing $K_4Fe(CN)_6^{-4/-3}$(1mM)+ $K_3Fe(CN)_6^{-4/-3}$(1 mM) compared with the stabilised cyclic voltammogram of a test solution at scan rate 100 mV s^{-1}.

The voltammogram of the carbon electrode on the silica monolith in the scan to positive displays an anodic peak centred at 0.143V. In the reverse scan, the faradic counter-process occurs at -0.143V. The peak separation between anodic and cathodic features (ΔE_P) is 286 mV. As a result, it can be observed that the reversibility of the redox process for the negatively charged redox couples decreases considerably at silica-modified electrodes. A similar results were obtained by other author [217].

Figure 4.25 shows the evolution of the peak separation at different scan rate immersed in solution and silica monolith containing $K_4Fe(CN)_6$(1mM)+ $K_3Fe(CN)_6$(1 mM).

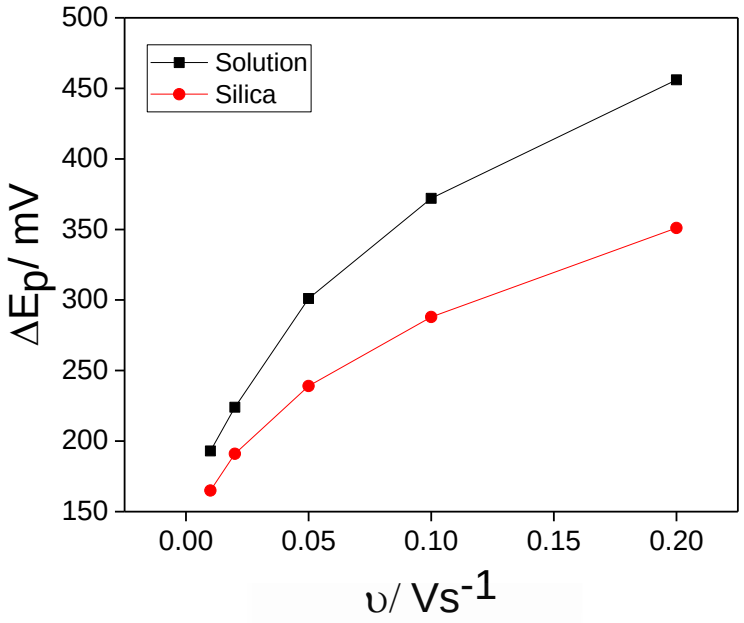

Figure 4.25. The evolution of the peak separation at different scan rate for carbon electrode immersed in solution and silica monolith containing $Fe(CN)_6^{-4/-3}$.

As observed in figure 4.25 at low scan rate (10 mV s^{-1}) the peak separation amounts 193 mV in a test solution and amounts 165 mV for the monolith of silica. When the scan rate is increased, the peak separation increases up to 456 mV in a test solution and 351 mV for the monolith of silica at scan rate (100 mVs^{-1}).

The values of Λ at different scan rates are collected in figure 4.26 for carbon electrode immersed in test solution of $K_4Fe(CN)_6$(1mM)+ $K_3Fe(CN)_6$(1 mM).

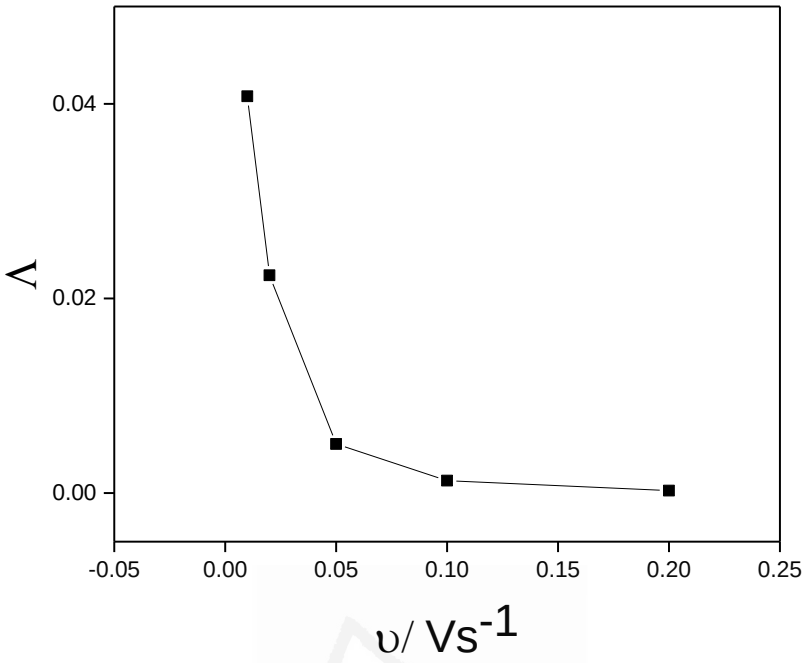

Figure 4.26. Values of Λ at different scan rate for $K_4Fe(CN)_6$(1mM)+ $K_3Fe(CN)_6$(1 mM) redox probe.

As observed in figure 4.26 at low scan rate (10 mV s^{-1}) the value of Λ is $4\times10^{-2}$and when the scan rate is increased, the value of Λ decreases to 1.2×10^{-3} at 100 mVs^{-1}. According to those data the redox probe can be classified kinetically as quasi-reversible in the whole range of scan rates.

Figure 4.27 shows the evolution of the corrected peak currents vs the scan rate of $Fe(CN)_6^{-4/-3}$ in solution.

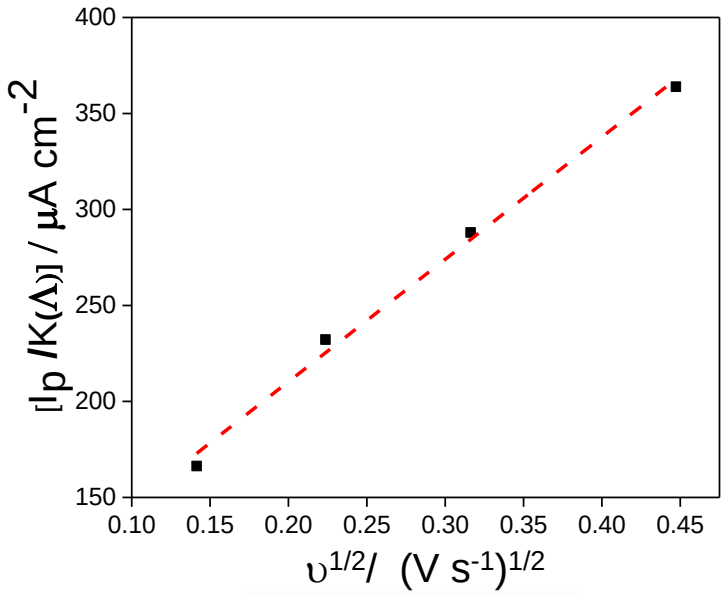

Figure 4.27. Randles–Sevcik plot obtained with the corrected value of current at different scan rates for the redox probe $Fe(CN)_6^{-4/-3}$ in solution.

The diffusion coefficient for solution of $Fe(CN)_6^{-4/-3}$ were calculated from the value of the slope linear fit in figure 4.27, $D=5.62\times10^{-6}cm^2\cdot s^{-1}$.

Figure 4.28 shows the evolution of the standard rate constant for the charge transfer k° at different scan rate for $Fe(CN)_6^{-4/-3}$ in solution.

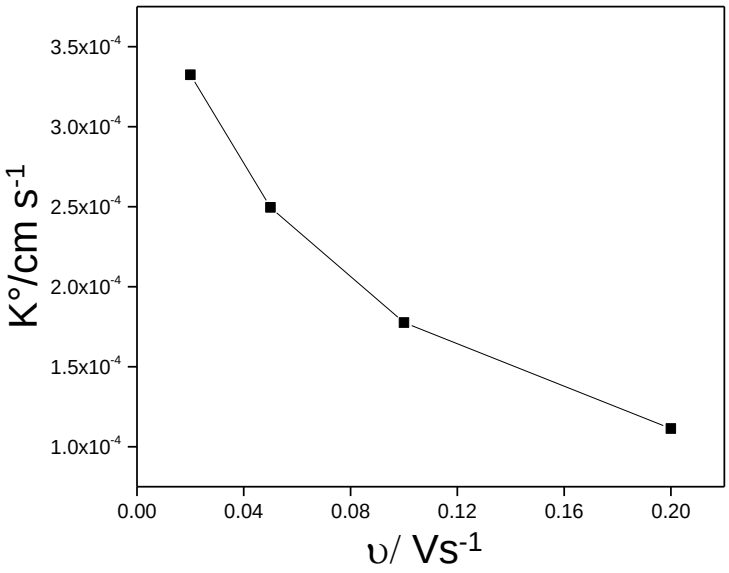

Figure 4.28. Evolution of the standard rate constant for the charge transfer k° at different scan rate for solution of $Fe(CN)_6^{-4/-3}$.

As observed in figure 4.28 at low scan rate (20 mV s^{-1}) the value of k°is 2.68×10^{-3} cm $s^{-1}$and when the scan rate is increased, the value decreases up to 8.98×10^{-4}cm s^{-1} at 200 mVs^{-1}.

Figure 4.29 shows the evolution of the corrected peak currents vs the scan rate of $Fe(CN)_6^{-4/-3}$ in silica.

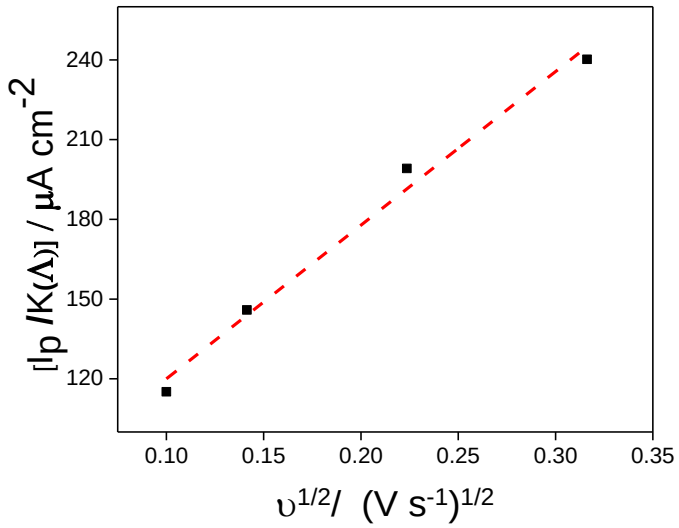

Figure 4.29. Randles–Sevcik plot obtained with the corrected value of current at different scan rates for the redox probe $Fe(CN)_6^{-4/-3}$ in silica.

The diffusion coefficient for silica of Fe $(CN)_6^{-4/-3}$ were calculated from the value of the slope linear fit in figure 4.29, it is of value $D=4.62\times10^{-6}cm^2.s^{-1}$. A similar results were obtained by other author[260]. This value is slightly smaller than the value in solution because this redox probe is more reversible in silica, so the diffusion coefficient decreases.

4.3.5. Electrochemical characterization of *p*-aminophenol encapsulated in ORMOSIL

Figure 4.30 shows stabilised cyclic voltammogram of carbon electrode immersed in monolith of silica of *p*-aminophenol and introducing Methyl, Propyl, Octyl and Phenyl group at different concentration (1,5,10 and 20%) in the gel composition at scan rate 100 mV s^{-1}. We observe that it is more reversible with organic functionalities at different concentrations than in conventional silica monolith (black voltammogram), so we focus the study of peak separation.

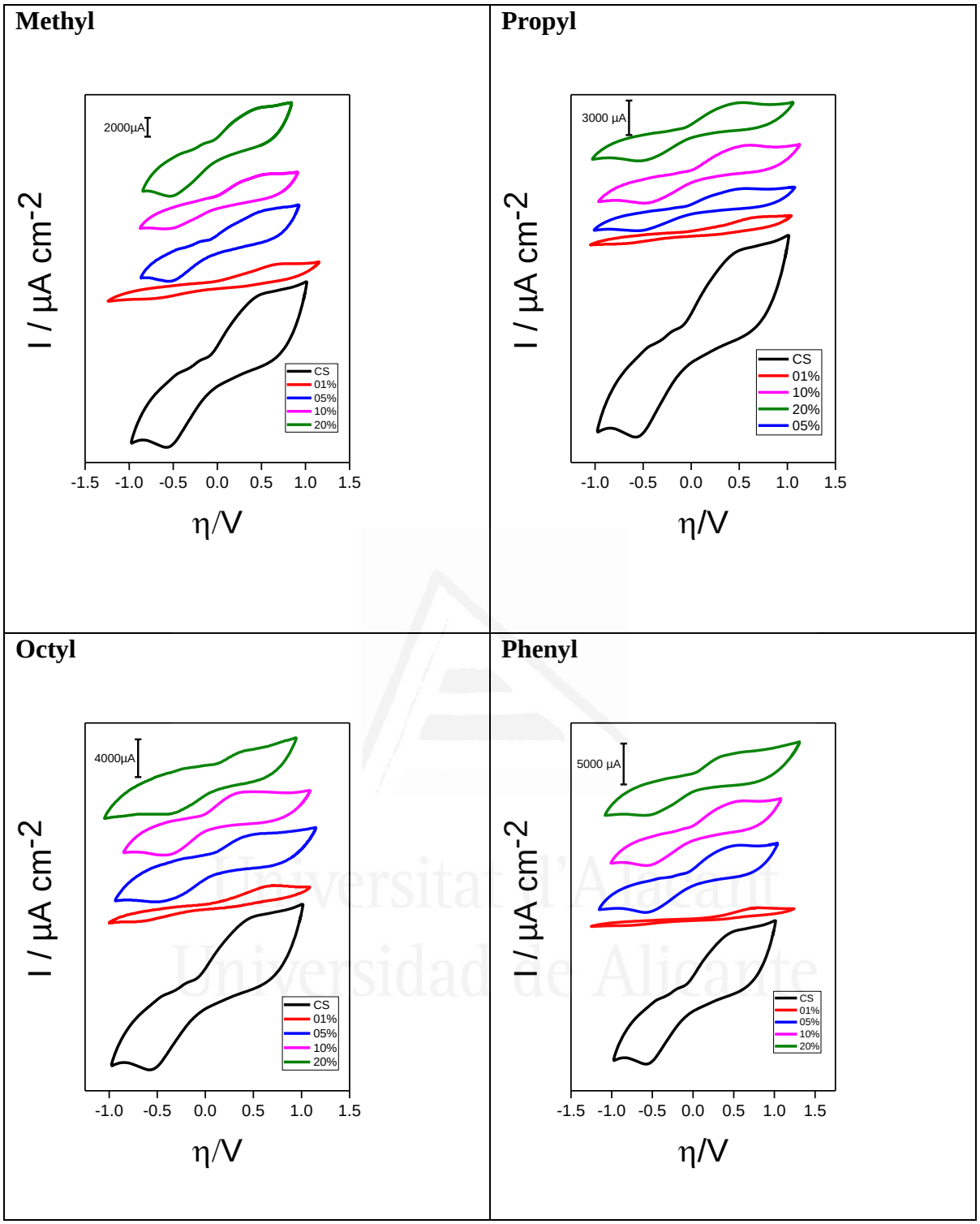

Figure 4.30. Stabilised cyclic voltammogram of carbon electrode immersed in monolith of silica of *p*-aminophenol and introducing Methyl, Propyl, Phenyl and Octyl group at different concentration (1-5-10 and 20%) from the bottom to up at scan rate 100 mV s^{-1}.

Table 4.6: Value of the peak separation of the *p*-aminophenol encapsulated in silica and modified with organic functionalities at different concentration.

	Methyl	**Propyl**	**Octyl**	**Phenyl**
ΔE_P 0%	1093	1093	1093	1093
ΔE_P 1%	1001	1013	1448	945
ΔE_P 5%	1020	1049	1419	985
ΔE_P 10%	1065	1097	967	1077
ΔE_P 20%	1100	1134	845	1149

This table shows the value of the peak separation of *p*-aminophenol of conventional silica monolith and after when we modify with organic functionalities at different concentration. First, with the methyl group it is more reversible with small concentration and it becomes irreversible with the concentration 20%. The propyl and phenyl group are similar than methyl group. In contrary with the octyl group it is more irreversible with the small concentration 1 and 5% and becomes reversible with the more concentration (10 and 20%), in this case of octyl group, the peak separation decreases with the increase of the concentration of organic functionalities. Figure 4.31 shows the evolution of the corrected peak currents vs the scan rate of *p*-aminophenol encapsulated with propyl group (5%).

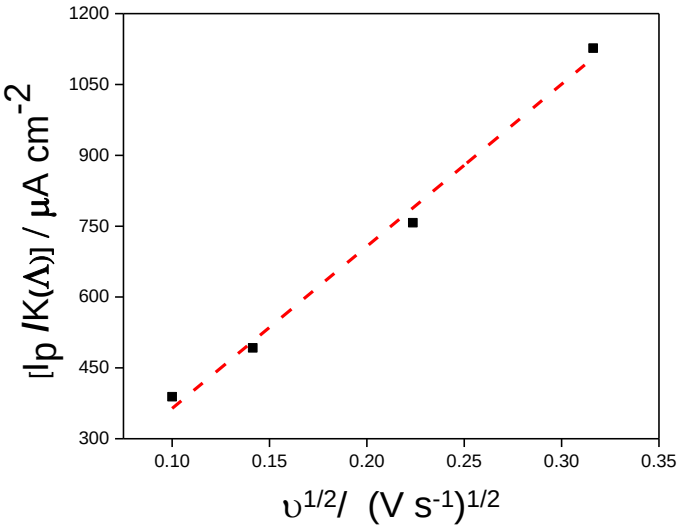

Figure 4.31. Randles–Sevcik plot obtained with the corrected value of current at different scan rates for *p*-aminophenol encapsulated with propyl group (5%).

Table 4.7: Value of the diffusion coefficient of *p*-aminophenol encapsulated in silica monolith and modified with organic functionalities at different concentration.

Diffusion Coefficient	**Methyl**	**Propyl**	**Octyl**	**Phenyl**
0%	8.51×10^{-6}	8.51×10^{-6}	8.51×10^{-6}	8.51×10^{-6}
1%	1.04×10^{-7}	1.36×10^{-7}	1.38×10^{-7}	1.56×10^{-7}
5%	1.45×10^{-7}	2.04×10^{-7}	3.87×10^{-7}	1.73×10^{-7}
10%	3.07×10^{-7}	3.98×10^{-7}	4.60×10^{-7}	4.07×10^{-7}
20%	4.09×10^{-7}	5.54×10^{-7}	8.82×10^{-7}	8.61×10^{-7}

The diffusion coefficient for solution of *p*-aminophenol were calculated from the value of the slope linear fit in figure 4.31, $D=2.04\times10^{-7}cm^2\cdot s^{-1}$. Similar calculations of diffusion coefficient were made for the other organic groups at different concentrations (1-5-10 and 20%), and data are collected in table 4.7.

Table 4.7 shows the value of diffusion coefficient of *p*-aminophenol of conventional silica monolith and after when we modify with organic functionalities at different concentration.

The diffusion coefficient in conventional silica is one order of magnitude higher than in monolith modified with organic functionalities. We observe for all the organic groups (methyl, propyl, octyl and phenyl) the diffusion coefficient increases with the increase of the concentration of the organic functionalities group.

4.3.6. Electrochemical characterization of Ferro / Ferricyanide redox probe encapsulated in ORMOSIL

Figure 4.32 shows stabilised cyclic voltammogram of carbon electrode immersed in monolith of silica of $Fe(CN)_6^{-4/-3}$ and introducing Methyl, Propyl, Octyl and Phenyl groups at different concentration (1-5-10 and 20%) in the gel composition at scan rate 100 mV s^{-1}. We observe that it is more reversible with organic functionalities at different concentrations than in conventional silica monolith (black voltammogram), the peak separation for the methyl group is around 100 and 180 mV, for the propyl and octyl group, the peak separation is around 100 and 118 mV and finally the phenyl group the peak separation is around 110 and 205 mV. For all cases the peak separation increases with the increase of the concentration of organic functionalities. Table 4.8 shows the value of the peak separation of ferrocyanide of conventional silica monolith and modified with organic functionalities at different concentration.

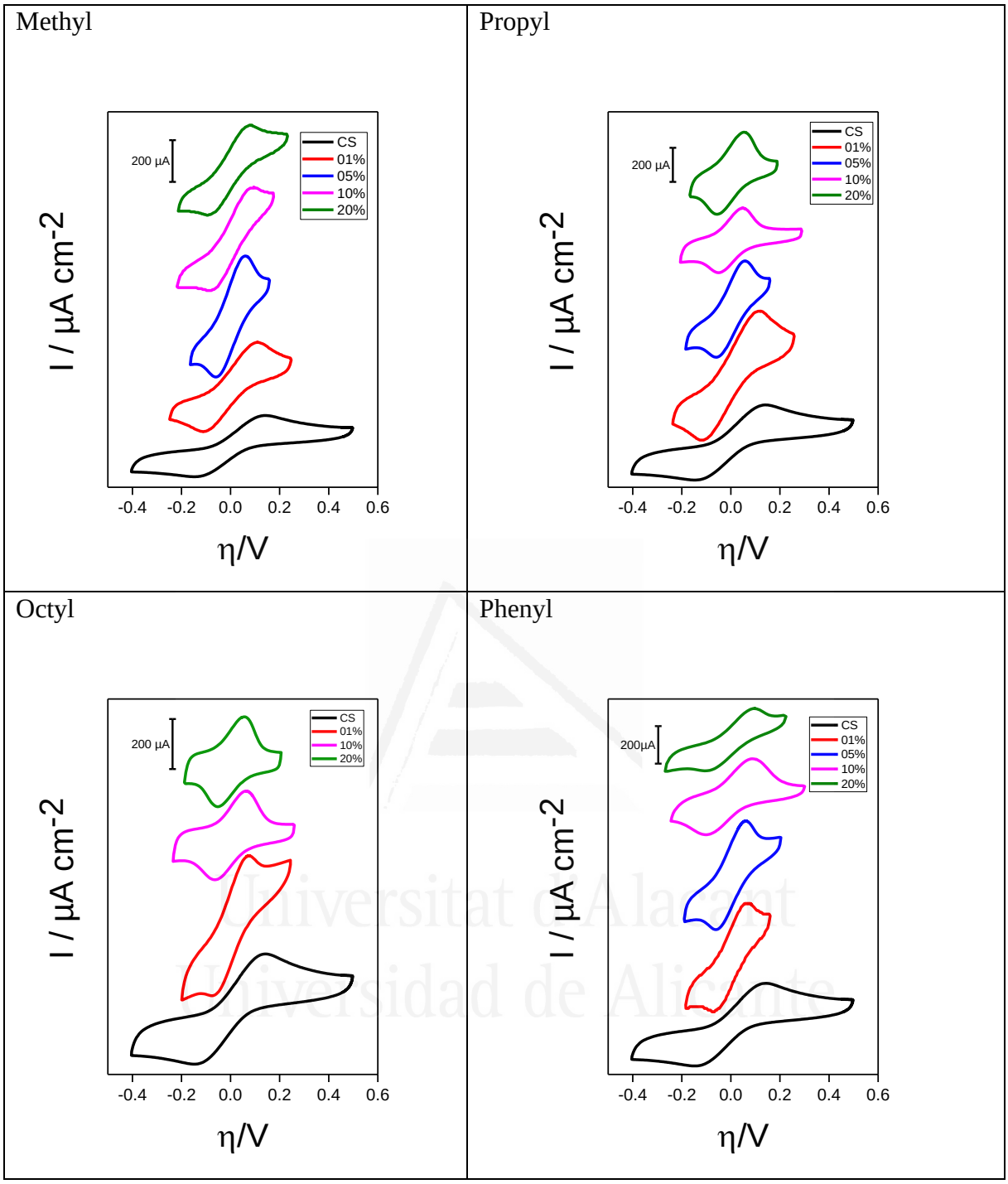

Figure 4.32: Stabilised cyclic voltammogram of carbon electrode immersed in monolith of silica of $Fe(CN)_6^{-4/-3}$ and introducing Methyl, Propyl, Octyl and Phenyl group at different concentration (1-5-10 and 20%) from the bottom to up at scan rate 100 mV s^{-1}.

Table 4.8: Value of the peak separation of the ferro / ferricyanide encapsulated in silica monolith and modified with organic functionalities at different concentration.

	Methyl	**Propyl**	**Octyl**	**Phenyl**
ΔE_P 0%	288	288	288	288
ΔE_P 1%	101	102	103	109
ΔE_P 5%	120	107	106	124
ΔE_P 10%	169	109	112	186
ΔE_P 20%	181	111	118	205

Figure 4.33 shows stabilized cyclic voltammogram of carbon electrode immersed in monolith of silica of $Fe(CN)_6^{-4/-3}$ introducing (propyl, octyl, phenyl and methyl) groups at concentration 10% at different scan rate.

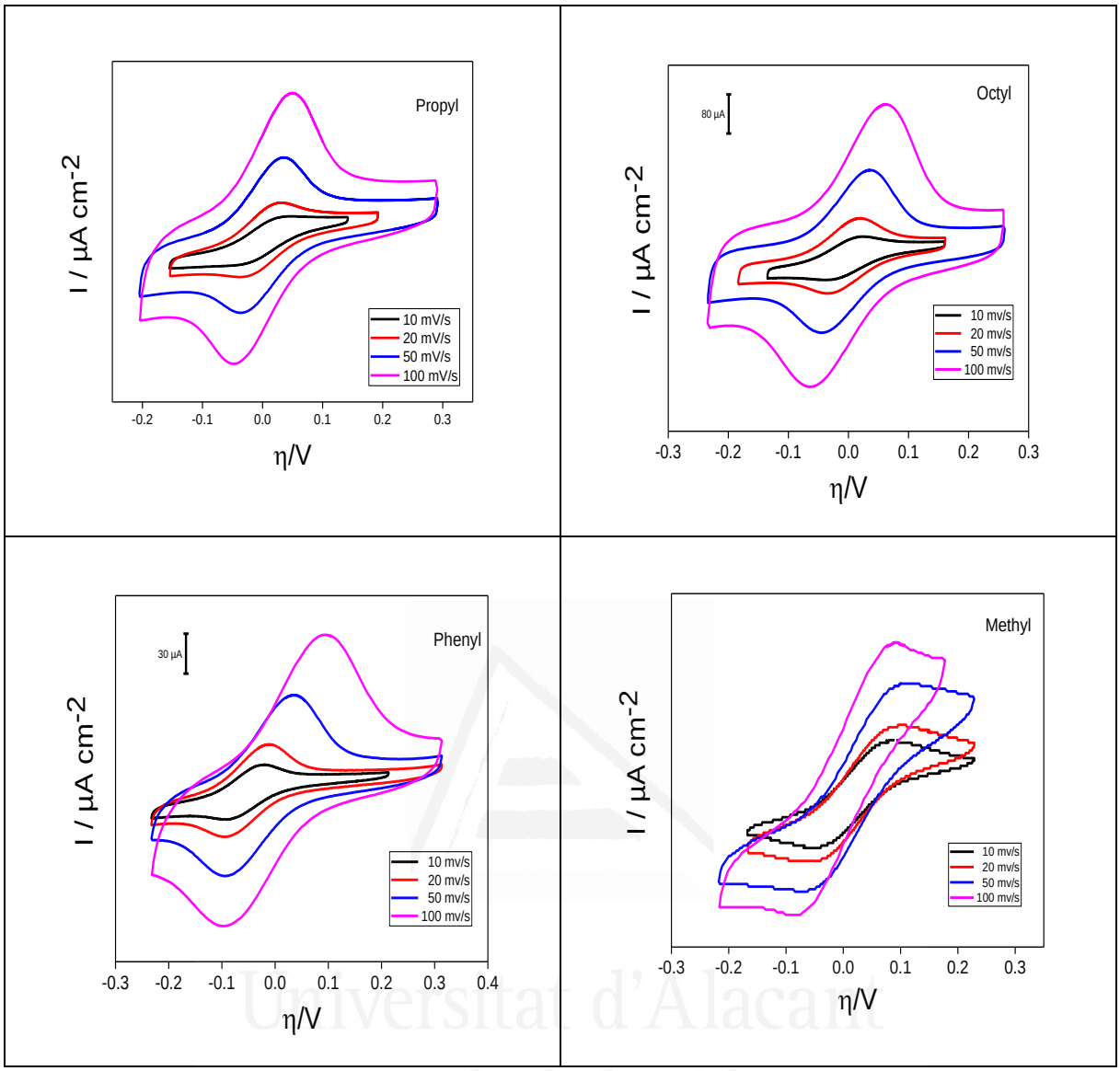

Figure 4.33. Stabilised cyclic voltammogram of carbon electrode immersed in monolith of silica of $Fe(CN)_6^{-4/-3}$ introducing (propyl, phenyl, octyl and methyl) groups at concentration 10% at different scan rates: 10, 20, 50, 100 and 200 mV s^{-1}.

As observed the intensity of the redox peaks processes increases as a function of the scan rate as expected. Figure 4.34 shows the evolution of the corrected peak currents vs the scan rate of Ferro / Ferricyanide encapsulated with propyl group (5%).

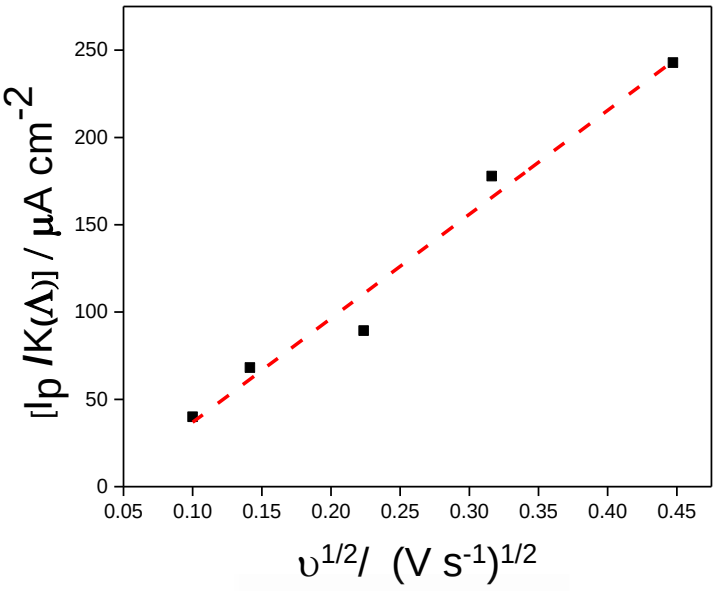

Figure 4.34: The evolution of the corrected peak currents vs the scan rate of Ferro / Ferricyanide encapsulated with propyl group (5%).

The diffusion coefficient for solution of *p*-aminophenol were calculated from the value of the slope linear fit in figure 4.33, $D=4.91\times10^{-6}cm^2\cdot s^{-1}$. Similar calculations of diffusion coefficient were made for the other organic groups at different concentrations (1-5-10 and 20%), and data are collected in table 4.9.

Table 4.9: Value of the diffusion coefficient of the ferro / ferricyanide encapsulated in silica monolith and modified with organic functionalities at different concentration.

Diffusion Coefficient	Methyl	Propyl	Octyl	Phenyl
0%	4.62×10^{-6}	4.62×10^{-6}	4.62×10^{-6}	4.62×10^{-6}
1%	4.66×10^{-6}	4.46×10^{-6}	3.7×10^{-6}	1.53×10^{-6}
5%	5.20×10^{-6}	4.91×10^{-6}	4.83×10^{-6}	2.10×10^{-6}
10%	6.50×10^{-6}	7.79×10^{-6}	7.39×10^{-6}	6.15×10^{-6}
20%	7.40×10^{-6}	8.34×10^{-6}	9.58×10^{-6}	7.25×10^{-6}

This table shows the value of diffusion coefficient of ferro / ferricyanide of conventional silica monolith and modified with organic functionalities at different concentration. It was calculated from the slope of Randles-Sevick plot obtained with the corrected value of current and equation 3. The diffusion coefficient increases with the increase of the concentration of the organic functionalities group.

4.4. Preliminary studies for the development of a biosensor based on ALP activity.

Alkaline phosphatase (ALP) is a hydrolase enzyme belonging to the group of phosphoric monoester hydrolases, and therefore, is capable of catalyzing the hydrolysis of a chemical bond. Its main activity is to carry out the dephosphorylation of certain molecules such as proteins, nucleotides and alkaloids, at alkaline pH, as its name suggests. For all this it is also called ortho-phosphoric-monoester hydrolase.

An alternative substrate is described for enzyme immunoassays with electrochemical detection. Alkaline phosphatase activity is determined by using *p*-aminophenyl phosphate as the enzyme substrate. Enzyme-generated *p*-aminophenol is detected amperometrically at a carbon electrode.

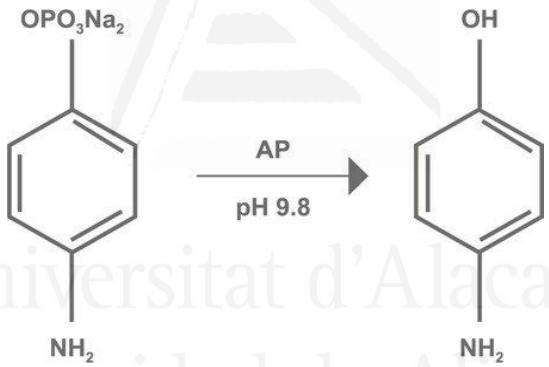

We start first with the study of *p*-aminophenyl phosphate and alkaline phosphatase in solution. Figure 4.35 shows the cyclic voltammogram of a carbon electrode immersed in a solution of *p*-aminophenyl phosphate (10mM) and Alkaline Phosphatase (30 µM).

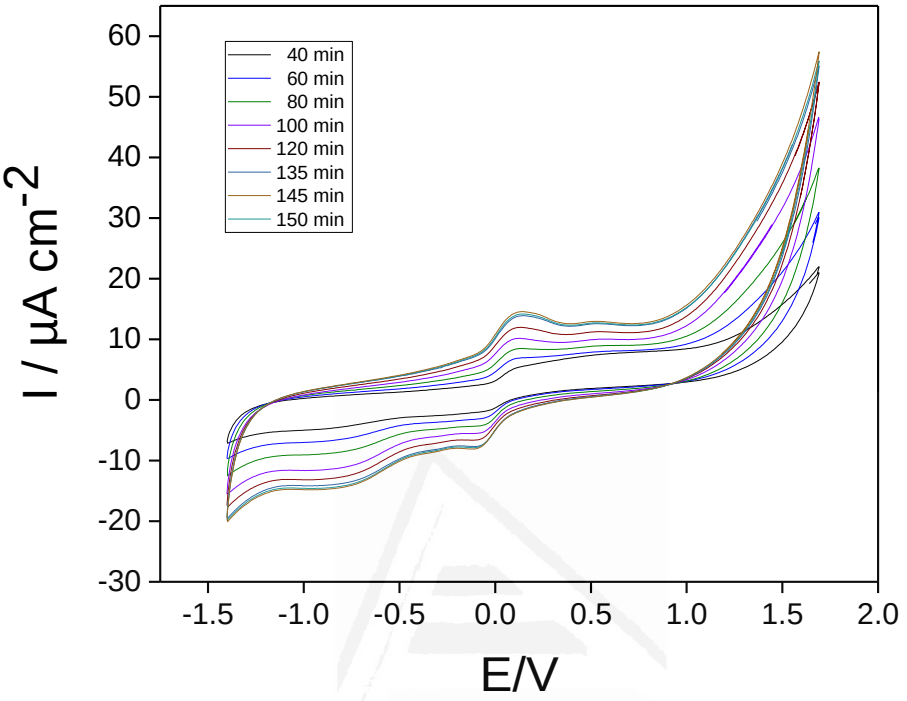

Figure 4.35. The cyclic voltammogram of a carbon electrode immersed in a solution of *p*-aminophenyl phosphate (10mM) and Alkaline Phosphatase (30 µM).

In the scan to positive potentials we observe emerging from 1.8V an oxidation current density, due to formation of *p*-aminophenol. Initially, the current density is near 0 on the zone potential between -1.4 and 1.8V, we observe the growing of current in this zone, but from 140 minutes it becomes stable.

Figure 4.36 shows the evolution of the current peak vs the time for carbon electrode immersed in a solution of *p*-aminophenyl phosphate and Alkaline Phosphatase.

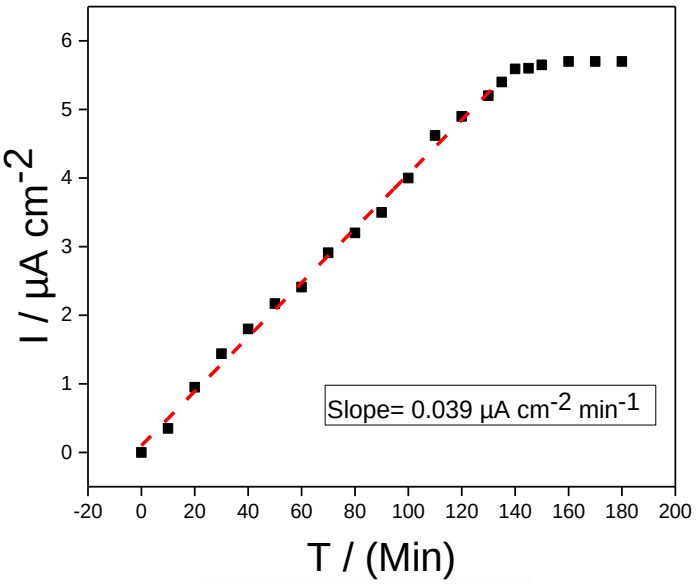

Figure 4.36. The evolution of the current peak vs the time for screen printed electrode immersed in a solution of p-aminophenyl phosphate and Alkaline Phosphatase. Kinetics of transformation.

The slope was calculated from the growth of the current until stabilization, which is of value 0.039 µA cm^{-2} min^{-1}.

Figure 4.37 shows the cyclic voltammogram of a carbon electrode immersed in a silica gel of *p*-aminophenyl phosphate (10mM) and Alkaline Phosphatase (30 µM).

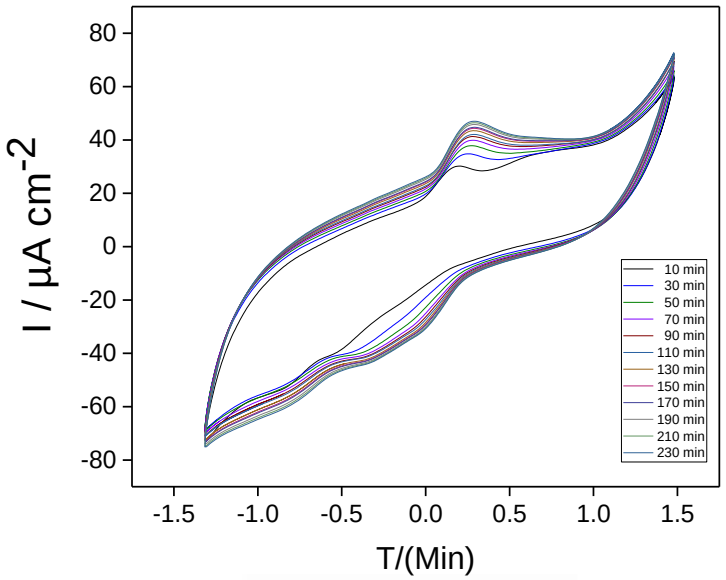

Figure4.37. The cyclic voltammogram of a carbon electrode immersed in a silica gel of *p*-aminophenyl phosphate (10mM) and Alkaline Phosphatase (30 µM).

In the scan to positive potentials we observe emerging from 1.5V an oxidation current density. Initially, the current density is near 0 on the zone potential between -1.4 and 1.5V, we observe the growing of current in this zone of potential, from 150 minutes it becomes stable.

Figure 4.38 shows the evolution of the current peak vs the time for the electrode immersed in silica of *p*-aminophenyl phosphate and Alkaline Phosphatase.

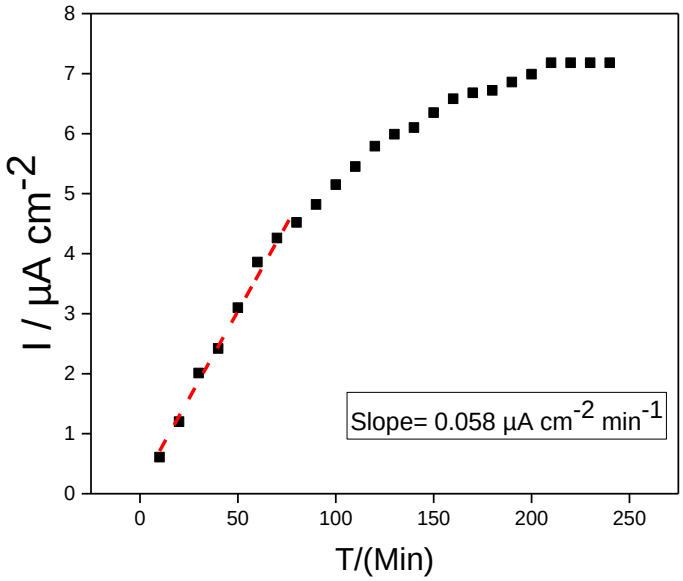

Figure4.38. The evolution of the current peak vs the time for screen printed electrode immersed in silica of *p*-aminophenyl phosphate and Alkaline Phosphatase. Kinetics of transformation

And also the slope was calculated with the growth of the current until stabilization which is of value 0.058µA cm^{-2} min^{-1}. After 150 minutes, the current becomes stable because all *p*-aminophenyl phosphate is converted into *p*-aminophenol.

The higher rate of *p*-aminophenol could be related with faster diffusion coefficient observed for this redox probe in silica as indicated in section 4.3.3.

5. General Conclusions

- Poly (3,4-ethylenedioxythiophene) doped with poly-(styrenesulfonate), PEDOT–PSS, films were synthesized by electrochemical methods from aqueous solution. The polymer thickness can be controlled by the potentiodynamic synthesis. Films synthesised deposited over a carbon support present smooth morphology due to the favorable interaction with the polymer.
- PEDOT-PSS thin films present a styrenesulfonate-to-EDOT ratio around 4, indicating that the overall charge of the film is negative. As polymer becomes thicker a progressive depletion of polyelectrolyte is observed.
- The electrocatalytic properties of PEDOT-PSS were studied against ferrocene redox probe. The electrochemical response of ferrocene can be clearly observed in thin polymer films. The heterogeneous constant for this transfer ranges between 2 and 6×10^{-3} cms^{-1}. The electrons transfer to the ferrocene seems progressively hindered as thicker the PEDOT-PSS films.
- The electroactive area for roughness factor that the transfer charge to the redox probe increases in thin PEDOT films but a gradual loss of the active area is observed in thicker films.
- Hybrid PEDOT-PSS silica films were prepared by electrochemical methods. The hybrid films present a dendritic morphology indicating the patterned growth of the polymer forced by the three- dimensional hollow structure of silica.
- PEDOT-PSS polymer grown across silica matrix present a styrenesulfonate-to-EDOT much higher than the polymer deposited over the bare surface, indicating that the doping level of PEDOT-PSS multiplied by a factor of 3 comparing with the film deposited on bare surface
- Conventional Silica and organically modified silica (ORMOSIL) monoliths were synthesized by sol-gel methodology, making use of tetraethylorthosilicate and alkyltriethoxysilane precursors.
- Silica monoliths were characterized by thermogravimetric analyses (TG), in all cases we detect in silica gel the presence of ethanol molecules that remained in the pores of silica coming from the precursor solution.
- TG and FTIR analyses allow the quantification of the organic group incorporated in ORMOSIL monoliths. In general terms as higher the concentration of alkylsilicate

precursor higher the concentration of organic group in the silica monolith, except in the case of methyl groups.

- The amount of organic groups in the silica gel is always higher than the calculated from the precursor solution composition except for the case of phenyl group where we observe a depletion of phenyl group in the gel.
- The electrochemical behaviour of *p*-aminophenol encapsulated in conventional silica and ORMOSIL monoliths were performed. The electrochemical response of *p*-aminophenol encapsulated in conventional silica is more irreversible than in solution, and the diffusion coefficient of *p*-aminophenol encapsulate in silica is near four times higher than in solution.
- The electrochemical behaviour of ferro/ferricyanide encapsulated in conventional silica and ORMOSIL monoliths were performed. The electrochemical response of ferro/ferricyanide encapsulated in conventional silica is more reversible than in solution, the diffusion coefficient for silica of ferro/ferricyanide is slightly smaller than the value in solution.
- The electrochemical response of *p*-aminophenol encapsulated in methyl, propyl and phenyl modified silica is more reversible than in conventional silica. As the concentration of this organic groups increases in the gel electrochemical reaction becomes more irreversible.
- The electrochemical response of *p*-aminophenol encapsulated in octyl modified silica is more reversible in low concentration of organic group become more reversible at higher concentration. The diffusion coefficient of *p*-aminophenol encapsulated in ORMOSIL in any composition is near one order of magnitude lower than in conventional silica. The diffusion coefficient increases as higher the concentration of organic groups.
- The electrochemical response of ferro/ferricyanide encapsulated in organic modified silica is more reversible than in conventional silica. As the concentration of this organic groups increases in the gel electrochemical reaction becomes more irreversible. The diffusion coefficient of ferro/ferricyanide encapsulated in silica are similar than in ORMOSIL. As higher the concentration of group increases the diffusion coefficient.
- Alkaline phosphatase was encapsulated in conventional silica monolith to develop a prototype of biosensor. Alkaline phosphatase presents activity in the hydrolysis of substrate (*p*-aminophenyl phosphate) to produce (*p*-aminophenol). The rate of *p*-aminophenol generation is faster in monolith than in solution.

6. Resumen

En los últimos años, la importancia de monitorear y controlar muchos parámetros diferentes en campos como los diagnósticos clínicos, la industria alimentaria, el medio ambiente, el análisis forense o el desarrollo de fármacos ha ido en aumento. Por lo tanto, existe la necesidad de contar con dispositivos analíticos confiables capaces de realizar análisis rápidos y precisos. Los métodos convencionales proporcionan alta sensibilidad y selectividad, pero son costosos, requieren mucho tiempo y requieren personal altamente capacitado. Una forma de superar muchas desventajas de estos métodos es desarrollar sensores.

Los sensores químicos son dispositivos que convierten la concentración de compuestos objetivo en una señal analítica. El término analítico implica el concepto de mensurabilidad. Luego, un sensor químico convierte la información sobre la presencia de compuestos objetivo en una cantidad medible. Actualmente, la electrónica es la tecnología que permite no solo la medición, sino también el uso eficiente de la información adquirida. Ejemplos de esto son el almacenamiento, el procesamiento, la comunicación y la utilización activa de la información para controlar las máquinas. La tecnología de sensores ha sido fundamental en la última extensión de la microelectrónica, y la extensión continua de las propiedades de los sensores está ganando campos de aplicaciones sin precedentes.

Un sensor puede definirse, de una manera muy general, como un dispositivo que responde a una señal o estímulo. Un estímulo puede entenderse como cualquier cantidad, propiedad o condición.En su gran mayoría, los sensores modernos no son dispositivos independientes. Forman parte de sistemas más grandes que pueden incorporar otros detectores, acondicionadores y procesadores de señal, dispositivos de memoria, grabadores de datos y transductores. En consecuencia, los sensores deben proporcionar una señal que sea legible por todos los demás elementos del sistema en el que están incorporados. Por eso, en la mayoría de los sistemas artificiales, la información sobre el estímulo, primero transmitida por la respuesta del sensor, se procesa y transmite. como una señal eléctrica: una tensión, una corriente o una carga. Esta señal eléctrica se puede describir con mayor detalle en términos de amplitud, frecuencia y / o fase[1,2].

Un sensor químico es un dispositivo analítico autónomo que puede proporcionar información sobre la composición química de su entorno, es decir, una fase líquida o gaseosa[4]. La información se proporciona en forma de una señal física medible que se correlaciona con la concentración de una determinada especie química (denominada analito). Dos pasos principales están involucrados en el funcionamiento de un sensor químico, a saber, el reconocimiento y la transducción. En la etapa de reconocimiento, las moléculas de analito interactúan selectivamente con las moléculas del receptor o los sitios incluidos en la estructura del elemento de reconocimiento del sensor. En consecuencia, un parámetro físico característico varía y esta variación se informa mediante un transductor integrado que genera la señal de salida. Un sensor químico basado en un elemento de reconocimiento hecho de un compuesto biológico es un biosensor. Sin embargo, como los materiales biomiméticos sintéticos van a sustituir, en cierta medida, los biomateriales de reconocimiento, una distinción entre un biosensor y un sensor químico estándar puede ser difícil. Los materiales biomiméticos típicos utilizados en el desarrollo de sensores son polímeros y aptámeros impresos molecularmente.

La química electroanalítica se utilizó para indicar el desarrollo de nuevos dispositivos y técnicas, y de nuevas metodologías para el uso correcto de las técnicas electroquímicas en química analítica. También incluía todas las técnicas (espectroscópicas, morfológicas, estructurales, etc.) adecuadas para caracterizar los materiales conductores de electricidad que constituyen el electrodo o las especies utilizadas como componente del electrodo. El término también incluye estas técnicas no electroquímicas siempre que se utilizan para identificar los efectos inducidos por la polarización del electrodo, como la transformación de especies, de la propia superficie del electrodo, etc.

Un sensor electroquímico es un dispositivo que transforma la información electroquímica en una señal analítica útil. Un sensor electroquímico está compuesto normalmente por un electrodo de trabajo, un electrodo de referencia y un contraelectrodo conectado a un potenciostato / galvanostato. El electrodo de trabajo actúa como receptor y también es un componente del transductor. La detección electroquímica es un campo analítico prometedor y ha encontrado su aplicabilidad en los campos de la energía, la salud, el medio ambiente, la industria alimentaria y farmacéutica[6]. La detección electroquímica da lugar al desarrollo de sensores químicos y biosensores. El sensor químico proporciona la información analítica sobre una cantidad particular de ciertas especies químicas en el ambiente circundante. Un biosensor es un dispositivo integrado que proporciona información analítica cuantitativa y semicuantitativa mediante el uso de un elemento de reconocimiento biológico que está en contacto espacial

directo con un elemento de transducción[7]. Los sensores electroquímicos tienen ciertas ventajas que incluyen su rentabilidad, aplicabilidad a una amplia gama de productos químicos, facilidad de uso y funcionalización, naturaleza robusta, alta sensibilidad y selectividad.

Hoy en día, el trabajo sobre biosensores y artículos publicados continúa avanzando utilizando diferentes elementos biológicos en combinación con varios tipos de transductores. En términos comerciales, los biosensores están adquiriendo rápidamente popularidad en el mercado global debido a su amplia variedad de aplicaciones en los campos de diagnóstico médico, productos farmacéuticos, biodefensa, industria alimentaria y procesos industriales. La mayor aplicación para biosensores sigue siendo los medidores de glucosa en sangre. Sin embargo, el mercado está cambiando hacia otras aplicaciones como la detección de enfermedades infecciosas, pruebas de colesterol, análisis de gases en sangre, pruebas de embarazo y aplicaciones en biología industrial, detección de toxicidad de alimentos y campo militar[19]. El término biosensores significa que el dispositivo es una combinación de tres partes: (i) un elemento de biorreconocimiento o bioreceptor, (ii) un elemento sensor también llamado transductor y (iii) un sistema de procesamiento de señales.

Los biosensores se pueden clasificar en cuatro grupos básicos diferentes en función de la transducción de señales: electroquímicos, ópticos, sensibles a la masa y sensores térmicos. Además, pueden clasificarse según el biorreceptor como: inmunoquímicos, enzimáticos, receptores no enzimáticos, células completas, biosensores de ácidos nucleicos y sensores biomiméticos. El pequeño tamaño de los electrodos y la posibilidad de miniaturización permiten la construcción de dispositivos de mano y / o en dispositivos de campo.

Muchas técnicas electroanalíticas tienen ventajas inherentes con propósitos variables y, por lo tanto, pueden utilizarse en una multitud de campos de estudio diferentes, que abarcan la catálisis enzimática[35], generación de radicales libres[36], conversión de energía solar[37]y miles de otros. Las principales ventajas de usar métodos voltamétricos sobre espectroscopia óptica o cromatografía incluyen su alta sensibilidad, precisión, precisión y rentabilidad. En concordancia con el mayor conocimiento de la electroquímica y una mejor comprensión de la síntesis y modificación de los electrodos, los sensores mejorarán considerablemente en términos de sensibilidad y límites de detección. Los microsensores y los nanosensores constituirán el siguiente paradigma disruptivo en el campo de la detección y la biosensibilidad. Los sensores electroquímicos se pueden dividir en tres tipos según su naturaleza y su principio

de funcionamiento, es decir, sensores potenciométricos, conductimétricos y amperométricos / voltamétricos.

diversa estrategias de inmovilización han sido reportadas. Los principales protocolos son: adsorciónfísica, unión covalente, atrapamiento, reticulación o unión por afinidad. En muchos casos, los métodos de inmovilización se basan en la combinación de varios métodos de inmovilización. Para estos cinco métodos básicos, se presenta una comparación a continuación: Según la naturaleza de unión, la adsorciónfísica implica enlaces débiles; el acoplamiento covalente es la unión química entre grupos funcionales de biomoléculas y el soporte; el atrapamiento es la incorporación de biomoléculas dentro de un gel o un polímero; la reticulación es un enlace entre biomoléculas, entrecruzante y molécula de inserción; la unión por afinidad implica un enlace entre un grupo funcional afín a una secuencia de proteínas. Los protocolos de inmovilización aparecen como un factor clave para desarrollar biosensores eficientes con rendimientos adecuados, como una buena estabilidad operativa y de almacenamiento, alta sensibilidad, alta selectividad, corto tiempo de respuesta y alta reproducibilidad. Las biomoléculas inmovilizadas deben mantener su estructura, su función, conservar su actividad biológica después de la inmovilización, permanecer estrechamente ligadas a la superficie y no desorberse durante el uso del biosensor. Además, un biosensor ideal debe ser estable para una aplicación a largo plazo. El tipo de método de inmovilización afecta la actividad y la estabilidad de los biosensores. Factores como la precisión de las mediciones, la reproducibilidad de un sensor a otro y la vida útil operacional se ven influenciados drásticamente por la estabilidad de las biomoléculas. Dado que los rendimientos analíticos de un biosensor se ven fuertemente afectados por el proceso de inmovilización, se han realizado intensos esfuerzos para desarrollar estrategias de inmovilización exitosas con el fin de asegurar una mayor sensibilidad y estabilidad de los biosensores. La elección de la técnica más apropiada y juiciosa también depende de la naturaleza de las biomoléculas, el transductor y el modo de detección asociado. El mejor método de inmovilización de biomoléculas varía si la aplicación del biosensor requiere una sensibilidad máxima o más bien se centra en la estabilidad. La reproducibilidad, el costo y la dificultad del proceso de inmovilización también deben ser considerados.

Los materiales de sílice porosos fabricados mediante el proceso de sol-gel a baja temperatura son matrices prometedoras para la encapsulación de biomoléculas. Hasta la fecha, los investigadores se han centrado en las rutas sol-gel utilizando alcóxidos como el tetrametilortosilicato (TMOS) y el tetraetilortosilicato (TEOS) para la encapsulación de biomoléculas. Estas rutas conducen a la formación de alcohol como un subproducto que puede

tener un efecto perjudicial sobre la actividad de las biomoléculas atrapadas. La síntesis de nanopartículas de sílice ha despertado gran interés en la investigación debido a su aplicación potencial en industrias (dispositivos electrónicos, aislantes, catálisis, etc.) y productos farmacéuticos (encapsulación de enzimas, administración de fármacos y marcadores celulares)[47,48]. El proceso Sol-gel se ha convertido en un área de investigación atractiva, en la que se han realizado amplios estudios sobre la síntesis de nanopartículas de sílice[49–51].

La encapsulación de enzimas y otras proteínas en materiales hospedantes inorgánicos que utilizan el procesamiento sol-gel ha atraído una atención considerable en los últimos años[52,53]. Esta investigación ha demostrado que las biomoléculas inmovilizadas en la matriz derivada de sol-gel conservan sus características funcionales en gran medida. Estos nuevos materiales compuestos son de interés para sus aplicaciones como biosensores de base óptica y electroquímica. La porosidad de los materiales sol-gel permite que pequeñas moléculas de analito se difundan en la matriz, mientras que las macromoléculas de proteínas grandes permanecen atrapadas físicamente en los poros. La transparencia de la matriz permite utilizar métodos de espectroscopía óptica para caracterizar las reacciones que ocurren en los poros del material. Los materiales sol-gel son condiciones ideales como hospedadores para dopantes biomoleculares porque se sintetizan a bajas temperaturas en condiciones de reacción bastante suaves[54].

En esta tesis se realiza un estudio de la modificación de electrodos mediante películas delgadas de sílice mediante el método sol-gel. La química Sol-gel ofrece un enfoque flexible para obtener una amplia gama de materiales. Permite lograr diferentes químicas y ofrece la capacidad de producir una amplia gama de nano / microestructuras[56]. La sílice existe bajo una amplia variedad de formas, con estructura cristalina y amorfa. Es un material que ha sido examinado exhaustivamente[47], Sus propiedades físicas y químicas son bien conocidas[54], lo que le otorga un número extraordinario de aplicaciones, como su uso en cromatografía, aislamiento térmico, catálisis y como soporte para catalizadores, se utiliza en el refuerzo de polímeros y como soporte para inmovilizar enzimas, entre otras. La sílice se puede modificar con una amplia variedad de grupos funcionales, lo que conduce a un considerable enriquecimiento y control de sus propiedades superficiales. Por ejemplo, estas propiedades han sido explotadas en gran medida en cromatografía, diseñando nuevas fases estacionarias. Además, la gran área de superficie combinada con las propiedades químicas de la superficie hace que la sílice sea un material excelente para usar como soporte de catalizador. A pesar de todas estas propiedades atractivas, el uso de sílice en métodos electroquímicos no fue generalizado. Los geles de sílice

preparados por la química sol-gel son materiales interesantes para la modificación de electrodos, y como no son electroactivos, pueden usarse como soporte para especies electroactivas, ya sea por adsorción o atrapamiento durante su formación, mejorando así su detección amperométrica[73–78]; Las propiedades más atractivas de los materiales de sílice son que tienen una gran capacidad para acumular varios analitos por adsorción, la sílice se puede modificar con grupos orgánicos de manera sencilla y estas modificaciones implican el desarrollo de una amplia gama de nuevos materiales. Además, estos materiales sirven como soporte para la inmovilización de enzimas en la fabricación de biosensores. Pero la razón fundamental para el uso de materiales sol-gel en la electroquímica es la existencia de múltiples formas de combinar las propiedades de los materiales inorgánicos con una amplia variedad de compuestos orgánicos a través de ORMOSIL.

La síntesis electroquímica es una técnica poderosa para la preparación de varios compuestos debido a su capacidad para controlar parámetros químicos y eléctricos que afectan la reacción general[110]. Los métodos electroquímicos pueden contribuir significativamente a la protección del medio ambiente a través de la minimización de la producción de residuos y materiales tóxicos. Por lo tanto, la electroquímica es un método ecológico para aplicaciones sintéticas[111]. Las películas finas de sílice se forman tradicionalmente a través de recubrimiento por rotación, recubrimiento por inmersión o recubrimiento por pulverización de un sol sobre una superficie plana[54,99,125]. En 1999, Mandler y sus colaboradores demostraron que es posible utilizar la electrodepósito para crear películas delgadas de sílice basadas en sol-gel sobre una superficie conductora[104]. En este caso, la película se preparó a partir de un sol prehidrolizado de metiltrimetoxisilano. Los iones hidróxido se formaron mediante la aplicación de un potencial suficientemente negativo para formar películas metiladas que varían en espesor desde nanómetros hasta micrómetros. En 2003, Collinson y sus colegas utilizaron la electrodeposición para crear películas de sílice delgadas sobre electrodos de carbono vítreos a partir de soles preparados únicamente a partir de tetrametoxisilano [96].

En el desarrollo de biosensores amperométricos es muy habitual usar ferroceno como transductor. El ferroceno (Fc) es un compuesto organometálico con excelentes propiedades redox[137,138]. El ferroceno tiene una buena estabilidad térmica y tolerancia al oxígeno debido a la interacción entre el átomo de hierro y el anillo de ciclopentadienilo. Esta interacción también facilita la síntesis de varios derivados de ferroceno[139]. Además, el ferroceno tiene un potencial de oxidación más bajo para perder un electrón debido a la oxidabilidad de su átomo de hierro y dos estados redox estables (ferroceno y ferricenio); en los sensores electroquímicos,

el componente que contiene ferroceno se utiliza como mediador o etiqueta. Se discuten el diseño arquitectónico, el efecto de mejora de los aditivos y las estructuras de los componentes que contienen ferroceno en los sensores correspondientes.

También es muy habitual el uso de a fosfatasa alcalina (ALP) como bioreceptor en biosensores amperométricos, la fosfatasa alcalina es una enzima de hidrólisis vital en el metabolismo del fosfato, que cataliza la hidrólisis de los grupos éster de fosfato en proteínas, ácidos nucleicos y otras moléculas pequeñas. Mientras tanto, una expresión normal de ALP se asocia con la aparición y el desarrollo de muchas enfermedades[161]. La fosfatasa alcalina (ALP) es una hidrolasa, que es responsable del proceso de desfosforilación de ácidos nucleicos, proteínas y algunas otras moléculas pequeñas [162], y se ha encontrado predominantemente en una variedad de tejidos de mamíferos, como hígado, hueso, riñón, placenta e intestino[163,164]. La enzima de la fosfatasa alcalina tiene un papel en el proceso de biomineralización[165]. Las fosfatasas alcalinas de varias fuentes se han estudiado intensamente en la interfaz aire-agua [166,167] .La importancia de las reacciones de transferencia de fosfato en los sistemas biológicos se refleja en la ubicuidad de los compuestos de fosfato. Los compuestos que contienen fosfato cumplen múltiples funciones biológicamente importantes, como ser metabolitos intermedios esenciales, materiales genéticos, fuentes de energía y depósitos de energía bioquímica [185]. Debido a las bajas velocidades de reacción de las hidrólisis del éster de fosfato, se requiere el uso de catalizadores. La superfamilia de enzimas llamadas fosfatasa tiene una maquinaria bioquímica que le permite hidrolizar los ésteres de fósforo rápidamente en condiciones celulares leves.

Se ha reportado la detección de *p*-aminofenol en el desarrollo de inmunosensores [187]. Una ventaja particular de *p*-AP es que es electroactivo, con un potencial de oxidación de 0.3 V [187], mientras que su precursor, el *p*-aminofenil fosfato no es electroactivo a este potencial, una etiqueta enzimática adecuada, p. ej. La fosfatasa alcalina (ALP), está unida al ADN objetivo por una molécula de biotina. Usamos *p*-aminofenilfosfato (*p*-APP) como sustrato para iniciar el proceso redox. La especie resultante de la reacción enzimática es para-aminofenol (*p*-AP). Tiene dos grupos electroquímicamente activos en la estructura del benceno. Él para-aminofenol se oxida a quinonaimina reversiblemente.

En el capitulo 2 se muestran las diferentes técnicas, reactivos y materiales utilizados durante este trabajo de tesis doctoral. También se describen las técnicas de funcionalización utilizadas para la preparación de los nuevos materiales. Sin embargo, las condiciones experimentales específicas se explicarán en detalle en cada capítulo. Existe una gran cantidad de técnicas electroquímicas disponibles para la caracterización. Se han utilizado celdas electroquímica con tres electrodos; voltamperometría cíclica (CV) cronoamperometría (CA); y muchas técnicas espectroscópicas se utilizan en la parte experimental de esta tesis; Espectroscopia fotoelectrónica de rayos X (XPS); Espectroscopia infrarroja transformada de Fourier (FTIR), y también hemos utilizado técnicas microscópicas como la microscopía electrónica de transmisión (TEM); Microscopía electrónica de barrido (SEM) y Microscopía electrónica de barrido de emisión de campo (FESEM). Las técnicas termogravimétricas se utilizan para determinar el peso de cada muestra en función de la temperatura, mientras que la muestra se somete a un programa de temperatura controlada en una atmósfera específica[203]. En Métodos experimentales explicamos cómo limpiar el material de vidrio y el tratamiento previo de los electrodos y hemos citado las soluciones, reactivos y electrodos.

En este capítulo 3 hemos visto la modulación del rendimiento electrocatalítico de PEDOT-PSS por inserción reactiva en una matriz de sílice sol-gel; Poli (3,4-etilendioxitiofeno) dopado con poli (estirenosulfonato), PEDOT-PSS, películas sintetizadas por métodos electroquímicos pueden considerarse como un pobre electrocatalizador para la oxidación del ferroceno en solución acuosa.

La modificación de la superficie del electrodo con un control preciso de los diversos componentes es capaz de producir sistemas moleculares integrados con aplicaciones extendidas en electroanálisis[205–207]. El uso de estos materiales modificados se extendió durante los últimos años y, particularmente, la ruta sol-gel ofreció la oportunidad de preparar películas similares a la cerámica en condiciones bastante suaves[61,208]. Esta síntesis de química suave mejoró la posibilidad de incorporar biomoléculas sensibles a la temperatura, como las enzimas a la capa huésped de sílice, dando como resultado materiales híbridos muy estables útiles para propósitos bioanalíticos [209]. La modificación de la superficie con geles de sílice se realiza típicamente mediante el recubrimiento del electrodo con películas delgadas obtenidas de un sol, que se obtiene mediante la hidrólisis de los precursores de alcóxidos metálicos en soluciones de agua / alcohol mediante técnicas convencionales como el recubrimiento por giro o inmersión o, incluso, mediante deposición electro-asistida[210,211]. Las propiedades electroquímicas mejoradas de los híbridos de polímeros conductores de sílice se utilizaron para desarrollar

electrodos para la electroquímica directa del citocromo c, cyt c, encapsulados dentro de una película de sílice. La inserción electroquímica de poli (3,4-etilendioxitiofeno) dopada con poli (estirenosulfonato), PEDOT-PSS, a través de los poros de sílice conecta eléctricamente las moléculas de proteínas, lo que da lugar a un aumento de 3 veces en la tasa de reducción electroquímica cyt c[213].

El presente trabajo se centra en la síntesis electroquímica de electrodos modificados que contienen películas PEDOT-PSS y su aplicación al estudio de las reacciones redox del ferroceno. De esta manera, el rendimiento electrocatalítico de los electrodos modificados con PEDOT-PSS se ajustará insertando este polímero conductor en matrices de sílice electrodepositada y, posteriormente, se explorará el rendimiento electroquímico del material híbrido para los procesos redox de ferroceno. Todas las modificaciones de los electrodos se realizarán, exclusivamente, por métodos electroquímicos. Las películas de PEDOT-PSS fueron caracterizadas con voltamogramas cíclicos registrados para un electrodo de carbono vítreo (GC) en el curso de la oxidación del monómero EDOT en una solución acuosa que contiene PSS como electrolito. Durante el primer barrido, la densidad de corriente es casi cero dentro de la región potencial comprendida entre 0,4 y 1,5 V. La oxidación del monómero comienza a aproximadamente 1,6 V y continúa con una cinética electroquímica rápida, como se deduce de la alta pendiente de la curva j-E. En ciclos potenciales sucesivos, el progreso de una meseta actual entre 0,4 V y 1,5 V revela la respuesta similar a la capacitancia de la película PEDOT-PSS depositada, mientras que la masa de polímero se puede determinar fácilmente en cualquier momento a partir de su carga de doble capa, suponiendo un valor de $70 Fg^{-1}$ para la capacitancia específica[213,232].

La morfología de la superficie de las películas PEDOT-PSS depositadas se examinó con la ayuda de un microscopio electrónico de emisión de campo. Obtuvimos varias micrografías para diferentes electrodos con una masa creciente de polímero depositado que oscila entre 46.5 y $815 \mu g cm^{-2}$. Todas las películas cubren uniformemente toda la superficie de los sustratos de GC, aunque se pueden observar con mayor claridad cuando se depositan grandes cantidades de material polimérico. El proceso de secado genera algunos defectos similares a grietas. Vale la pena mencionar que la homogeneidad de la superficie de estas películas PEDOT-PSS contrasta con algunos datos de la literatura. Por ejemplo, se informó un aspecto granular cuando el material se deposita a partir de disolventes orgánicos [233] o una estructura agregada, similar a la coliflor, cuando se depositó a partir de soluciones acuosas sobre sustratos de oro[234]. La

interacción favorable entre el soporte de carbono y la capa de polímero parece ser el origen de la morfología más suave mostrada por nuestras muestras.

La espectroscopía fotoelectrónica de rayos X de alta resolución (XPS) se ha empleado para caracterizar la estructura química de los recubrimientos PEDOT-PSS. Un electrodo de carbono vítreo cubierto con una masa de polímero depositado cerca de 202 $\mu g cm^{-2}$, se transfirió a la cámara UHV, donde se analizaron las regiones espectrales C, O y S. El espectro de nivel de núcleo de C 1s registrado, donde se pueden distinguir claramente tres contribuciones principales a 284.5, 285.5 y 286.8eV. El pico a menor energía de unión corresponde al carbono localizado en el esqueleto aromático de PEDOT o en los restos fenilo de PSS. Además, la contribución a 285.5eV se origina a partir de átomos de C unidos directamente a los átomos de S, como los presentes en las unidades EDOT y PSS. Finalmente, el elemento de alta energía en 286.8eV se puede asignar a las estructuras C-O-C presentes en los restos EDOT[235–237].

En el comportamiento electroquímico del ferroceno en películas PEDOT-PSS no modificadas en esta parte, examinamos primero el rendimiento electrocatalítico de las películas PEDOT-PSS prístinas hacia un mediador redox típico como el ferroceno. Con fines comparativos, la actividad electroquímica de un electrodo de carbono vítreo desnudo también se ha incluido en el estudio. La oxidación electroquímica del centro redox del ferroceno, $Fe^{2+} \rightarrow Fe^{3+}$, en los sustratos de GC se caracteriza por la presencia de un pico anódico reversible centrado a 0.515 V en medio ácido. El contra-proceso farádico ocurre a 0.385 V durante el escaneo inverso. Como resultado, la separación máxima entre las características anódicas y catódicas, ΔE_P, es de 130 mV en las condiciones experimentales empleadas.

Se realizó un análisis adicional sobre los resultados voltamétricos para evaluar la cinética de la transferencia de electrones a través del polímero. La reversibilidad cinética de la reacción electroquímica se evaluó a partir de la separación del pico del proceso redox de los experimentos de voltametría cíclica aplicando el método de Nicholson[240]. En tales experimentos, se obtuvieron voltamogramas cíclicos estabilizados para electrodos de GC desnudos y películas PEDOT-PSS sumergidas en soluciones de prueba que contienen ferroceno a diferentes velocidades de escaneo que oscilan entre 10 y 200 mVs^{-1}. Los valores de separación de picos para una velocidad de barrido 100 mVs^{-1}.

Se estudió el comportamiento electroquímico del ferroceno en los electrodos híbridos de sílice PEDOT-PSS. Se sabe que las matrices de SiO_2 poroso químicamente modificadas poseen la capacidad de mejorar la cinética de varias reacciones electroquímicas[212,217,242]. Este efecto se logra gracias al entorno particular proporcionado por los poros de sílice, que puede reorganizar las moléculas electroactivas, cambiar sus propiedades de transporte de difusión e incluso estimular interacciones electrostáticas favorables o adversas. En esta sección, trataremos de modificar la actividad de PEDOT-PSS hacia la oxidación del ferroceno insertando el polímero a través de una matriz de sílice tridimensional depositada previamente en la superficie GC[212]. Después de que la sílice se depositó en GC, el electrodo se enjuagó con agua ultrapura y se mantuvo húmedo (en estado de hidrogel) para sumergirlo en una solución acuosa que contenía tanto EDOT como PSS. El polímero se depositó potenciodinámicamente hasta que se alcanzó una capacitancia de 14.1 $mFcm^{-2}$. En una superficie plana de GC, tal valor de capacitancia corresponde a una densidad de masa PEDOT-PSS cercana a 202μgcm^{-2}[232]. Sin embargo, cuando el polímero crece dentro de la plantilla de sílice, esos 14.1 $mFcm^{-2}$ significa que se han depositado cantidades equivalentes de material electroactivo.

El PEDOT-PSS se puede electrodepositar en superficies desnudas de GC a partir de soluciones acuosas que contienen monómero EDOT en presencia de aniones PSS. Después de la electropolimerización, XPS reveló un exceso de dopante PSS para muestras extremadamente delgadas y un descanso progresivo de estos iones polielectrolitos a medida que aumenta la cantidad de polímero depositado. El material PEDOT-PSS no modificado es un electrocatalizador deficiente para la oxidación del ferroceno. De hecho, se ha encontrado que la velocidad de transferencia de electrones disminuye progresivamente a medida que aumenta la cantidad de polímero depositado.

El modesto rendimiento electroquímico de las películas PEDOT-PSS prístinas se puede mejorar haciendo crecer el polímero a través de una matriz de sílice depositada previamente en la superficie GC. Al contrario de la superficie lisa de las películas PEDOT-PSS no modificadas, el material híbrido orgánico-inorgánico exhibe estructuras tridimensionales, como resultado del crecimiento modelado. La constante de transferencia de electrones para la oxidación del ferroceno casi se duplica cuando se produce la reacción electroquímica en este polímero modificado y, además, el nivel de dopaje de PEDOT se multiplica por un factor de tres de los encontrados para películas de masa electroactiva similar depositada en superficies de GC

desnudas. Tal efecto está acompañado por un aumento significativo en el área activa verdadera disponible para la transferencia de electrones a la sonda redox.

En conclusión la velocidad de transferencia de electrones a sonda redox decae progresivamente a medida que aumenta la cantidad de polímero depositado y el área electroactiva disponible para la reacción electroquímica muestra cifras bastante modestas. Presentamos aquí una forma alternativa y sencilla de mejorar las propiedades de este material que utiliza, exclusivamente, métodos de síntesis electroquímica. El rendimiento electrocatalítico se puede mejorar significativamente insertando el polímero dentro de una matriz de sílice porosa tridimensional pre-depositada que forma un material híbrido interpenetrante. Por un lado, el PEDOT-PSS modificado muestra niveles de dopaje que triplican el material no modificado. Por otro lado, la constante de transferencia de electrones y el área electroactiva real para la oxidación del ferroceno aumentaron en un factor de 2 y 4, respectivamente.

En este capítulo 4 hemos visto el comportamiento electroquímico de las sondas redox encapsuladas en monolitos de sílice sol-gel: Como plataforma para el desarrollo de biosensores, hemos sintetizado monolitos de sílice utilizando la metodología sol-gel. Dos sondas redox fueron encapsuladas en los monolitos *p*-aminofenol y ferro/ferricianuro. El hidrogel monolítico se ha utilizado como medio electrolítico para una celda electroquímica, en contacto con un electrodo de carbón serigrafiado. Esto permitió el estudio del comportamiento electroquímico de las sondas ferro / ferricianuro y *p*-aminofenol encapsuladas. La respuesta electroquímica de estas sondas en disolución se comparó con la obtenida en el hidrogel.

El carácter químico de la sílice se moduló mediante la introducción de funcionalidades orgánicas (grupos metilo, propilo, octilo y fenilo). La sonda p-aminofenol se estudió en estos sistemas ya que esta especie es el producto generado por la enzima fosfatasa alcalina, que nos permitirá desarrollar biosensores basados en esta proteína y su sustrato (*p*-aminofenilfosfato). Se ha demostrado que estas proteínas pueden incluirse dentro de las matrices sol-gel de sílice y conservar su actividad dentro del monolito [248].

Para la preparación de TEOS hidrolizados, en un vial, se preparó una solución de sílice a temperatura ambiente, mezclando TEOS (5,6 ml) con ETANOL (7,6 ml) y HCl 2,7 M (0,01 M). La disolución, con dos fases claramente diferenciadas, se agitó vigorosamente durante

aproximadamente una hora, el tiempo necesario para que el TEOS se hidrolice. La aparición de una sola fase se usó como un indicador visual para saber que la hidrólisis había terminado.

La rotaevaporación del TEOS hidrolizado, se realizó para la eliminación completa del etanol residual generado durante el proceso de hidrólisis, ya que puede interferir negativamente con las biomoléculas inmovilizadas y en las proteínas, inducir un desnaturalizacion total o parcial de su conformación nativa.

La fabricación de monolitos utilizando la técnica sol-gel se utilizó comométodo de inmovilización de enzima, el proceso sol-gel es uno de los más utilizados debido a las muchas ventajas que posee. Los monolitos obtenidos con ella presentan, entre otros beneficios, estabilidad térmica y química, posibilidad de variar el número y tamaño de sus poros, estabilidad de las biomoléculas encapsuladas en su interior y resistencia a la pérdida y desorción de las mismas.

Se prepararon matrices con la enzima ALP y el *p*-APP, una vez obtenido el TEOS hidrolizado, 1 ml de este últimodisolución con 1 ml de solución de ALP y 1 ml de solución de *p*-APP se ha mezclado, la mezcla se agitó con cuidado para formar burbujas. Siguiendo este protocolo, la formación de gel se produjo en aproximadamente 15 minutos a temperatura y presión ambiente.

Al caracterizan los geles de sílice por TG se observa que al aumentar la temperatura la pérdida de masa para la sílice es bastante similar, en todos los casos la pérdida de masa oscila entre el 3 y el 5%. Los resultados del análisis termogravimétrico para muestras de sílice modificadas con diferentes concentraciones de grupos metilo en la disolución del precursor,% molar de grupos metilo (M), fórmula teórica (obtenida de la solución del precursor) y fórmula medida por TG. En todos los casos, entre 38 y 49% de los grupos metilo se han incorporado independientemente de la concentración de precursor utilizada en la solución precursora. Se obtuvieron resultados similares de Porcel-Valenzuela sobre gel de sílice obtenido por deposición electroquímica [250].

Se observa que la cantidad de grupos propilo incorporados en el gel aumenta con la cantidad creciente de grupos propilo en la solución precursora. En términos generales, la concentración de grupos incorporados en sílice es más alta que en la solución precursora. Para la sílice modificada con grupos propilo, la descomposición de la materia orgánica tiene lugar a temperaturas entre 550 y 750ºC. La descomposición se produce a valores de temperatura

más bajos a medida que aumenta la cantidad de grupo orgánico en la sílice, es decir, se obtienen geles más térmicamente estables utilizando concentraciones más bajas de precursor orgánico.

Los precursores de sílice convencionales contienen cuatro grupos alcóxido idénticos que son hidrolizables (enlaces Si-O), generalmente grupos etóxido; mientras que para obtener sílice modificada orgánicamente, se utilizan precursores que contienen grupos alquilo no hidrolizables (enlaces Si-C): metilo (M), n-propilo (P), octilo (O) y fenilo (Ph). El uso de la espectroscopia infrarroja revela la existencia de monolitos químicamente diferentes y comparables según la naturaleza de los precursores utilizados.

Se estudió el comportamiento electroquímico de *p*-aminofenol en disolución y en sílice convencional y se muestra la actividad electroquímica de un electrodo de carbono frente la sonda redox de *p*-aminofenol. El voltamograma muestra en el barrido positivo un pico anódico centrado en 0.418V, que está relacionado con la oxidación de (*p*-aminofenol). En el escaneo inverso, el contra-proceso farádico ocurre a -0,400V. La separación de picos es de 818 mV. Para estas sondas, determinamos el potencial de equilibrio (Eq) de la sonda redox y, después, deducimos el sobrepotencial $\eta = E\text{-}Eq$. La separación de picos entre las características anódicas y catódicas, el sobrepotencial es la diferencia de potencial (voltaje) entre el potencial de reducción determinado termodinámicamente de una media reacción y el potencial en el que se observa experimentalmente el evento redox.

Hemos sintetizado monolitos de sílice utilizando la metodología sol-gel como se indica en la sección experimental. Esto permitió el estudio del comportamiento electroquímico del p-aminofenol encapsulado, y el comportamiento electroquímico de ferro/ferricyanideen disolución y en sílice. Estudiamos el comportamiento electroquímico de la sonda encapsulada con sílice; El coeficiente de difusión para sílice de $Fe(CN)_6^{-4/-3}$se calculó a partir del valor del ajuste lineal de pendiente en la figura 4.29, tiene un valor $D=4.62\times10^{-6}cm^2.s^{-1}$. Un resultado similar fue obtenido por otrosautores[260]. Este valor es ligeramente más pequeño que el valor en disolución porque estas sondas redox son más reversibles en sílice, por lo que el coeficiente de difusión disminuye.

El carácter químico de la sílice se moduló mediante la introducción de funcionalidades orgánicas y se estudió con la sonda redox de *p*-aminofenol se obtuvo.El voltagrama cíclico estabilizado de electrodo de carbono sumergido en monolito de sílice de *p*-aminofenol e introduciendo el grupo metilo, propilo, octilo y fenilo en diferentes concentraciones (1-20%)

en la composición de gel a una velocidad de barrido de 100 mV s^{-1}. Observamos que esta sonda es más reversible con funcionalidades orgánicas en diferentes concentraciones que en el monolito de sílice convencional, por lo que enfocamos el estudio de la separación de picos, el valor de la separación de picos de *p*-aminofenol del monolito de sílice convencional y luego, cuando modificamos con funcionalidades orgánicas en diferente concentración, es más reversible con una pequeña concentración de funcionalidades orgánicas que en el monolito de sílice convencional, excepto con el grupo octilo, es más reversible con una mayor concentración de funcionalidades orgánicas (10 y 20%).

El carácter químico de la sílice se moduló mediante la introducción de funcionalidades orgánicas y se estudió frente la sonda redox Ferro/Ferricianuro, se obtuvo el voltagrama cíclico estabilizado de electrodo de carbono sumergido en monolito de sílice con Ferro/Ferricianuroe overcome introduciendo el grupo metilo, propilo, fenilo y octilo a diferentes concentraciones (1-20%) una velocidad de barrido de 100 mV s^{-1}. Observamos que es más reversible con funcionalidades orgánicas en diferentes concentraciones que en el monolito de sílice convencional, por lo que enfocamos el estudio de la separación de picos. El valor de la separación de picos del ferrocianuro del monolito de sílice convencional y la modificamos con funcionalidades orgánicas a diferentes niveles concentración. Este proceso es más reversible con funcionalidades orgánicas que en el monolito de sílice convencional.

Los estudios preliminares para el desarrollo de un biosensor basado en la actividad de la fosfatasa alcalina fueron estudiados. La fosfatasa alcalina (ALP) es una enzima hidrolasa que pertenece al grupo de las hidrolasas fosfóricas y, por lo tanto, es capaz de catalizar la hidrólisis de un enlace químico. Su actividad principal es llevar a cabo la desfosforilación de ciertas moléculas como proteínas, nucleótidos y alcaloides, a pH alcalino, como sugiere su nombre. Por todo esto también se le llama hidrolasa orto-fosfórica-monoéster. Se describe un sustrato alternativo para los inmunoensayos enzimáticos con detección electroquímica. La actividad de la fosfatasa alcalina se determina utilizando fosfato de *p*-aminofenilo como el sustrato enzimático. El *p*-aminofenol generado por la enzima se detecta amperométricamente en un electrodo de carbono. Comenzamos primero con el estudio de *p*-aminofenil fosfato y fosfatasa alcalina en solución, tomamos 1.5 ml de cada solución. El voltagrama cíclico de un electrodo de carbono sumergido en una solución de *p*-aminofenil fosfato (10 mM) y fosfatasa alcalina. En el barrido a potenciales positivos observamos que emergen a 1.8 V una densidad de corriente de oxidación, debido a la formación de *p*-aminofenol. Inicialmente, la densidad de corriente es cercana a 0 en el potencial de la zona entre -1.4 y 1.8 V, observamos el crecimiento de la

corriente en esta zona, pero a partir de 140 minutos se estabiliza; la evolución del pico de corriente frente al tiempo para el electrodo de carbono sumergido en una solución de p-aminofenil fosfato y fosfatasa alcalina; La evolución del pico actual frente al tiempo para el electrodo serigrafiado sumergido en una solución de *p*-aminofenil fosfato y Fosfatasa Alcalina. Hicimos el mismo estudio, pero encapsulando en sílice. Y se observó una cinética de formación de *p*-aminofenol similar.

7. References

[1] J. Farden, Handbook of modern sensors : physics, designs, and applications, 3rd editio, Springer-Verlag, 2003.

[2] Sensor Technology Handbook - Jon S. Wilson - Google Livres, (n.d.).

[3] R.M. White, A Sensor Classification Scheme, IEEE Trans. Ultrason. Ferroelectr. Freq. Control. 34 (1987) 124–126. doi:10.1109/T-UFFC.1987.26922.

[4] F.G. Banica, Chemical Sensors and Biosensors: Fundamentals and Applications, John Wiley & Sons Inc, 2012.

[5] Electroanalytical Chemistry: A Series of Advances: - Google Livres, (n.d.).

[6] F. Faridbod, V.K. Gupta, H.A. Zamani, Electrochemical Sensors and Biosensors, 2011 (2011) 2–4. doi:10.4061/2011/352546.

[7] D.R. Thévenot, K. Toth, R.A. Durst, G.S. Wilson, ELECTROCHEMICAL BIOSENSORS: RECOMMENDED DEFINITIONS AND CLASSIFICATION *, Anal. Lett. 34 (2001) 635–659. doi:10.1081/AL-100103209.

[8] A. Mardegan, P. Scopece, P. Ugo, L.M. Moretto, Ensembles of Gold Nanowires for the Anodic Stripping Voltammetric Determination of Inorganic Arsenic, J. Nanosci. Nanotechnol. 15 (2015) 3417–3422. doi:10.1166/jnn.2015.10213.

[9] M. De Leo, A. Kuhn, P. Ugo, 3D-Ensembles of Gold Nanowires: Preparation, Characterization and Electroanalytical Peculiarities, Electroanalysis. 19 (2007) 227–236. doi:10.1002/elan.200603724.

[10] F. Arduini, C. Zanardi, S. Cinti, F. Terzi, D. Moscone, G. Palleschi, R. Seeber, Effective electrochemical sensor based on screen-printed electrodes modified with a carbon black-Au nanoparticles composite, Sensors Actuators B Chem. 212 (2015) 536–543. doi:10.1016/J.SNB.2015.02.051.

[11] I. Gualandi, E. Scavetta, Y. Vlamidis, A. Casagrande, D. Tonelli, Co/Al layered double hydroxide coated electrode for in flow amperometric detection of sugars, Electrochim. Acta. 173 (2015) 67–75. doi:10.1016/J.ELECTACTA.2015.04.172.

[12] L.C. Clark, C. Lyons, ELECTRODE SYSTEMS FOR CONTINUOUS

MONITORING IN CARDIOVASCULAR SURGERY, Ann. N. Y. Acad. Sci. 102 (2006) 29–45. doi:10.1111/j.1749-6632.1962.tb13623.x.

[13] G.G. Guilbault, J.G. Montalvo, Urea-specific enzyme electrode, J. Am. Chem. Soc. 91 (1969) 2164–2165. doi:10.1021/ja01036a083.

[14] W. Mindt, P. Racine, Stimulating electrode with low energy consumption, Med. Biol. Eng. 11 (1973) 659–660. doi:10.1007/BF02477420.

[15] A.H. Clemens, P.H. Chang, R.W. Myers, [Development of an automatic system of insulin infusion controlled by blood sugar, its system for the determination of glucose and control algorithms]., Journ. Annu. Diabetol. Hotel. Dieu. (1976) 269–78.

[16] E.F. Pfeiffer, W. Beischer, C. Thum, A.H. Clemens, [The artificial endocrine pancreas in clinical medicine and in research., Journ. Annu. Diabetol. Hotel. Dieu. (1976) 279–96.

[17] K. Cammann, Bio-sensors based on ion-selective electrodes, Fresenius' Zeitschrift Für Anal. Chemie. 287 (1977) 1–9. doi:10.1007/BF00539519.

[18] R. Renneberg, D. Pfeiffer, F. Lisdat, G. Wilson, U. Wollenberger, F. Ligler, A.P.F. Turner, Frieder Scheller and the Short History of Biosensors, in: Biosensing 21st Century, Springer Berlin Heidelberg, Berlin, Heidelberg, 2008: pp. 1–18. doi:10.1007/10_2007_086.

[19] Global Biosensors Market - Industry Analysis, Size, Share, Growth, Trends and Forecast 2014-2020, (n.d.).

[20] F.W. Scheller, U. Wollenberger, A. Warsinke, F. Lisdat, Research and development in biosensors, Curr. Opin. Biotechnol. 12 (2001) 35–40. doi:10.1016/S0958-1669(00)00169-5.

[21] A. Rahman, M.J.A. Shiddiky, J. Park, Y. Shim, An impedimetric immunosensor for the label-free detection of bisphenol A, 22 (2007) 2464–2470. doi:10.1016/j.bios.2006.09.010.

[22] A.J. Baeumner, Biosensors for environmental pollutants and food contaminants, Anal. Bioanal. Chem. 377 (2003) 434–445. doi:10.1007/s00216-003-2158-9.

[23] A.L. Jenkins, R. Yin, J.L. Jensen, Molecularly imprinted polymer sensors for pesticide and insecticide detection in water., Analyst. 126 (2001) 798–802.

[24] F.L. Dickert, O. Hayden, K.P. Halikias, Synthetic receptors as sensor coatings for molecules and living cells, Analyst. 126 (2001) 766–771. doi:10.1039/b009893k.

[25] B. Hock, M. Seifert, K. Kramer, Engineering receptors and antibodies for biosensors, Biosens. Bioelectron. 17 (2002) 239–249. doi:10.1016/S0956-5663(01)00267-6.

[26] M.B. Gu, R.J. Mitchell, B.C. Kim, Whole-Cell-Based Biosensors for Environmental Biomonitoring and Application, in: Springer, Berlin, Heidelberg, 2004: pp. 269–305. doi:10.1007/b13533.

[27] P. Fromherz, Electrical Interfacing of Nerve Cells and Semiconductor Chips, ChemPhysChem. 3 (2002) 276.

[28] R. Shoji, Y. Sakai, A. Sakoda, M. Suzuki, Development of a rapid and sensitive bioassay device using human cells immobilized in macroporous microcarriers for the on-site evaluation of environmental waters, Appl. Microbiol. Biotechnol. 54 (2000) 432–438.

[29] H. Schulze, S. Vorlová, F. Villatte, T.T. Bachmann, R.D. Schmid, Design of acetylcholinesterases for biosensor applications, Biosens. Bioelectron. 18 (2003) 201–209.

[30] P. Leonard, S. Hearty, J. Brennan, L. Dunne, J. Quinn, T. Chakraborty, R. O'Kennedy, Advances in biosensors for detection of pathogens in food and water, Enzyme Microb. Technol. 32 (2003) 3–13.

[31] J. Tamayo, M. Alvarez, L.M. Lechuga, Digital tuning of the quality factor of micromechanical resonant biological detectors, Sensors Actuators B Chem. 89 (2003) 33–39.

[32] H.. Lang, M.. Baller, R. Berger, C. Gerber, J.. Gimzewski, F.. Battiston, P. Fornaro, J.. Ramseyer, E. Meyer, H.. Güntherodt, An artificial nose based on a micromechanical cantilever array, Anal. Chim. Acta. 393 (1999) 59–65.

[33] R. Raiteri, M. Grattarola, H.-J. Butt, P. Skládal, Micromechanical cantilever-based biosensors, Sensors Actuators B Chem. 79 (2001) 115–126.

[34] K. Ramanathan, B. Danielsson, Principles and applications of thermal biosensors, Biosens. Bioelectron. 16 (2001) 417–423.

[35] Y.-M. Li, X.-T. Chen, J. Li, H.-H. Liu, Direct voltammetry and catalysis of hemoenzymes in methyl cellulose film, Electrochim. Acta. 49 (2004) 3195–3200.

[36] L.J. Núnez-Vergara, D. Farias, S. Bollo, J.A. Squella, An electrochemical evidence of free radicals formation from flutamide and its reactivity with endo/xenobiotics of pharmacological relevance, Bioelectrochemistry. 53 (2001) 103–110.

[37] G. Angulo, A. Kapturkiewicz, A. Palmaerts, L. Lutsen, T.J. Cleij, D. Vanderzande, Cyclic voltammetry studies of n-type polymers with non-alternant fluoranthene units, Electrochim. Acta. 54 (2009) 1584–1588.

[38] Y. Wang, H. Xu, J. Zhang, G. Li, Electrochemical Sensors for Clinic Analysis., Sensors (Basel). 8 (2008) 2043–2081.

[39] N.R. Stradiotto, H. Yamanaka, M.V.B. Zanoni, Electrochemical sensors: a powerful tool in analytical chemistry, J. Braz. Chem. Soc. 14 (2003) 159–173.

[40] J. Bobacka, A. Ivaska, A. Lewenstam, Potentiometric Ion Sensors, Chem. Rev. 108 (2008) 329–351.

[41] E. Bakker, E. Pretsch, Nanoscale potentiometry, TrAC Trends Anal. Chem. 27 (2008) 612–618.

[42] M. Rumyantseva, M. Labeau, G. Delabouglise, L. Ryabova, I. Kutsenok, A. Gaskov, Copper and nickel doping effect on interaction of SnO2 films with H2S, J. Mater. Chem. 7 (1997) 1785–1790.

[43] M. Fleischer, H. Meixner, Sensitive, selective and stable CH4 detection using semiconducting Ga2O3 thin films, Sensors Actuators B Chem. 26 (1995) 81–84.

[44] B.P.J. de Lacy Costello, P. Evans, N.M. Ratcliffe, Preparation of polypyrrole composites and the effect of volatile amines on their electrical properties, Analyst. 121 (1996) 793.

[45] V. Smyntyna, V. Golovanov, S. Kacˇiulis, G. Mattogno, G. Righini, Influence of chemical composition on sensitivity and signal reproducibility of CdS sensors of

oxygen, Sensors Actuators B Chem. 25 (1995) 628–630.

[46] W. Qu, J.-U. Meyer, Thick-film humidity sensor based on porous material, Meas. Sci. Technol. 8 (1997) 593–600.

[47] R.K. Iler, The chemistry of silica : solubility, polymerization, colloid and surface properties, and biochemistry, Wiley, 1979.

[48] L.L. Hench, J.K. West, The sol-gel process, Chem. Rev. 90 (1990) 33–72. doi:10.1021/cr00099a003.

[49] T. Matsoukas, E. Gulari, Dynamics of growth of silica particles from ammonia-catalyzed hydrolysis of tetra-ethyl-orthosilicate, J. Colloid Interface Sci. 124 (1988) 252–261.

[50] T. Matsoukas, E. Gulari, Monomer-addition growth with a slow initiation step: A growth model for silica particles from alkoxides, J. Colloid Interface Sci. 132 (1989) 13–21.

[51] G.. Bogush, C.. Zukoski, Uniform silica particle precipitation: An aggregative growth model, J. Colloid Interface Sci. 142 (1991) 19–34.

[52] D. Avnir, S. Braun, O. Lev, M. Ottolenghi, Enzymes and Other Proteins Entrapped in Sol-Gel Materials, Chem. Mater. 6 (1994) 1605–1614.

[53] B.C. Dave, B. Dunn, J.S. Valentine, J.I. Zink, Sol-gel encapsulation methods for biosensors, Anal. Chem. 66 (1994) 1120A–1127A.

[54] C.J. Brinker, G.W. Scherer, Sol-gel science : the physics and chemistry of sol-gel processing, Academic Press, 1990.

[55] H.H. DABAGHI, M. KAZEMZAD, Y. GANJKHANLOU, A.A. YUZBASHI, Electrochemical preparation of new organosilicone compounds for functionalizing of mesoporous silica., Funct. Mater. Lett. 06 (2013) 1350031.

[56] G.J. Owens, R.K. Singh, F. Foroutan, M. Alqaysi, C.-M. Han, C. Mahapatra, H.-W. Kim, J.C. Knowles, Sol–gel based materials for biomedical applications, Prog. Mater. Sci. 77 (2016) 1–79. doi:10.1016/J.PMATSCI.2015.12.001.

[57] A.P. Legrand, H. Hommel, A. Tuel, A. Vidal, H. Balard, E. Papirer, P. Levitz, M.

Czernichowski, R. Erre, H. Van Damme, J.P. Gallas, J.F. Hemidy, J.C. Lavalley, O. Barres, A. Burneau, Y. Grillet, Hydroxyls of silica powders, Adv. Colloid Interface Sci. 33 (1990) 91–330. doi:10.1016/0001-8686(90)80027-W.

[58] W. Stöber, A. Fink, E. Bohn, Controlled growth of monodisperse silica spheres in the micron size range, J. Colloid Interface Sci. 26 (1968) 62–69. doi:10.1016/0021-9797(68)90272-5.

[59] G.H. Bogush, M.A. Tracy, C.F. Zukoski, Preparation of monodisperse silica particles: Control of size and mass fraction, J. Non. Cryst. Solids. 104 (1988) 95–106. doi:10.1016/0022-3093(88)90187-1.

[60] G.. Bogush, C.. Zukoski, Studies of the kinetics of the precipitation of uniform silica particles through the hydrolysis and condensation of silicon alkoxides, J. Colloid Interface Sci. 142 (1991) 1–18. doi:10.1016/0021-9797(91)90029-8.

[61] M.M. Collinson, A.R. Howells, Peer Reviewed: Sol–Gels and Electrochemistry: Research at the Intersection., Anal. Chem. 72 (2000) 702 A-709 A. doi:10.1021/ac0029556.

[62] D. Avnir, D. Levy, R. Reisfeld, The nature of the silica cage as reflected by spectral changes and enhanced photostability of trapped Rhodamine 6G, J. Phys. Chem. 88 (1984) 5956–5959. doi:10.1021/j150668a042.

[63] D. Avnir, Organic Chemistry within Ceramic Matrices: Doped Sol-Gel Materials, Acc. Chem. Res. 28 (1995) 328–334. doi:10.1021/ar00056a002.

[64] O. Lev, M. Tsionsky, L. Rabinovich, V. Glezer, S. Sampath, I. Pankratov, J. Gun, Organically modified sol-gel sensors, Anal. Chem. 67 (1995) 22A–30A. doi:10.1021/ac00097a001.

[65] Optical and Electronic Phenomena in Sol-Gel Glasses and Modern Application, Springer Berlin Heidelberg, Berlin, Heidelberg, 1996. doi:10.1007/BFb0111486.

[66] B. Dunn, G.C. Farrington, B. Katz, Sol-gel approaches for solid electrolytes and electrode materials, Solid State Ionics. 70–71 (1994) 3–10. doi:10.1016/0167-2738(94)90281-X.

[67] A. Walcarius, M.M. Collinson, Analytical Chemistry with Silica Sol-Gels: Traditional

Routes to New Materials for Chemical Analysis, Annu. Rev. Anal. Chem. 2 (2009) 121–143. doi:10.1146/annurev-anchem-060908-155139.

[68] M.M. Collinson, Sol-Gel Strategies for the Preparation of Selective Materials for Chemical Analysis, Crit. Rev. Anal. Chem. 29 (1999) 289–311. doi:10.1080/10408349891199310.

[69] D. Avnir, T. Coradin, O. Lev, J. Livage, Recent bio-applications of sol–gel materials, J. Mater. Chem. 16 (2006) 1013–1030. doi:10.1039/B512706H.

[70] O. Lev, Z. Wu, S. Bharathi, V. Glezer, A. Modestov, J. Gun, A. L. Rabinovich, S. Sampath, Sol−Gel Materials in Electrochemistry, (1997). doi:10.1021/CM970367B.

[71] K.S. Alber, J.A. Cox, Electrochemistry in solids prepared by sol-gel processes, Mikrochim. Acta. 127 (1997) 131–147. doi:10.1007/BF01242718.

[72] I.A. Rahman, V. Padavettan, Synthesis of Silica Nanoparticles by Sol-Gel: Size-Dependent Properties, Surface Modification, and Applications in Silica-Polymer Nanocomposites—A Review, J. Nanomater. 2012 (2012) 1–15. doi:10.1155/2012/132424.

[73] M. Kopanica, V. Stará, Silica gel modified carbon composite electrodes, Electroanalysis. 3 (1991) 13–16. doi:10.1002/elan.1140030103.

[74] M.A. Ruiz Barrio, J.M. Pingarrón Carrazón, Voltammetric determination of pentachlorophenol with a silica gel-modified carbon paste electrode, Fresenius. J. Anal. Chem. 344 (1992) 34–38. doi:10.1007/BF00324838.

[75] R.J. Barrio, Z. Gomez de Balugera, M. Aranzazu Goicolea, Utilization of a silica-modified carbon paste electrode for the direct determination of todralazine in biological fluids, Anal. Chim. Acta. 273 (1993) 93–99. doi:10.1016/0003-2670(93)80148-E.

[76] A. Arranz, S.F. de Betoño, J.M. Moreda, A. Cid, J.F. Arranz, Preconcentration and voltammetric determination of the herbicide metamitron with a silica-modified carbon paste electrode, Microchim. Acta. 127 (1997) 273–279. doi:10.1007/BF01242735.

[77] A. Arranz, M.F. Villalba, S.F. de Betoño, J.M. Moreda, J.F. Arranz, Anodic voltammetric assay of the herbicide Metamitron on a carbon paste electrode, Fresenius. J. Anal. Chem. 357 (1997) 768–772. doi:10.1007/s002160050246.

[78] A. Walcarius, J. Bessiere, Silica-modified carbon paste electrode for copper determination in ammoniacal medium, Electroanalysis. 9 (1997) 707–713. doi:10.1002/elan.1140090910.

[79] O. Nadzhafova, M. Etienne, A. Walcarius, Direct electrochemistry of hemoglobin and glucose oxidase in electrodeposited sol–gel silica thin films on glassy carbon, Electrochem. Commun. 9 (2007) 1189–1195. doi:10.1016/J.ELECOM.2007.01.010.

[80] J. Joseph, H. Gomathi, G. Prabhakara Rao, Electrochemical characteristics of thin films of nickel hexacyanoferrate formed on carbon substrates, Electrochim. Acta. 36 (1991) 1537–1541. doi:10.1016/0013-4686(91)85003-P.

[81] G.A.P. Zaldivar, Y. Gushikem, L.T. Kubota, Tin(IV) oxide grafted on a silica gel surface as a conducting substrate base for cupric hexacyanoferrate, J. Electroanal. Chem. Interfacial Electrochem. 318 (1991) 247–254. doi:10.1016/0022-0728(91)85307-B.

[82] L.T. Kubota, Y. Gushikem, Cyclic voltammetric study of [Fe(CN)6]3−/4− immobilized on silica gel surface coated with titanium(IV) oxide, Electrochim. Acta. 37 (1992) 2477–2480. doi:10.1016/0013-4686(92)87087-G.

[83] Y. Gushikem, C.R.M. Peixoto, U.P.R. Filho, L.T. Kubota, E. Stadler, Electrochemical Properties of [Ru(edta)(H2O)]−Immobilized on a Zirconium(IV) Oxide-Coated Silica Gel Surface, J. Colloid Interface Sci. 184 (1996) 236–240. doi:10.1006/JCIS.1996.0616.

[84] E.F. Perez, L.T. Kubota, A.A. Tanaka, G. De Oliveira Neto, Anodic oxidation of cysteine catalysed by nickel tetrasulphonated phthalocyanine immobilized on silica gel modified with titanium (IV) oxide, Electrochim. Acta. 43 (1998) 1665–1673. doi:10.1016/S0013-4686(97)00323-X.

[85] M.M. Collinson, Recent trends in analytical applications of organically modified silicate materials, TrAC Trends Anal. Chem. 21 (2002) 31–39. doi:10.1016/S0165-9936(01)00125-X.

[86] S. Dash, S. Mishra, S. Patel, B.K. Mishra, Organically modified silica: Synthesis and applications due to its surface interaction with organic molecules, Adv. Colloid Interface Sci. 140 (2008) 77–94. doi:10.1016/J.CIS.2007.12.006.

[87] S.L. Burkett, S.D. Sims, S. Mann, Synthesis of hybrid inorganic–organic mesoporous silica by co-condensation of siloxane and organosiloxane precursors, Chem. Commun. 0 (1996) 1367–1368. doi:10.1039/CC9960001367.

[88] D.J. Macquarrie, D.B. Jackson, J.E.G. Mdoe, J.H. Clark, Organomodified hexagonal mesoporous silicates, New J. Chem. 23 (1999) 539–544. doi:10.1039/a900839j.

[89] D.J. Macquarrie, D.B. Jackson, Aminopropylated MCMs as base catalysts: a comparison with aminopropylated silica, Chem. Commun. 0 (1997) 1781–1782. doi:10.1039/a704156j.

[90] C.E. Fowler, S.L. Burkett, S. Mann, Synthesis and characterization of ordered organo–silica–surfactant mesophases with functionalized MCM-41-type architecture, Chem. Commun. 0 (1997) 1769–1770. doi:10.1039/a704644h.

[91] J.H. Clark, D.J. Macquarrie, Catalysis of liquid phase organic reactions using chemically modified mesoporous inorganic solids, Chem. Commun. 0 (1998) 853–860. doi:10.1039/a709143e.

[92] M.A. Marshall, H.A. Mottola, Synthesis of Silica-Immobilized 8-Quinolinol with (Aminophenyl)trimethoxysilane, Anal. Chem. 55 (1983) 2089–2093. doi:10.1021/ac00263a019.

[93] M.E. Diaz-Garcia, R.B. Lainno, Molecular Imprinting in Sol-Gel Materials: Recent Developments and Applications, Microchim. Acta. 149 (2005) 19–36. doi:10.1007/s00604-004-0274-7.

[94] S. American Association of Immunologists., The journal of immunology : official journal of the American Association of Immunologists., Williams & Wilkins, 1950. http://www.jimmunol.org/content/23/6/423.short (accessed February 22, 2019).

[95] L. Pauling, A Theory of the Structure and Process of Formation of Antibodies, (2002). doi:10.1021/JA01867A018.

[96] P. N. Deepa, Mandakini Kanungo, Greg Claycomb, A. Peter M. A. Sherwood, M.M. Collinson, Electrochemically Deposited Sol−Gel-Derived Silicate Films as a Viable Alternative in Thin-Film Design, (2003). doi:10.1021/AC026459O.

[97] M.D. Petit-Dominguez, Hong Shen, A. William R. Heineman, C.J. Seliskar,

Electrochemical Behavior of Graphite Electrodes Modified by Spin-Coating with Sol−Gel-Entrapped Ionomers, (1997). doi:10.1021/AC960839Q.

[98] Y.-Y. Huang, K.-S. Chou, Studies on the spin coating process of silica films, Ceram. Int. 29 (2003) 485–493. doi:10.1016/S0272-8842(02)00191-8.

[99] C.J. Brinker, G.C. Frye, A.J. Hurd, C.S. Ashley, Fundamentals of sol-gel dip coating, Thin Solid Films. 201 (1991) 97–108. doi:10.1016/0040-6090(91)90158-T.

[100] A.-W. Xu, J.C. Yu, H.-X. Zhang, L.-Z. Zhang, A. Dai-Bin Kuang, Yue-Ping Fang, Continuous Formation of Supported Unusual Mesostructured Silica Films by Sol−Gel Dip Coating, (2002). doi:10.1021/LA026035P.

[101] A.R. Di Giampaolo Conde, M. Puerta, H. Ruiz, J.L. Olivares, Thick aluminosilicate coatings on carbon steel via sol-gel, J. Non. Cryst. Solids. 147–148 (1992) 467–473. doi:10.1016/S0022-3093(05)80660-X.

[102] J. Puetz, G. Gasparro, M.A. Aegerter, Liquid film spray deposition of transparent conducting oxide coatings, Thin Solid Films. 442 (2003) 40–43. doi:10.1016/S0040-6090(03)00936-2.

[103] A. Walcarius, D. Mandler, J.A. Cox, M. Collinson, O. Lev, Exciting new directions in the intersection of functionalized sol–gel materials with electrochemistry, J. Mater. Chem. 15 (2005) 3663. doi:10.1039/b504839g.

[104] R. Shacham, D. Avnir, D. Mandler, Electrodeposition of Methylated Sol-Gel Films on Conducting Surfaces, Adv. Mater. 11 (1999) 384–388. doi:10.1002/(SICI)1521-4095(199903)11:5<384::AID-ADMA384>3.0.CO;2-M.

[105] A.T. Kuhn, C.Y. Chan, pH changes at near-electrode surfaces, J. Appl. Electrochem. 13 (1983) 189–207. doi:10.1007/BF00612481.

[106] D. Kriz, O. Ramström, K. Mosbach, Peer Reviewed: Molecular Imprinting: New Possibilities for Sensor Technology, Anal. Chem. 69 (1997) 345A–349A. doi:10.1021/ac971657e.

[107] J.E. Lofgreen, G.A. Ozin, Controlling morphology and porosity to improve performance of molecularly imprinted sol-gel silica., Chem. Soc. Rev. 43 (2014) 911–33. doi:10.1039/c3cs60276a.

[108] A.C. West, C. Cheng, B.C. Baker, Pulse Reverse Copper Electrodeposition in High Aspect Ratio Trenches and Vias, J. Electrochem. Soc. 145 (1998) 3070. doi:10.1149/1.1838766.

[109] D.A. Gamero Quijano, Desarrollo de electrodos modificados con matrices de sílice para posibles aplicaciones en sensores y biosensores electroquímicos, (2014). http://rua.ua.es/dspace/handle/10045/41427 (accessed February 26, 2019).

[110] A.M. Osman, F. El-Cheikh, Z.H. Khalill, A.I. Khodair, Studies on the electrosynthesis of organic compounds II. Reducibility of some Schiff's bases on lead and copper cathodes, J. Appl. Chem. Biotechnol. 26 (2007) 126–130. doi:10.1002/jctb.5020260120.

[111] B.A. Frontana-Uribe, R.D. Little, J.G. Ibanez, A. Palma, R. Vasquez-Medrano, Organic electrosynthesis: a promising green methodology in organic chemistry, Green Chem. 12 (2010) 2099. doi:10.1039/c0gc00382d.

[112] M.M. Collinson, A.R. Howells, Sol-gels and electrochemistry: research at the intersection., Anal. Chem. 72 (2000) 702A–709A. http://www.ncbi.nlm.nih.gov/pubmed/11080854 (accessed February 20, 2019).

[113] O. Lev, Z. Wu, S. Bharathi, V. Glezer, A. Modestov, J. Gun, A. L. Rabinovich, S. Sampath, Sol−Gel Materials in Electrochemistry, (1997). doi:10.1021/CM970367B.

[114] A. Walcarius†, Electrochemical Applications of Silica-Based Organic−Inorganic Hybrid Materials, (2001). doi:10.1021/CM0110167.

[115] U. Narang, P.N. Prasad, F. V. Bright, K. Ramanathan, N.D. Kumar, B.D. Malhotra, M.N. Kamalasanan, S. Chandra, Glucose Biosensor Based on a Sol-Gel-Derived Platform, Anal. Chem. 66 (1994) 3139–3144. doi:10.1021/ac00091a023.

[116] J.W. Long, B. Dunn, A. Debra R. Rolison, Henry S. White, Three-Dimensional Battery Architectures, (2004). doi:10.1021/CR020740L.

[117] R.W. Hart, H.S. White, B. Dunn, D.R. Rolison, 3-D microbatteries, Electrochem. Commun. 5 (2003) 120–123. doi:10.1016/S1388-2481(02)00556-8.

[118] J.S. Sakamoto, B. Dunn, Hierarchical battery electrodes based on inverted opal structures, J. Mater. Chem. 12 (2002) 2859–2861. doi:10.1039/b205634h.

[119] J. Wang, P.V.A. Pamidi, Sol−Gel-Derived Gold Composite Electrodes, Anal. Chem. 69 (1997) 4490–4494. doi:10.1021/ac970680x.

[120] M. Tsionsky, G. Gun, V. Glezer, O. Lev, Sol-Gel-Derived Ceramic-Carbon Composite Electrodes: Introduction and Scope of Applications, Anal. Chem. 66 (1994) 1747–1753. doi:10.1021/ac00082a024.

[121] S.S. And, O. Lev, Inert Metal-Modified, Composite Ceramic−Carbon, Amperometric Biosensors: Renewable, Controlled Reactive Layer, (1996). doi:10.1021/AC951094B.

[122] D. Avnir, M. Ottolenghi, S. Braun, O. Lev, D. Levy, Organically Doped Sol-Gel Porous Glasses: Chemical Sensors, Enzymatic Sensors, Electrooptical Materials, Luminescent Materials and Photochromic Materials, in: Sol-Gel Opt., Springer US, Boston, MA, 1994: pp. 539–582. doi:10.1007/978-1-4615-2750-3_23.

[123] O. Lev, M. Tsionsky, L. Rabinovich, V. Glezer, S. Sampath, I. Pankratov, J. Gun, Organically modified sol-gel sensors, Anal. Chem. 67 (1995) 22A–30A. doi:10.1021/ac00097a001.

[124] O.S. Wolfbeis, R. Reisfeld, I. Oehme, Sol-gels and chemical sensors, in: Opt. Electron. Phenom. Sol-Gel Glas. Mod. Appl., Springer Berlin Heidelberg, Berlin, Heidelberg, n.d.: pp. 51–98. doi:10.1007/BFb0111488.

[125] C.J. Brinker, A.J. Hurd, P.R. Schunk, G.C. Frye, C.S. Ashley, Review of sol-gel thin film formation, J. Non. Cryst. Solids. 147–148 (1992) 424–436. doi:10.1016/S0022-3093(05)80653-2.

[126] A. Walcarius, E. Sibottier, Electrochemically-Induced Deposition of Amine-Functionalized Silica Films on Gold Electrodes and Application to Cu(II) Detection in (Hydro)Alcoholic Medium, Electroanalysis. 17 (2005) 1716–1726. doi:10.1002/elan.200503300.

[127] N.A. Carrington, L. Yong, Z.-L. Xue, Electrochemical deposition of sol–gel films for enhanced chromium(VI) determination in aqueous solutions, Anal. Chim. Acta. 572 (2006) 17–24. doi:10.1016/j.aca.2006.05.020.

[128] M. Sheffer, A. Groysman, D. Mandler, Electrodeposition of sol–gel films on Al for corrosion protection, Corros. Sci. 45 (2003) 2893–2904. doi:10.1016/S0010-

938X(03)00106-9.

[129] Z. Zhang, L. Nie, S. Yao, Electrodeposited sol-gel-imprinted sensing film for cytidine recognition on Au-electrode surface., Talanta. 69 (2006) 435–42. doi:10.1016/j.talanta.2005.10.008.

[130] Emilie Sibottier, Stéphanie Sayen, and Fabien Gaboriaud, A. Walcarius*, Factors Affecting the Preparation and Properties of Electrodeposited Silica Thin Films Functionalized with Amine or Thiol Groups, (2006). doi:10.1021/LA060984R.

[131] R. Shacham, D. Avnir, D. Mandler, Electrodeposition of Methylated Sol-Gel Films on Conducting Surfaces, Adv. Mater. 11 (1999) 384–388.

[132] R. Shacham, D. Avnir, D. Mandler, Electrodeposition of Dye-Doped Titania Thin Films, J. Sol-Gel Sci. Technol. 31 (2004) 329–334. doi:10.1023/B:JSST.0000048012.14882.38.

[133] R. Shacham, D. Mandler, D. Avnir, Electrochemically Induced Sol–Gel Deposition of Zirconia Thin Films, Chem. - A Eur. J. 10 (2004) 1936–1943. doi:10.1002/chem.200305469.

[134] M. Etienne, A. Goux, E. Sibottier, A. Walcarius, Oriented mesoporous organosilica films on electrode: a new class of nanomaterials for sensing., J. Nanosci. Nanotechnol. 9 (2009) 2398–406.

[135] A. Walcarius, E. Sibottier, M. Etienne, J. Ghanbaja, Electrochemically assisted self-assembly of mesoporous silica thin films, Nat. Mater. 6 (2007) 602–608. doi:10.1038/nmat1951.

[136] Y. Guillemin, M. Etienne, E. Aubert, A. Walcarius, Electrogeneration of highly methylated mesoporous silica thin films with vertically-aligned mesochannels and electrochemical monitoring of mass transport issues, J. Mater. Chem. 20 (2010) 6799. doi:10.1039/c0jm00305k.

[137] A. Togni, T. Hayashi, Ferrocenes : homogeneous catalysis, organic synthesis, materials science, VCH Publishers, 1995.

[138] D. (Didier) Astruc, Organometallic chemistry and catalysis, Springer, 2007.

[139] L.-X. Dai, Tao Tu, Shu-Li You, A. Wei-Ping Deng, X.-L. Hou, Asymmetric Catalysis with Chiral Ferrocene Ligands, (2003). doi:10.1021/AR020153M.

[140] B. Fabre, Ferrocene-Terminated Monolayers Covalently Bound to Hydrogen-Terminated Silicon Surfaces. Toward the Development of Charge Storage and Communication Devices, Acc. Chem. Res. 43 (2010) 1509–1518. doi:10.1021/ar100085q.

[141] H. Nishihara, Redox chemistry and functionalities of conjugated ferrocene systems, Adv. Inorg. Chem. 53 (2002) 41–86. doi:10.1016/S0898-8838(02)53003-8.

[142] Nlate, Ruiz, Sartor, Navarro, Blais, Astruc, Molecular batteries: ferrocenylsilylation of dendrons, dendritic cores, and dendrimers: new convergent and divergent routes to ferrocenyl dendrimers with stable redox activity, Chemistry. 6 (2000) 2544–53.

[143] L. Deng, L. Wang, H. Yu, X. Dong, J. Huo, Recent progress in synthesis of ferrocenyl dendrimers and their application in anion recognition, Des. Monomers Polym. 10 (2007) 131–143. doi:10.1163/156855507780378258.

[144] W.A. Amer, L. Wang, H. Yu, A.M. Amin, Y. Wang, Synthesis and Properties of a Ferrocene-based Metallomesogenic Polymer Containing Bis(4-hydroxyoctoxyphenyl)sulfone, J. Inorg. Organomet. Polym. Mater. 22 (2012) 1229–1239. doi:10.1007/s10904-012-9717-5.

[145] K. Tamura, N. Akutagawa, M. Satoh, J. Wada, T. Masuda, Charge/Discharge Properties of Organometallic Batteries Fabricated with Ferrocene-Containing Polymers, Macromol. Rapid Commun. 29 (2008) 1944–1949. doi:10.1002/marc.200800526.

[146] A. Miodek, G. Castillo, T. Hianik, H. Korri-Youssoufi, Electrochemical Aptasensor of Human Cellular Prion Based on Multiwalled Carbon Nanotubes Modified with Dendrimers: A Platform for Connecting Redox Markers and Aptamers, Anal. Chem. 85 (2013) 7704–7712. doi:10.1021/ac400605p.

[147] C. Gondran, M. Orio, D. Rigal, B. Galland, L. Bouffier, T. Gulon, S. Cosnier, Electropolymerized biotinylated poly (pyrrole–viologen) film as platform for the development of reagentless impedimetric immunosensors, Electrochem. Commun. 12 (2010) 311–314. doi:10.1016/j.elecom.2009.12.026.

[148] F. Canonne, M. Perrée-Fauvet, J.P. Mahy, H. Korri-Youssoufi, Electrochemical Detection of DNA Sequences Based on Metalloporphyrins-Polypyrrole Towards a Multi-Detection Analysis, Sens. Lett. 6 (2008) 570–576. doi:10.1166/sl.2008.432.

[149] M. Topcu Sulak, M.T. Sulak, E. Erhan, B. Keskinler, Applied biochemistry and biotechnology : ABAB., Humana Press, n.d.

[150] R. Pilloton, Determination of phenolic acids using Trametes versicolor laccase - D Odaci, S Timur, N Pazarlioglu, MR Montereali, W Vastarella, R Pilloton, Azmi Telefonvcu - Talanta 71 (2007) 312–317, (n.d.).

[151] M. Şenel, E. Çevik, M.F. Abasıyanık, Amperometric hydrogen peroxide biosensor based on covalent immobilization of horseradish peroxidase on ferrocene containing polymeric mediator, Sensors Actuators B Chem. 145 (2010) 444–450. doi:10.1016/j.snb.2009.12.055.

[152] P. Stepnicka, Ferrocenes : ligands, materials and biomolecules, J. Wiley, 2008.

[153] H.-S. Wang, Q.-X. Pan, G.-X. Wang, H.-S. Wang, Q.-X. Pan, G.-X. Wang, A Biosensor Based on Immobilization of Horseradish Peroxidase in Chitosan Matrix Cross-linked with Glyoxal for Amperometric Determination of Hydrogen Peroxide, Sensors. 5 (2005) 266–276. doi:10.3390/s5040266.

[154] Z. Jiang, Y. Shangguan, Q. Zheng, Ferrocene-Modified Polyelectrolyte Film-Coated Electrode and Its Application in Glucose Detection, Polymers (Basel). 11 (2019) 551. doi:10.3390/polym11030551.

[155] H.Z. Kaya, S. Söylemez, Y.A. Udum, L. Toppare, Application of an Efficient Amperometric Glucose Sensing Electrode Based on a Bilayer Polymer Film Platform, J. Electrochem. Soc. 165 (2018) B939–B945. doi:10.1149/2.1121816jes.

[156] A. Jędrzak, T. Rębiś, Ł. Klapiszewski, J. Zdarta, G. Milczarek, T. Jesionowski, Carbon paste electrode based on functional GOx/silica-lignin system to prepare an amperometric glucose biosensor, Sensors Actuators B Chem. 256 (2018) 176–185. doi:10.1016/j.snb.2017.10.079.

[157] M. Dervisevic, E. Dervisevic, M. Senel, E. Cevik, H.B. Yildiz, P. Camurlu, Construction of ferrocene modified conducting polymer based amperometric urea

biosensor, Enzyme Microb. Technol. 102 (2017) 53–59. doi:10.1016/j.enzmictec.2017.04.002.

[158] J. Zhou, H. Li, H. Yang, H. Cheng, G. Lai, Immobilization of Glucose Oxidase on a Carbon Nanotubes/Dendrimer-Ferrocene Modified Electrode for Reagentless Glucose Biosensing, J. Nanosci. Nanotechnol. 17 (2017) 212–216. doi:10.1166/jnn.2017.12388.

[159] N.P. Godman, J.L. DeLuca, S.R. McCollum, D.W. Schmidtke, D.T. Glatzhofer, Electrochemical Characterization of Layer-By-Layer Assembled Ferrocene-Modified Linear Poly(ethylenimine)/Enzyme Bioanodes for Glucose Sensor and Biofuel Cell Applications, Langmuir. 32 (2016) 3541–3551. doi:10.1021/acs.langmuir.5b04753.

[160] B. Feng, Y.N. Liu, A disposable cholesterol enzyme biosensor based on ferrocene-capped gold nanoparticle modified screen-printed carbon electrode, Int. J. Electrochem. Sci. 10 (2015) 4770–4778.

[161] Y. Wang, L. Yang, N. Li, C. Sun, Y. Xia, L. Yuan, J. Lu, F. Liu, X. Xing, A versatile assay for alkaline phosphatase detection based on thymine-HgII-thymine structure generation mediated by TdT, Talanta. 195 (2019) 566–572. doi:10.1016/j.talanta.2018.11.061.

[162] J.E. Coleman, Structure and Mechanism of Alkaline Phosphatase, Annu. Rev. Biophys. Biomol. Struct. 21 (1992) 441–483. doi:10.1146/annurev.bb.21.060192.002301.

[163] J.L. Millán, Alkaline Phosphatases, Purinergic Signal. 2 (2006) 335–341. doi:10.1007/s11302-005-5435-6.

[164] Y. Liu, E. Xiong, X. Li, J. Li, X. Zhang, J. Chen, Sensitive electrochemical assay of alkaline phosphatase activity based on TdT-mediated hemin/G-quadruplex DNAzyme nanowires for signal amplification, Biosens. Bioelectron. 87 (2017) 970–975. doi:10.1016/j.bios.2016.09.069.

[165] J.P. Bilezikian, L.G. (Lawrence G. Raisz, G.A. Rodan, Principles of bone biology, Academic Press, 2002.

[166] A. Petrigliano, A. Tronin, C. Nicolini, Deposition and enzymatic activity of Langmuir-Blodgett films of alkaline phosphatase, Thin Solid Films. 284–285 (1996) 752–756. doi:10.1016/S0040-6090(95)08438-X.

[167] L. Caseli, D.C. Masui, R.P.M. Furriel, F.A. Leone, M.E.D. Zaniquelli, Incorporation conditions guiding the aggregation of a glycosylphosphatidyl inositol (GPI)-anchored protein in Langmuir monolayers., Colloids Surf. B. Biointerfaces. 46 (2005) 248–54. doi:10.1016/j.colsurfb.2005.11.007.

[168] H. Wang, L. Mu, G. She, H. Xu, W. Shi, Fluorescent biosensor for alkaline phosphatase based on fluorescein derivatives modified silicon nanowires, Sensors Actuators B Chem. 203 (2014) 774–781. doi:10.1016/J.SNB.2014.07.047.

[169] P. Colombatto, A. Randone, G. Civitico, J. Monti Gorin, L. Dolci, N. Medaina, F. Oliveri, G. Verme, G. Marchiaro, R. Pagni, P. Karayiannis, H.C. Thomas, G. Hess, F. Bonino, M.R. Brunetto, Hepatitis G virus RNA in the serum of patients with elevated gamma glutamyl transpeptidase and alkaline phosphatase: a specific liver disease? [corrected]., J. Viral Hepat. 3 (1996) 301–6.

[170] S. Sardiwal, P. Magnusson, D.J.A. Goldsmith, E.J. Lamb, Bone Alkaline Phosphatase in CKD–Mineral Bone Disorder, Am. J. Kidney Dis. 62 (2013) 810–822. doi:10.1053/j.ajkd.2013.02.366.

[171] D.M. Goldberg, J. V Martin, A.H. Knight, Elevation of serum alkaline phosphatase activity and related enzymes in diabetes mellitus., Clin. Biochem. 10 (1977) 8–11.

[172] J.A. Lorente, H. Valenzuela, J. Morote, A. Gelabert, Serum bone alkaline phosphatase levels enhance the clinical utility of prostate specific antigen in the staging of newly diagnosed prostate cancer patients., Eur. J. Nucl. Med. 26 (1999) 625–32.

[173] S. Ito, S. Yamazaki, K. Kano, T. Ikeda, Highly sensitive electrochemical detection of alkaline phosphatase, 424 (2000) 57–63.

[174] I. Bronstein, C.S. Martin, J.J. Fortin, C.E. Olesen, J.C. Voyta, Chemiluminescence: sensitive detection technology for reporter gene assays., Clin. Chem. 42 (1996) 1542–6.

[175] F.W. Scheller, C.G. Bauer, A. Makower, U. Wollenberger, A. Warsinke, F.F. Bier, COUPLING OF IMMUNOASSAYS WITH ENZYMATIC RECYCLING ELECTRODES, Anal. Lett. 34 (2001) 1233–1245. doi:10.1081/AL-100104149.

[176] A. Benez, A. Geiselhart, R. Handgretinger, U. Schiebel, G. Fierlbeck, Detection of

circulating melanoma cells by immunomagnetic cell sorting, J. Clin. Lab. Anal. 13 (1999) 229–233. doi:10.1002/(SICI)1098-2825(1999)13.

[177] C. C. Ruan, H. H. Wang, Y. Y. Li, A BIENZYME ELECTROCHEMICAL BIOSENSOR COUPLED WITH IMMUNOMAGNETIC SEPARATION FOR RAPID DETECTION OF ESCHERICHIA COLI O157:H7 IN FOOD SAMPLES, Trans. ASAE. 45 (2002) 249. doi:10.13031/2013.7853.

[178] J. Tian, Y. Yang, M. Huang, C. Zhou, J. Lu, Photoelectrochemical determination of alkaline phosphatase activity based on a photo-excited electron transfer strategy, Talanta. 196 (2019) 293–299. doi:10.1016/j.talanta.2018.12.079.

[179] M. Nausch, Alkaline phosphatase activities and the relationship to inorganic phosphate in the Pomeranian Bight (southern Baltic Sea), Aquat. Microb. Ecol. 16 (1998) 87–94. doi:10.3354/ame016087.

[180] R.B. McComb, G.N. Bowers, S. Posen, Alkaline Phosphatase, Springer US, Boston, MA, 1979. doi:10.1007/978-1-4613-2970-1.

[181] R.H. Plimmer, The Metabolism of Organic Phosphorus Compounds. Their Hydrolysis by the Action of Enzymes., Biochem. J. 7 (1913) 43–71.

[182] R. Robison, The Possible Significance of Hexosephosphoric Esters in Ossification., Biochem. J. 17 (1923) 286–93.

[183] J.L. Millán, M.P. Whyte, Alkaline Phosphatase and Hypophosphatasia, Calcif. Tissue Int. 98 (2016) 398–416. doi:10.1007/s00223-015-0079-1.

[184] J.C. RATHBUN, Hypophosphatasia; a new developmental anomaly., Am. J. Dis. Child. 75 (1948) 822–31.

[185] F.H. Westheimer, Why nature chose phosphates., Science. 235 (1987) 1173–8. doi:10.1126/SCIENCE.2434996.

[186] E.J. Wood, Principles and techniques of practical biochemistry (5th Ed.): Wilson, K., Walker, J. (eds.), Biochem. Mol. Biol. Educ. 30 (2002) 214–215. doi:10.1002/bmb.2002.494030030062.

[187] O. Niwa, Y. Xu, H.B. Halsall, W.R. Heineman, Small-volume voltammetric detection

of 4-aminophenol with interdigitated array electrodes and its application to electrochemical enzyme immunoassay, Anal. Chem. 65 (1993) 1559–1563. doi:10.1021/ac00059a013.

[188] F. Hofmann, A. Frey, B. Holzapfl, M. Schienle, C. Paulus, P. Schindler-Bauer, R. Hintsche, E. Nebling, J. Albers, W. Gumbrecht, R. Thewes, Passive DNA sensor with gold electrodes fabricated in a CMOS backend process, Eur. Solid-State Device Res. Conf. (2002) 487–490. doi:10.1109/ESSDERC.2002.194974.

[189] M.S. Islam, K. Sazawa, N. Hata, K. Sugawara, H. Kuramitz, Determination of heavy metal toxicity by using a micro-droplet hydrodynamic voltammetry for microalgal bioassay based on alkaline phosphatase, Chemosphere. 188 (2017) 337–344. doi:10.1016/j.chemosphere.2017.09.008.

[190] M.K. Sharma, G.S. Agarwal, V.K. Rao, S. Upadhyay, G.P. Rai, R. Vijayaraghavan, Amperometric Biosensor for the Sensitive Detection of Plasmodium falciparum Histidine Rich Protein-2 Antigen, Sens. Lett. 9 (2011) 1363–1369. doi:10.1166/sl.2011.1681.

[191] G.A. Messina, N. V. Panini, N.A. Martinez, J. Raba, Microfluidic immunosensor design for the quantification of interleukin-6 in human serum samples, Anal. Biochem. 380 (2008) 262–267. doi:10.1016/j.ab.2008.05.055.

[192] G.A. Messina, I.E. De Vito, J. Raba, Screen-printed immunosensor for quantification of human serum IgG antibodies to Helicobacter pylori, Sensors Actuators B Chem. 128 (2007) 23–30. doi:10.1016/j.snb.2007.05.024.

[193] M.P. Kreuzer, R. McCarthy, M. Pravda, G.G. Guilbault, Development of Electrochemical Immunosensor for Progesterone Analysis in Milk, Anal. Lett. 37 (2004) 943–956. doi:10.1081/AL-120030289.

[194] M.P. Kreuzer, M. Pravda, C.K. O'Sullivan, G.G. Guilbault, Novel electrochemical immunosensors for seafood toxin analysis, Toxicon. 40 (2002) 1267–1274. doi:10.1016/S0041-0101(02)00132-0.

[195] A.J. Bard, L.R. Faulkner, Electrochemical methods : fundamentals and applications, Wiley, 2001.

[196] J. Wang, Analytical electrochemistry, Wiley-VCH, 2006.

[197] D.A. Skoog, F.J. Holler, S.R. Crouch, Principles of instrumental analysis, Thomson, Brooks/Cole, Belmont, CA :, 2007. https://ua.on.worldcat.org/search?queryString=no%3A+1058011927#/oclc/1058011927 (accessed February 5, 2019).

[198] C.R. Brundle, C.A. Evans, S. Wilson, Encyclopedia of materials characterization : surfaces, interfaces, thin films, Butterworth-Heinemann, 1992.

[199] E. Raymundo-Piñero, D. Cazorla-Amorós, A. Linares-Solano, J. Find, U. Wild, R. Schlögl, Structural characterization of N-containing activated carbon fibers prepared from a low softening point petroleum pitch and a melamine resin, Carbon N. Y. 40 (2002) 597–608. doi:10.1016/S0008-6223(01)00155-5.

[200] B.C. Smith, Fundamentals of Fourier transform infrared spectroscopy, CRC Press, 2011.

[201] Y. (Yang) Leng, Materials characterization : introduction to microscopic and spectroscopic methods,

[202] R. (Roland) Wiesendanger, Scanning probe microscopy and spectroscopy : methods and applications, Cambridge University Press, 1994.

[203] T. Hatakeyama, F.X. Quinn, Thermal analysis : fundamentals and applications to polymer science, Wiley, 1999.

[204] D.A. Skoog, F.J. Holler, S.R. Crouch, Principles of instrumental analysis, n.d.

[205] M. Labib, E.H. Sargent, S.O. Kelley, Electrochemical Methods for the Analysis of Clinically Relevant Biomolecules, Chem. Rev. 116 (2016) 9001–9090. doi:10.1021/acs.chemrev.6b00220.

[206] B.J. Sanghavi, O.S. Wolfbeis, T. Hirsch, N.S. Swami, Nanomaterial-based electrochemical sensing of neurological drugs and neurotransmitters, Microchim. Acta. 182 (2015) 1–41. doi:10.1007/s00604-014-1308-4.

[207] A. Walcarius, Template-directed porous electrodes in electroanalysis, Anal. Bioanal. Chem. 396 (2010) 261–272. doi:10.1007/s00216-009-3069-1.

[208] R.M. and, M.M. Collinson*, Template Recognition in Inorganic−Organic Hybrid Films Prepared by the Sol−Gel Process, (1998). doi:10.1021/CM9801136.

[209] Annette R. Howells, and Pedro J. Zambrano, M.M. Collinson*, Diffusion of Redox Probes in Hydrated Sol−Gel-Derived Glasses, (2000). doi:10.1021/AC000910Z.

[210] D. Salinas-Torres, F. Montilla, F. Huerta, E. Morallón, All electrochemical synthesis of polyaniline/silica sol–gel materials, Electrochim. Acta. 56 (2011) 3620–3625. doi:10.1016/J.ELECTACTA.2010.11.059.

[211] A. Walcarius, Electrochemical Applications of Silica-Based Organic−Inorganic Hybrid Materials, (2001). doi:10.1021/CM0110167.

[212] M. Porcel-Valenzuela, A. Salinas-Castillo, E. Morallón, F. Montilla, Molecularly imprinted silica films prepared by electroassisted deposition for the selective detection of dopamine, Sensors Actuators B Chem. 222 (2016) 63–70. doi:10.1016/J.SNB.2015.08.042.

[213] S. López-Bernabeu, A. Gamero-Quijano, F. Huerta, E. Morallón, F. Montilla, Enhancement of the direct electron transfer to encapsulated cytochrome c by electrochemical functionalization with a conducting polymer, J. Electroanal. Chem. 793 (2017) 34–40. doi:10.1016/J.JELECHEM.2016.12.044.

[214] I. Gill, A. Ballesteros, Bioencapsulation within synthetic polymers (Part 1): sol-gel encapsulated biologicals., Trends Biotechnol. 18 (2000) 282–96.

[215] A. Salinas-Castillo, J.F. Fernández-Sánchez, A. Segura-Carretero, A. Fernández-Gutiérrez, Solid-surface phosphorescence characterization of polycyclic aromatic hydrocarbons and selective determination of benzo(a)pyrene in water samples, Anal. Chim. Acta. 550 (2005) 53–60. doi:10.1016/j.aca.2005.06.046.

[216] F. Montilla, M.A. Cotarelo, E. Morallón, Hybrid sol–gel–conducting polymer synthesised by electrochemical insertion: tailoring the capacitance of polyaniline, J. Mater. Chem. 19 (2009) 305–310. doi:10.1039/B813323A.

[217] A. Gamero-Quijano, F. Huerta, D. Salinas-Torres, E. Morallón, F. Montilla, Electrochemical Behaviour of PSS-Functionalized Silica Films Prepared by Electroassisted Deposition of Sol–Gel Precursors, Electrocatalysis. 6 (2015) 33–41.

doi:10.1007/s12678-014-0215-0.

[218] S.Y. Yang, J.A. Defranco, Y.A. Sylvester, T.J. Gobert, D.J. Macaya, R.M. Owens, G.G. Malliaras, Integration of a surface-directed microfluidic system with an organic electrochemical transistor array for multi-analyte biosensors., Lab Chip. 9 (2009) 704–8. doi:10.1039/b811606g.

[219] D. Liu, M.M. Rahman, C. Ge, J. Kim, J.J. Lee, Highly stable and conductive PEDOT:PSS/graphene nanocomposites for biosensor applications in aqueous medium, New J. Chem. 41 (2017) 15458–15465. doi:10.1039/c7nj03330c.

[220] M. Mazloum-Ardakani, E. Amin-Sadrabadi, A. Khoshroo, Enhanced activity for non-enzymatic glucose oxidation on nickel nanostructure supported on PEDOT:PSS, J. Electroanal. Chem. 775 (2016) 116–120. doi:10.1016/J.JELECHEM.2016.05.044.

[221] G.-X. Wang, Y. Qian, X.-X. Cao, X.-H. Xia, Direct electrochemistry of cytochrome c on a graphene/poly (3,4-ethylenedioxythiophene) nanocomposite modified electrode, Electrochem. Commun. 20 (2012) 1–3. doi:10.1016/J.ELECOM.2012.03.029.

[222] S. López-Bernabeu, F. Huerta, E. Morallón, F. Montilla, Direct Electron Transfer to Cytochrome *c* Induced by a Conducting Polymer, J. Phys. Chem. C. 121 (2017) 15870–15879. doi:10.1021/acs.jpcc.7b05204.

[223] J. Park, H.K. Kim, Y. Son, Glucose biosensor constructed from capped conducting microtubules of PEDOT, Sensors Actuators B Chem. 133 (2008) 244–250. doi:10.1016/J.SNB.2008.02.029.

[224] P. Santhosh, K.M. Manesh, S. Uthayakumar, S. Komathi, A.I. Gopalan, K.-P. Lee, Fabrication of enzymatic glucose biosensor based on palladium nanoparticles dispersed onto poly(3,4-ethylenedioxythiophene) nanofibers., Bioelectrochemistry. 75 (2009) 61–6. doi:10.1016/j.bioelechem.2008.12.001.

[225] R.L. McCreery, Advanced Carbon Electrode Materials for Molecular Electrochemistry, Chem. Rev. 108 (2008) 2646–2687. doi:10.1021/cr068076m.

[226] G. Liu, J. Liu, T. Böcking, P.K. Eggers, J.J. Gooding, The modification of glassy carbon and gold electrodes with aryl diazonium salt: The impact of the electrode materials on the rate of heterogeneous electron transfer, Chem. Phys. 319 (2005) 136–

146. doi:10.1016/j.chemphys.2005.03.033.

[227] John F. Smalley, Harry O. Finklea, Christopher E. D. Chidsey, Matthew R. Linford, Stephen E. Creager, John P. Ferraris, Keli Chalfant, Thomas Zawodzinsk, and Stephen W. Feldberg, M.D. Newton, Heterogeneous Electron-Transfer Kinetics for Ruthenium and Ferrocene Redox Moieties through Alkanethiol Monolayers on Gold, (2003). doi:10.1021/JA028458J.

[228] N.J. Ronkainen, H.B. Halsall, W.R. Heineman, Electrochemical biosensors, Chem. Soc. Rev. 39 (2010) 1747. doi:10.1039/b714449k.

[229] E.-H. Yoo, S.-Y. Lee, Glucose Biosensors: An Overview of Use in Clinical Practice, Sensors. 10 (2010) 4558–4576. doi:10.3390/s100504558.

[230] L. Setti, A. Fraleoni-Morgera, I. Mencarelli, A. Filippini, B. Ballarin, M. Di Biase, An HRP-based amperometric biosensor fabricated by thermal inkjet printing, Sensors Actuators B Chem. 126 (2007) 252–257. doi:10.1016/J.SNB.2006.12.015.

[231] L. Setti, A. Fraleoni-Morgera, B. Ballarin, A. Filippini, D. Frascaro, C. Piana, An amperometric glucose biosensor prototype fabricated by thermal inkjet printing, Biosens. Bioelectron. 20 (2005) 2019–2026. doi:10.1016/j.bios.2004.09.022.

[232] J. Bobacka, A. Lewenstam, A. Ivaska, Electrochemical impedance spectroscopy of oxidized poly(3,4-ethylenedioxythiophene) film electrodes in aqueous solutions, J. Electroanal. Chem. 489 (2000) 17–27. doi:10.1016/S0022-0728(00)00206-0.

[233] K.C. (nee Włodarczyk), J. Karczewski, P. Jasiński, Influence of electropolymerization conditions on the morphological and electrical properties of PEDOT film, Electrochim. Acta. 176 (2015) 156–161. doi:10.1016/J.ELECTACTA.2015.07.006.

[234] V. Castagnola, C. Bayon, E. Descamps, C. Bergaud, Morphology and conductivity of PEDOT layers produced by different electrochemical routes, Synth. Met. 189 (2014) 7–16. doi:10.1016/J.SYNTHMET.2013.12.013.

[235] A. Lachkar, A. Selmani, E. Sacher, M. Leclerc, R. Mokhliss, Metallization of polythiophenes I. Interaction of vapor-deposited Cu, Ag and Au with poly(3-hexylthiophene) (P3HT), Synth. Met. 66 (1994) 209–215. doi:10.1016/0379-6779(94)90069-8.

[236] S.K.. Jönsson, J. Birgerson, X. Crispin, G. Greczynski, W. Osikowicz, A.. Denier van der Gon, W.. Salaneck, M. Fahlman, The effects of solvents on the morphology and sheet resistance in poly(3,4-ethylenedioxythiophene)–polystyrenesulfonic acid (PEDOT–PSS) films, Synth. Met. 139 (2003) 1–10. doi:10.1016/S0379-6779(02)01259-6.

[237] M.M. Nasef, H. Saidi, H.M. Nor, M.A. Yarmo, XPS studies of radiation grafted PTFE-g-polystyrene sulfonic acid membranes, J. Appl. Polym. Sci. 76 (2000) 336–349. doi:10.1002/(SICI)1097-4628(20000418)76:3<336::AID-APP9>3.0.CO;2-E.

[238] G. Greczynski, T. Kugler, W.. Salaneck, Characterization of the PEDOT-PSS system by means of X-ray and ultraviolet photoelectron spectroscopy, Thin Solid Films. 354 (1999) 129–135. doi:10.1016/S0040-6090(99)00422-8.

[239] X. Crispin, S. Marciniak, W. Osikowicz, G. Zotti, A.W.D. van der Gon, F. Louwet, M. Fahlman, L. Groenendaal, F. De Schryver, W.R. Salaneck, Conductivity, morphology, interfacial chemistry, and stability of poly(3,4-ethylene dioxythiophene)-poly(styrene sulfonate): A photoelectron spectroscopy study, J. Polym. Sci. Part B Polym. Phys. 41 (2003) 2561–2583. doi:10.1002/polb.10659.

[240] Allen J. Bard and Larry R. Faulkner, Electrochemical Methods: Fundamentals and Applications, New York: Wiley, 2001, 2nd ed., Russ. J. Electrochem. 38 (2002) 1364–1365. doi:10.1023/A:1021637209564.

[241] D. Salinas-Torres, F. Huerta, F. Montilla, E. Morallón, Study on electroactive and electrocatalytic surfaces of single walled carbon nanotube-modified electrodes, Electrochim. Acta. 56 (2011) 2464–2470. doi:10.1016/J.ELECTACTA.2010.11.023.

[242] A. Gamero-Quijano, F. Huerta, D. Salinas-Torres, E. Morallón, F. Montilla, Enhancement of the Electrochemical Performance of SWCNT dispersed in a Silica Sol-gel Matrix by Reactive Insertion of a Conducting Polymer, Electrochim. Acta. 135 (2014) 114–120. doi:10.1016/J.ELECTACTA.2014.04.172.

[243] J.A. Taylor, G.M. Lancaster, A. Ignatiev, J.W. Rabalais, Interactions of ion beams with surfaces. Reactions of nitrogen with silicon and its oxides, J. Chem. Phys. 68 (1978) 1776–1784. doi:10.1063/1.435869.

[244] Bell, Ley, Photoemission study of SiOx (0, Phys. Rev. B. Condens. Matter. 37 (1988)

8383–8393. http://www.ncbi.nlm.nih.gov/pubmed/9944177 (accessed February 18, 2019).

[245] X.-R. Yu, H. Hantsche, Vertical differential charging in monochromatized small spot X-ray photoelectron spectroscopy, Surf. Interface Anal. 20 (1993) 555–558. doi:10.1002/sia.740200702.

[246] T. Gross, M. Ramm, H. Sonntag, W. Unger, H.M. Weijers, E.H. Adem, An XPS analysis of different SiO2 modifications employing a C 1s as well as an Au 4f7/2 static charge reference, Surf. Interface Anal. 18 (1992) 59–64. doi:10.1002/sia.740180110.

[247] S.S. Jedlicka, J.L. Rickus, D.Y. Zemlyanov, Surface Analysis by X-ray Photoelectron Spectroscopy of Sol−Gel Silica Modified with Covalently Bound Peptides, J. Phys. Chem. B. 111 (2007) 11850–11857. doi:10.1021/jp0744230.

[248] A. Gamero-Quijano, F. Huerta, E. Morallón, F. Montilla, Modulation of the silica sol-gel composition for the promotion of direct electron transfer to encapsulated cytochrome c, Langmuir. 30 (2014) 10531–10538. doi:10.1021/la5023517.

[249] M. Zaharescu, A. Jitianu, A. Brăileanu, J. Madarász, C. Novák, G. Pokol, Composition and thermal stability of SiO2-based hybrid materials TEOS-MTEOS system, J. Therm. Anal. Calorim. 71 (2003) 421–428. doi:10.1023/A:1022883221776.

[250] M.P. Valenzuela, afinidad preparados por electrodepósito para la detección de neurotransmisores María Porcel Valenzuela, (n.d.).

[251] R. Al-Oweini, H. El-Rassy, Synthesis and characterization by FTIR spectroscopy of silica aerogels prepared using several Si(OR)4 and R″Si(OR′)3 precursors, J. Mol. Struct. 919 (2009) 140–145. doi:10.1016/j.molstruc.2008.08.025.

[252] C.J. Brinker, G.W. Scherer, Sol-gel science : the physics and chemistry of sol-gel processing, Academic Press, 1990.

[253] G. Socrates, Infrared and raman characteristic group frequencies : tables and charts., John Wiley & Sons, 2007.

[254] P. Innocenzi, Infrared spectroscopy of sol–gel derived silica-based films: a spectra-microstructure overview, J. Non. Cryst. Solids. 316 (2003) 309–319. doi:10.1016/S0022-3093(02)01637-X.

[255] A. Bertoluzza, C. Fagnano, M. Antonietta Morelli, V. Gottardi, M. Guglielmi, Raman and infrared spectra on silica gel evolving toward glass, J. Non. Cryst. Solids. 48 (1982) 117–128. doi:10.1016/0022-3093(82)90250-2.

[256] R.S. Nicholson, Theory and Application of Cyclic Voltammetry for Measurement of Electrode Reaction Kinetics., Anal. Chem. 37 (1965) 1351–1355. doi:10.1021/ac60230a016.

[257] E. Mahé, D. Devilliers, C. Comninellis, Electrochemical reactivity at graphitic micro-domains on polycrystalline boron doped diamond thin-films electrodes, Electrochim. Acta. 50 (2005) 2263–2277. doi:10.1016/j.electacta.2004.10.060.

[258] H. Matsuda, Y. Ayabe, Zur Theorie der Randles-Sevčikschen Kathodenstrahl-Polarographie, Zeitschrift Für Elektrochemie, Berichte Der Bunsengesellschaft Für Phys. Chemie. 59 (1955) 494–503. doi:10.1002/BBPC.19550590605.

[259] D. Robinson, J.E. Anderson, J.L. Lin, Measurement of diffusion coefficients of some indoles and ascorbic acid by flow injection analysis, J. Phys. Chem. 94 (1990) 1003–1005. doi:10.1021/j100365a092.

[260] M.M. Collinson, P.J. Zambrano, H. Wang, J.S. Taussig, Diffusion Coefficients of Redox Probes Encapsulated within Sol−Gel Derived Silica Monoliths Measured with Ultramicroelectrodes, Langmuir. 15 (1999) 662–668. doi:10.1021/la980764g.